ACOUSTICAL COMMUNICATIONS FOR WIRELESS DOWNHOLE TELEMETRY SYSTEMS

A Dissertation

by

ABDALLAH KAYED FARRAJ

Submitted to the Office of Graduate Studies of
Texas A&M University
in partial fulfillment of the requirements for the degree of

DOCTOR OF PHILOSOPHY

Approved by:

Co-Chairs of Committee,	Scott L. Miller
	Khalid A. Qaraqe
Committee Members,	Deepa Kundur
	Jim X. Ji
	Mahmoud El-Halwagi
Department Head,	Costas N. Georghiades

December 2012

Major Subject: Electrical Engineering

ABSTRACT

This dissertation investigates the use of advanced acoustical communication techniques for wireless downhole telemetry systems. Using acoustic waves for downhole telemetry systems is investigated in order to replace the wired communication systems currently being used in oil and gas wells. While the acoustic technology offers great benefits, a clear understanding of its propagation aspects inside the wells is lacking. This dissertation describes a testbed that was designed to study the propagation of acoustic waves over production pipes. The wireless communication system was built using an acoustic transmitter, five connected segments of seven inch production pipes, and an acoustic receiver. The propagation experiments that were conducted on this testbed in order to characterize the channel behavior are explained as well. Moreover, the large scale statistics of the acoustic waves along the pipe string are described. Results of this work indicate that acoustic waves experience a frequency-dependent attenuation and dispersion over the pipe string. In addition, the testbed was modified by encasing one pipe segment in concrete in order to study the effect of concrete on wave propagation. The concrete was found to filter out many of the signal harmonics; accordingly, the acoustic waves experienced extra attenuation and dispersion. Signal processing techniques are also investigated to address the effects of multipaths and attenuation in the acoustic channel; results show great enhancements in signal qualities and the usefulness of these algorithms for downhole communication systems. Furthermore, to explore an alternative to vibrating the body of a cemented pipe string, a testbed was designed to investigate the propagation aspects of sound waves inside the interior of the production pipes. Results indicate that some low-frequency sound waves can travel for thousands of feet inside a cemented pipe string

and can still be detected reliably.

DEDICATION

To my wonderful family...

Salam Noor,

Malak Rahma,

Laila Ward,

and Eman

ACKNOWLEDGEMENTS

First and foremost, I would like to praise God Almighty for all the blessings I have. I wish to express my sincere gratitude to my advisor, Dr. Scott Miller, for his guidance, time, encouragement, continuous support, and help. Thank you for the many hours of assistance in preparing and running the experiments and analyzing the results.

I would like to thank Dr. Khalid Qaraqe for his support. I am very grateful to my committee members; Dr. Deepa Kundur, Dr. Jim Ji, and Dr. Mahmoud El-Halwagi for their time and efforts in helping me complete this dissertation. I would like to thank all the professors who have taught me throughout my graduate study. I also thank all the staff at the Department of Electrical and Computer Engineering, Sponsored Students Office, and the Office of Graduate Studies at Texas A&M University.

I am thankful to RasGas Ltd. for their generous support of this project; Paul Tubel, Scott Kruegel, and Clark Bergeron from ZIEBEL US Inc. for their useful suggestions and help; Anantharaman Balasubramanian, Eser Ustunel, Nariman Rahimian, and Kiran Gummuluri for their help in running the experiments; and Paula Evans for her administrative assistance.

I am grateful for the support and good wishes I always get from my colleagues and friends. I would like to deeply thank my family for their support, prayers, and patience. Last but not the least, I would love to say thank you to my wonderful wife, Eman, for her wisdom, encouragement, unlimited love, and tireless efforts to push me forward. Your support made this journey meaningful.

TABLE OF CONTENTS

LIST OF FIGURES

Page

LIST OF TABLES

1. Introduction

New challenges for well drilling, completion, and production have changed the role of technology in the oil and gas industry. For example, there has been a significant increase in the need for advanced technologies in the exploration and production sectors; the ability to communicate between downhole and surface instruments in oil and gas wells is becoming a critical need as well operators seek production and operations efficiency.

Especially in remote operating environments, the monitoring of flow rate, temperature, and pressure data has become essential in order to facilitate well performance optimization and help in maintenance by providing valuable information about corrosion, flow blockages, and leaks. Sensor technology along with communications techniques provide an on-demand access to the information necessary to optimize production levels and achieve costs goals.

1.1 Background and Motivation

The use of wire line tools for communication between downhole and surface instruments is common in the oil and gas industry, but these installations present cost, maintenance, and reliability issues. Wireless communication systems offer a significant advantage over the existing wired technologies as they eliminate the need for cables, clamps, external pressure and temperature sensors, as well as splices on the cable that can fail inside the wellbore. Sometimes it is typical to shut down production in order to get measurements down the well in such wired systems. Therefore, alternatively, the existing wired systems can be replaced with wireless communication systems to acquire the vital data without interrupting production.

It is estimated that the deployment cost savings of using wireless tools over wire

line tools for a single well can reach a few hundreds of thousands of dollars. With this kind of savings potential for each deployment, the development of reliable wireless communication tools for downhole applications became a significant industry need. Wireless communication techniques have recently been investigated to decrease the cost of exploring for oil and gas as several companies have developed new technologies involving sensors and wireless telemetry which provide valuable real time process monitoring information. An illustration of a typical wireless downhole telemetry system is shown in Figure 1.1.

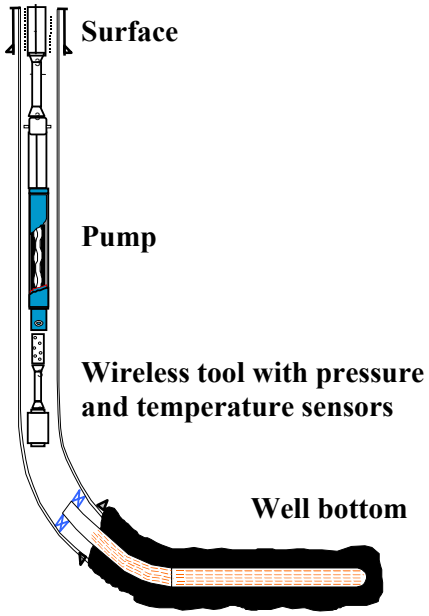

Figure 1.1: Typical wireless downhole telemetry system

Using electromagnetic waves to conduct wireless communications in such configurations is an infeasible option as there are conducting mediums, like the steel pipe string and the formation around it, that will decay the electromagnetic waves and limit the propagation to unpractical distances. On the other hand, acoustic waves,

which either propagate by vibrating the body of the pipe string or propagate using the medium inside the pipe string, will not have such problems. This makes the acoustic waves an interesting option to conduct wireless communications using pipe strings for downhole systems.

Using acoustic waves as a means to carry information for downhole telemetry systems is a technology currently being investigated by companies and researchers in order to replace the wired communication systems currently being used in oil and gas wells. While this technology offers great benefits, a clear understanding of its propagation aspects inside the wells is lacking.

The use of acoustic waves to conduct wireless downhole communications is investigated in this dissertation. A testbed that was designed to study the propagation of acoustic waves over production pipes is described. This wireless communication system was built using an acoustic transmitter, pipe string composed of connected segments of production pipes, and an acoustic receiver. Acoustic waves propagate in this setup from one point to another by vibrating the body of the pipe string. Propagation experiments were conducted on this testbed in order to characterize the acoustic channel behavior. The experimental results for this setup are discussed as well. Some signal processing techniques are also investigated in order to address the effects of dispersion and attenuation in the acoustic channel.

It is interesting to investigate the effect of encasing the exterior of a pipe segment in concrete on the propagation of acoustic waves in this testbed. It was expected that concrete would have a significant impact on the propagation of acoustic waves that vibrate the tubing. Consequently, part of the pipe string was encased in a doughnut-shaped concrete segment, and the propagation aspects of the acoustic waves are investigated as well.

To study the feasibility of using the interior of the pipe string as a propagation

medium for sound waves, a wireless communication system was built using a speaker and microphone while the propagation medium for the sound wave is the air inside the pipe string. Propagation results are discussed in this work including signal decay rate and delay spread measures.

1.2 Summary of Contributions

Contributions of this work include:

- Building a testbed for 2-7/8" and 7" pipes
- Building the acoustic receiver circuit and software
- Conducting acoustical propagation experiments on this testbed
- Extracting the channel large scale statistics
- Encasing parts of the pipe string into concrete and studying the effect of concrete on signal propagation
- Developing signal processing algorithms to counter the damaging effects of the concrete and the acoustic channel and enhance the measurements' quality

1.3 Notation

In this dissertation, matrices are represented in bold upper case symbols, vectors in bold lower case symbols, and real or complex scalars in italic lower case symbols.

1.4 Dissertation Organization

The rest of the dissertation is organized as follows: Chapter 2 provides an overview of acoustic telemetry systems and a brief literature review is given. An overview of the testbed and experiment design is given in Chapter 3. Measurement results are shown and discussed in Chapter 4 for the 2-7/8" pipe string case and in

Chapter 5 for the 7" pipe string case. Chapter 6 introduces some signal processing algorithms that enhance the experimental results. Chapter 7 describes channel characterization experiments and results. An overview of the sound propagation inside the production pipe string experiment and some results are described in Chapter 8. Finally, Chapter 9 contains discussions and conclusions.

2. Downhole Communication Systems

Downhole telemetry systems are described in this chapter. The current well logging techniques are described in Section 2.1. A literature review about acoustic communication systems is provided in Section 2.2. A review of some results from acoustic downhole systems is given in Section 2.3.

2.1 Well Logging Systems

Well logging is a record of information that provides documentation of one or more physical measurements as a function of well depth [1, 2]. The accurate knowledge of the potential production status of any drilled well is an essential need to avoid bypassing a good productive well or avoid wasting money trying to make production out of a non-commercial well. Production logging is taken to provide valuable information on downhole production activity of the well [3].

Logging equipment is lowered through the well tubing in order to make downhole measurements. The measurements are recorded using an equipment at the surface and then analyzed to get an idea about the well conditions. Logging can provide valuable information about the physical conditions of the well, the types of fluids within the formation, effectiveness of stimulation methods, and temperature, pressure, and rate of the gas or oil inside the well [3]. The transmission of well downhole information can be achieved using a data transmission cable containing a shielding conductor or an optical fiber bundle with a tool attached to its end. This cable can be installed as part of the well completion process, and this will need special handling in the packers and wellhead [2].

To acquire some information while drilling a well, measurement-while-drilling techniques can be used. Mud logging is one famous method to achieve that. Mud is

a term used to refer to the drilling liquid mixture that is used to cool and lubricate the drilling bit, condition the formation wall, and remove the cuttings from inside the well. Mud logging refers to the practice of analyzing the samples of the circulated drilling mud to detect signs of fluids or formations which have entered the mud [1]. The mud logger tries to identify, record, and evaluate the drilling parameters, then this data is correlated with that of other wells in order to decide if the well is capable of producing hydrocarbons. Mud logging is also used to monitor wellbore stability [4].

The logging-while-drilling systems mainly use the mud-pulse telemetry systems to transmit the measured data from the bottom of the well up to the surface. The transmission rate for the mud systems is very low, and this puts limitations on using those systems to accomplish real-time communications. More information about well logging techniques and mud-pulse telemetry systems can be found in [5, 6, 7, 8, 9, 10, 11].

Acoustic logging refers to the logs produced by devices that detect and measure the amplitudes of sound waves in the audible frequency range inside the well. In acoustic logging, a transmitter located inside the well is used to emit some sort of mechanical energy that propagates along the well; this energy is detected, measured, and recorded by one or more acoustic receivers located in the borehole some distance away from the transmitter tool [12].

2.2 Acoustic Communication Systems

2.2.1 Background

An acoustic wave is a type of pressure fluctuations that can exist in a compressible (or longitudinal) medium. A sound wave is a specific type of acoustic waves. The audible spectrum covers frequencies from 20 Hz to 20 kHz for humans, but for marine

mammals and other species the audible spectrum can extend beyond the human hearing range. In addition to sound waves, acoustic waves include ultrasonic and infrasonic waves whose frequencies lie outside the limits of hearing.

Longitudinal waves are waves that have the same direction of vibration along their direction of propagation. This means that the vibration of the medium is in the same direction as the motion of the wave; in other words, the motion of the medium particles goes back and forth along the same direction in which the wave travels [13]. Mechanical longitudinal waves are also called compressional or compression waves. The rate of change of these pressure fluctuations determines the frequency of the wave.

A transverse wave is a moving wave that consists of vibrations occurring perpendicular to the direction of wave propagation. Shear waves can travel through the interior of solid materials. In addition, shear waves create an elastic deformation of the medium in a direction that is perpendicular to propagation; i.e., they are considered transverse waves [13]. Fluids, such as air, gas, or water, cannot sustain a shear deformation; therefore, there will only be compressional waves propagating through air or water. At the water-solid interface, new wave types can be generated through energy conversion, and shear waves and other surface waves can be present.

Sound travels at a speed that is dependent on the propagation medium. For example, sound travels at a speed around 340 m/sec in air, while its speed in water is around 1500 m/sec [14]. The speed of propagation of longitudinal waves in stainless steel is about 5790 m/sec [15]. Speed of propagation is also a function of temperature. For example, for the case of pure water, the speed of sound is around 1402.4 m/sec at 0°C, 1542.5 m/sec at 50°C, and about 1555.1 m/sec at 75°C [15]. The relationship between speed of sound in pure water and temperature can be approximated as [15]

$$C_s = 1402.4 + 5.01\ T_c - 0.055\ {T_c}^2 + 0.00022\ {T_c}^3 \tag{2.1}$$

where C_s is the speed of a sound wave in pure water in m/sec, and T_c is the temperature in Celsius degrees.

A thorough analysis of acoustics is available in [16]. Sound wave equations, sound reflection and transmission, sound radiation and reception, sound absorption and attenuation, and underwater acoustics are some of the topics tackled in this book. Moreover, [17] treats the problem of elastic wave propagation in periodic structures, while [18] studies sound wave propagation in and transmission through sandwich plates. In addition, [19, 20, 21, 22] provide studies of elastic and acoustic waves propagation inside periodic and multi-layer structures. Analysis of acoustic and elastic waves propagation in solids can be found in [23, 24, 25, 26]. Wave propagation in nonlinear fluids and solids is also introduced in [27].

Using acoustic waves to carry information is a promising way to conduct wireless downhole communications. Acoustic waves can propagate from one point to another through vibrating the production tubing. While offering substantial potential benefits, this technology is still in its infancy and is currently not suitable for some large diameter tubings and longer distances. Obviously, there is a need to study the behavior of the acoustic channel for this technology. Understanding the channel nature is essential in order to design a successful communication system.

2.2.2 Literature Survey

There have been many attempts to use and understand acoustic downhole communication systems in the past few years. For example, [28] and [29] provide an early analysis of the problem, predicting that the frequency response of the communication channel will have alternating pass bands and stop bands. Signal transmission is

possible within pass bands. However, because attenuation is very high, propagation is not possible in stop bands.

Drumheller [30] states that the fundamental problem in designing a successful acoustic telemetry system is analyzing the frequency response of the pipe string. The acoustic impedance changes over the pipe string and this produces an unusual scattering pattern in the acoustic transmission, which causes distortion of the acoustic waves. It is mentioned that the original attempts to develop an acoustic telemetry system failed because of the use of a narrow-pulse transmission scheme. This transmission method will spread the limited energy over a broad band of frequencies, echoes will disperse the waves and attenuate the energy, and finally the pipe string will block large bands of acoustic energy.

Pipe strings are assembled from 30 to 45 foot sections of pipe, which are connected through joints. The cross sectional area of the pipe joints is significantly greater than that of the pipe. For a compression wave propagating over pipes, the channel acoustic impedance is the product of the pipe mass density, wave bar velocity, and pipe cross sectional area [31]. This will result in the pipe joint having a higher acoustic impedance than the rest of the pipe body. As expected, any spatial variations in the acoustic impedance along the pipe string will result in partial reflections and/or transmissions of the acoustic energy. Eventually, the pipe joints will cause multiple reflections to the acoustic wave, but since the joints occur at periodic intervals along the pipe string, signal transmission is still possible within pass bands [31]. When pipe segments are not exactly of the same length, the width and center of the pass bands are found to change [32].

Computation of linear, one-dimensional, extensional stress waves in an elastic waveguide using a time-domain approach is considered in [33]. The time-domain algorithm includes a combination of finite-difference and characteristics methods.

Attenuation of sound waves inside drill strings is studied in [34]. It was reported that mode conversion between extensional and bending waves and reflections due to deviations in periodic spacing between tool joins (due to the pipe segments not having the same length) are believed to be a major factor contributing to wave attenuation in the pipe string.

Interaction between extensional and bending waves in elastic waveguides is studied in [35]. Different linear elastic waves can propagate inside long rods. Waves do not interact in straight rods, but if curved rods are used as waveguides, wave energy is exchanged between extensional and bending waves [35]. In addition to viscous dissipation, mode conversion from extensional waves to bending waves was suggested to account for signal decay.

Wave impedance of a pipe string is studied in [36]. It was found that for a pipe string the wave impedance is in general a complex number, but at discrete physical locations the wave impedance reduces to a real number. In these locations, acoustic repeaters can be located, provided the repeater has a matching acoustic impedance, without causing any reflections to the acoustic wave.

Attempts to model acoustic signals propagating over pipes in the time domain can be found in [37], where the propagation of sound energy pulses through the pipe string and the effect of multiple reflections and/or transmissions during this propagation are described using a Markov chain. A time-domain algorithm is developed for the propagation of one-dimensional waves including transducer sources and sensors in [38]. Moreover, [39, 40] study acoustic transmission through fluid-filled pipes in boreholes. In addition, a multi-layered waveguide is suggested in [41] to understand how sound waves propagate axially in drilling boreholes.

The propagation of plane sound waves in gases contained in cylindrical tubes of a large range of diameters is considered in [42]. Experimental results are presented in

[43] to show a mode selective transfer of energy from sound waves propagating inside a circular pipe to pipe wall vibration. An experimental study of sound waves propagation in liquids contained by pipes constructed of polymeric materials is discussed in [44]. Moreover, [45] investigates the noise sound propagation in a tunnel with emphasis on the behavior of sound waves near the tunnel outlet. In addition, [46] investigates the problem of acoustical wave propagation in cylindrically layered media, and specifically the case of water-filled underground pipes is considered. Sound propagation without airflow through circular ducts with a spiral element inside is examined in [47].

Analogies between electromagnetic and acoustic systems are found in [48, 49, 50] where understanding of the propagation and absorbtion of electromagnetic fields is used to approach the acoustic waves propagation and attenuation problem. A review of electrical and electromagnetic borehole measurement methods is presented in [51]. In addition, [52] presents a coreless electromagnetic coupling-based telemetry system using dual electronic gauges.

Underwater acoustic telemetry systems use acoustic waves for communication underwater [53, 54, 55]. An overview of such acoustic systems is given in [56], and a review of the underwater channel and the limitations it imposes upon acoustic telemetry systems is provided. Some the civilian systems that have been built are also discussed. An introduction to underwater acoustics systems and their applications is provided in [57]. High data rate transmission requires a wide bandwidth which is severely constrained in the ocean because of the absorption of high-frequency energy. Accordingly, spread spectrum communication methods are suggested to conduct underwater acoustic systems in [58]. The advantages of using spread spectrum include the ability to provide low probability of intercept in hostile environments, enable multiple access capability in systems shared by many users, and achieve processing

gain in channels where the transmitted signal is distorted by multipath propagation. A design and implementation of an all-digital transceiver for real-time underwater acoustic communications using digital signal processors is presented in [59]. The design of the transceiver was based on using a direct-sequence spread spectrum method, an equal-gain combiner, and an adaptive decision-feedback equalizer to enhance the interference rejection capability under multipath fading environments.

2.3 Acoustic Downhole Communication Systems

The work of [60] describes the development, design of a prototype, and the testing that was performed to confirm the acoustic communication behavior in the annulus of a production well. Well tests were performed to determine the acoustic signal attenuation, effect of fluid viscosity, effect of head pressure, acoustic noise levels, and their effect on the baud rate. A measurement-while-drilling system using acoustic telemetry system is proposed in [61]; the design was based on the principle of elastic wave propagation and magnetostrictive technology. The system was intended to achieve data transmission through jointed drill strings with higher reliability and transmission efficiency.

A successful wireless acoustic telemetry system for surface read-out of downhole data is described in [62, 63]. A real time half duplex communications wireless gauge that is used to monitor deep well gas production is described in [64]; this system used acoustic waves to carry communication between the downhole and surface. In addition, [65] describes an acoustic downhole communication system; the design used a high power acoustic transmitter driven by a signal processor that maximizes input energy in certain frequency bands in order to minimize the dispersion and distortion effects.

Due to severe attenuation for acoustic signals in very long drill strings, surface

noise becomes dominant over the actual signal. Accordingly, [66, 67, 68] discuss a signal processing algorithm that uses two acoustic receivers in order to suppress the surface noise. The channel capacity was reported to improve over the single receiver case. Channel capacity and the use of the water filling method are explored for a pipe string channel model in [69, 70, 71]. Results indicated that for a bit error rate comparable to that in the current mud-pulse telemetry systems, the acoustic telemetry system is capable of transmission at higher data rates.

A wireless acoustic telemetry system for sending real-time downhole pressure and temperature data to well surface is investigated in [72, 73]. The application of the acoustic telemetry system was found to enhance safety and operations flexibility. Maximizing fidelity of real time logging data transmitted via digital telemetry systems is discussed in [74]; the proposed design criterion was to minimize the end-to-end distortion instead of minimizing the average bit error rate. In addition, [75] discusses designing a downhole communication system using multi-carrier modulation techniques. A transfer matrix method is used in [76] to study the acoustic property of drill strings. A waveform design of an acoustic signal is proposed to be used in data transmission using drill strings in logging-while-drilling systems in [77]. The design involved specifying the baseband signal, carrier frequency, and bandwidth consideration.

Field test results of some proposed acoustic measurement-while-drilling telemetry systems are described in [78, 79]. Some of the reported findings in the test telemetry systems are that significant variations in signal-to-noise ratio were observed. Type of pipes, type of formation, and density of fluid inside the string are some factors reported to affect signal attenuation. In addition, results indicate that as the data rate and/or transmission depth increases, the percentage of data recovery at the receiver was found to decrease. Normal drilling operations were also found to produce

in-band acoustic noise at intensities comparable to that of the acoustic transducer output [66].

Technological advances in real-time well testing and operations are discussed in [80]. Moreover, [81] introduces a complete real-time communication system that has been adapted to well testing operations in the oil and gas industry to improve the efficiency, safety, and decision-making processes. The work of [82] discusses a wireless communication solution for real time reservoir surveillance that will be used to acquire well critical data; this solution was proposed to help operators to effectively manage and optimize well production. Real time transmission of high resolution downhole images using telemetry systems along with image compression techniques is discussed in [83].

Some differences between logging-while-drilling and wireline-conveyed logging tools and methods are discussed in [84]. Finally, a review of some seismic-while-drilling techniques used by the industry is presented in [85]; some strategies for data acquisition and sensor deployment are also detailed.

3. Testbed Design and Signal Analysis

The testbed that was designed to investigate the propagation aspects of acoustic signals for downhole telemetry systems is described in this chapter. The testbed main blocks are summarized in Section 3.1. A detailed description of the transmitter unit, production pipes, and receiver unit is provided in Sections 3.2, 3.3, and 3.4, respectively. Setup limitations are discussed in Section 3.5. Signal analysis measures used in this dissertation are presented in Section 3.6; these measures include the power spectral density, signal-to-noise ratio, signal decay rate, power delay profile, mean excess delay, root mean square excess delay spread, maximum excess delay (X dB), and coherence bandwidth.

3.1 Testbed Design

To study the usefulness of using acoustic waves in conducting wireless downhole communication systems, a testbed was designed to examine the propagation of acoustic waves over cemented production pipes. The testbed comprises three main components: an acoustic transmitter tool, a pipe string as the communication medium for the acoustic waves, and an acoustic receiver unit.

The acoustic transmitter main component is a piezoelectric transducer. This wireless tool transmits data from inside the wellbore to the surface without cables; consequently, it does not block the fluid flow inside the well tubing. The transmitter output is a compression acoustic signal in the form of a burst that propagates by vibrating the pipe string. The input to the acoustic transmitter in this testbed is a voltage signal provided by a function generator. The function generator creates a pulsed sinusoid signal on a given input frequency; this signal is fed to the acoustic transmitter, and the transmitter tool generates the acoustic wave accordingly. Fre-

quency ranges from 100 Hz to 2000 Hz were used to generate the input signals; lower or higher frequencies were not tested due to limitations on the transmitter tool.

The acoustic receiver was internally-developed; it consists of a 50G piezoelectric accelerometer, a clamp to attach this sensor to the pipe string, an interface circuitry to power the sensor, an anti-aliasing low-pass filter, a data acquisition card, and a computer that runs software that was internally developed. The piezoelectric accelerometer measures the vibrations produced by the transmitter over the pipe string. The accelerometer, along with the interface circuit, works as an acoustic sensor that converts the acoustic vibrations into a voltage signal. The data acquisition card connects the sensor output with the computer, and it samples the measurements at a rate of around 47 kHz. The computer is used to capture, display, and analyze the measured signals.

In order to simulate a communication medium, two pipe strings were assembled. At first, eight segments of 2-7/8" pipes were connected to form the pipe string for the 2-7/8" experiment described in Chapter 4. Next, five segments of 7 inch production tubing were assembled to form a long pipe string for the 7" experiment described in Chapter 5. Extensive propagation experiments were conducted on this testbed in order to find the acoustic channel response as a function of distance and frequency. Signal measurements were taken at the beginning, middle, and end of each pipe segment. In each measurement, five pulses were recorded for each input frequency. Acoustic signals with different input frequencies were transmitted over the pipe and data were measured over the pipe segments using the acoustic receiver.

It is interesting to see how other external factors can affect acoustic wave propagation; the effect of encasing the exterior of a pipe segment in concrete is one interesting thing to investigate in this testbed. It was expected that this concrete would have a significant impact on the propagation of acoustic waves through the tubing. In

order to investigate this effect for the 7" pipe string, the exterior of the first half of the third pipe segment (around 20 feet) was encased in a doughnut-shaped concrete segment of 3/4 inch thickness. The propagation measurements were repeated for this setup. Next, the later part of the third pipe was encased in concrete. The concrete segment was around 20 feet of length and 3/4 inch of thickness. The aforementioned propagation measurements were repeated on this setup.

3.2 Transmitter Unit

The transmitter unit is composed of the function generator and the acoustic wireless tool. Figure 3.1 shows a picture of the transmitter tool.

Figure 3.1: Photograph of the transmitter tool

3.2.1 Function Generator

The input to the acoustic transmitter in this testbed is a voltage signal provided by a function generator. The function generator creates a periodic burst signal that has a duration around 44 ms on a given input frequency. This signal is fed to the

acoustic transmitter and the transmitter tool generates the acoustic waves according to the input frequency. Frequencies ranging from 100 Hz to 2000 Hz were used to generate the signal bursts. The actual duration for each input frequency is shown in Table 3.1.

Table 3.1: Function generator's actual burst duration per input frequency

Frequency (Hz)	100	200	300	400	500
Number of Cycles Per Burst	4	9	13	18	22
Actual Burst Duration (ms)	40	45	43.333	45	44
Frequency (Hz)	600	700	800	900	1000
Number of Cycles Per Burst	26	31	35	40	44
Actual Burst Duration (ms)	43.333	44.286	43.75	44.444	44
Frequency (Hz)	1100	1200	1300	1400	1500
Number of Cycles Per Burst	48	53	57	62	66
Actual Burst Duration (ms)	43.636	44.167	43.846	44.286	44
Frequency (Hz)	1600	1700	1800	1900	2000
Number of Cycles Per Burst	70	75	79	84	88
Actual Burst Duration (ms)	43.75	44.118	43.889	44.211	44

3.2.2 Acoustic Tool

The acoustic transmitter was provided by Ziebel Inc.; its main component is a piezoelectric transducer, and it is controlled via computer through a serial port using HyperTerminal. This tool is battery operated; its length is 7.5 feet and diameter is 2-7/8 inches. This wireless tool transmits data from inside the wellbore to the surface without cables, and so it does not block the fluid flow inside the well tubing. The trigger input to the transmitter is either a voltage signal provided by a function generator or a predetermined command from a computer. The end of the transmitter tool connects directly through the production tubing string with an 8-Round EUE R2 connection. The transmitter output is a compression acoustic signal in the form of a burst that propagates over the pipe string.

3.3 Pipe String

The pipe string is the most important part in the testbed as it resembles the communication medium in which the acoustic waves propagate. Two pipe strings were investigated in this work: 2-7/8" pipe sting and 7" pipe string. A picture of the pipe string is shown in Figure 3.2.

Figure 3.2: Photograph of the pipe string

3.3.1 2-7/8" Pipes

In order to simulate a communication medium, eight segments of 2-7/8 inch production tubing were assembled to form the pipe string. Each pipe segment is around 30 feet long, so the overall length of the pipe string is around 240 feet. Moreover, in order to minimize the interface between the pipes and earth, the pipe segments were positioned over concrete blocks. The wireless tool connects directly to the pipe string in this case.

3.3.2 7" Pipes

The communication medium was made of five assembled segments of 7 inch production tubing that form the pipe string. Each pipe segment is around 40 feet long, so the overall length of the pipe string is around 200 feet. In addition, to minimize the interface between the pipes and earth, the pipe segments were positioned over wooden blocks. The wireless tool, with a diameter of 2-7/8 inch, connects to the pipe string, which has a 7 inch diameter, through a swedge.

3.4 Receiver Unit

The acoustic receiver was internally-developed; it consists of the following components:

1. 50G piezoelectric accelerometer
2. Interface circuitry
3. Anti-aliasing low-pass filter
4. Data acquisition card
5. Computer software and hardware

A picture of the receiver unit when connected to the pipe string is shown in Figure 3.3.

3.4.1 Accelerometer

The accelerometer used in the receiver unit is a 50G accelerometer provided by ENDEVCO with a model of 752A12. The symbol "G" is used to denote the average acceleration produced by gravity at the Earth's surface around sea level, and so "G" is often used as a unit of acceleration. The acoustic sensor is a piezoelectric

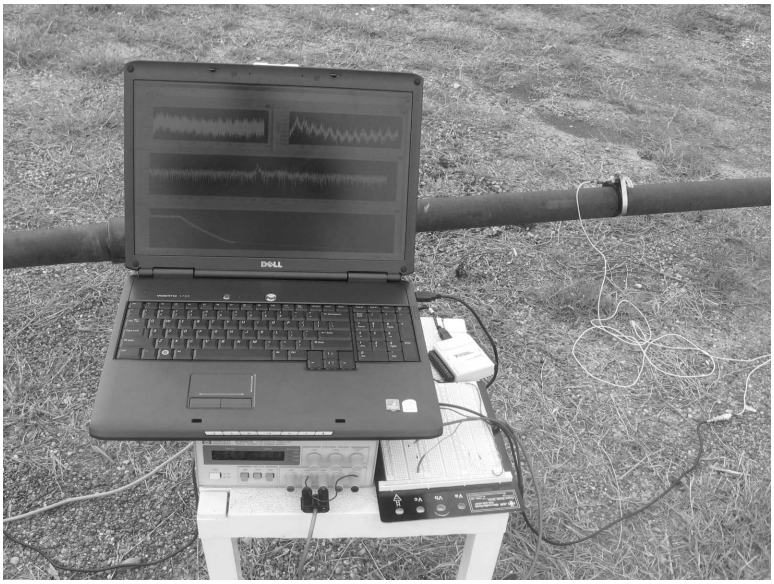

Figure 3.3: Photograph of the receiver unit

accelerometer with integral electronics; it supports an acceleration range of -50 to 50G and a frequency range of 1 to 10 kHz. The device voltage sensitivity is 100 mV/G at 100 Hz. In addition, a clamp was used to attach the accelerometer to the pipe string at the required location.

3.4.2 Interface Circuit

The goal of the interface, also referred to as the conditioning, circuit is to provide a constant current to power the accelerometer. The circuit is comprised of a +18 to +24 V DC power supply or battery that powers this setup, an optional diode that can have a model of 1N456A or 1N4148, a 4.7 mA constant current diode that can have a model of 1N5314, and a blocking capacitor that can have a value of 0.1 μF. The input signal originating from the accelerometer is inserted into this circuit at the point where the capacitor and the current limiting diode meet. The output signal is taken from the other end of the blocking capacitor. The circuit is shown in Figure 3.4.

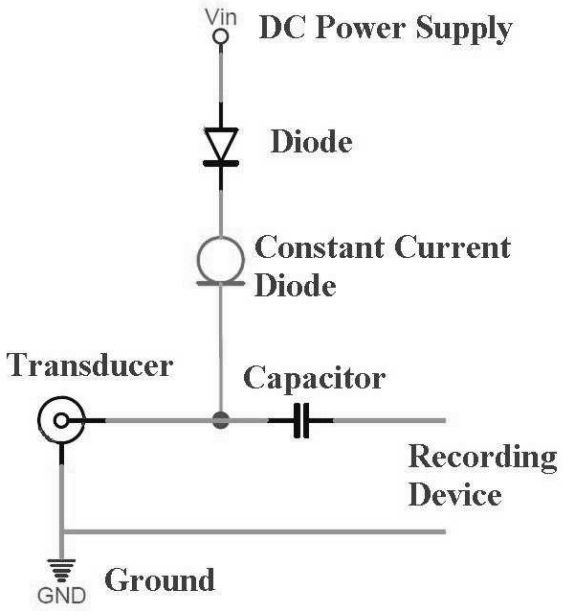

Figure 3.4: Conditioning circuit used to power the accelerometer

3.4.3 Anti-Aliasing Filter

The anti-aliasing filter is a low-pass filter that is used between the conditioning circuit and the sampling circuit. Its goal is to restrict the bandwidth of the analog measurement in order to satisfy the Nyquist sampling limit and so prevent signal aliasing in the sampled signals. The designed filter is an active 8th-order low-pass elliptic filter. This active device is an MAX7400 filter provided by Maxim Integrated Products. The cutoff frequency of the filter was selected, using external capacitors, to be around 20.1 kHz.

3.4.4 Data Acquisition Card

The data acquisition card (DAQ) works as an analog-to-digital convertor; it samples and digitizes the signal coming from the anti-aliasing filter and passes those samples to the computer. The used DAQ is an NI USB-6009 card provided by

National Instruments. This card has a maximum sampling frequency of 48,000 sample/sec and it uses 14 bits to digitize the samples. The card connects to the computer through the USB port. A sampling frequency of around 47 kHz was used to sample the measurements for the propagation experiments.

3.4.5 Computer Software and Hardware

A LabView software was develop in order to capture, display, save, and analyze the measured signals. A snapshot of the software program is shown in Figure 3.5. A Dell laptop was used to host the software and connect with the DAQ through the USB port. This computer has a VOSTRO 1700 model with Windows Vista; it has 2 GB of RAM memory and its processor is an Intel Core 2 Duo CPU that runs at 1.6 GHz.

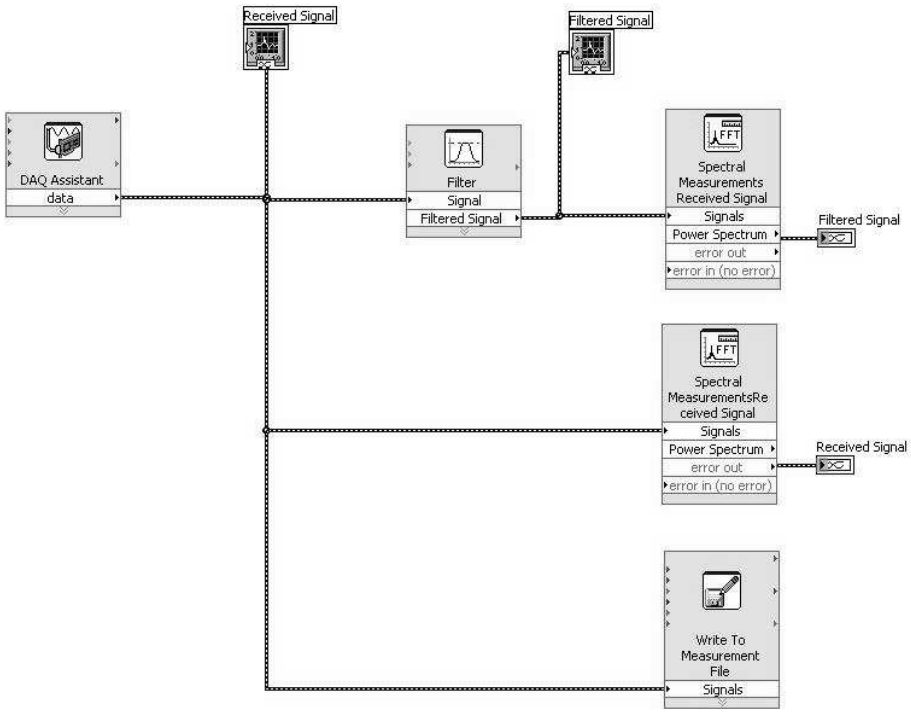

Figure 3.5: Snapshot of LabView software

3.5 Setup Limitations

While working on the testbed, some challenges were faced. The limitations of the experimental setup include:

- Piezoelectric accelerometer: the sensor is very sensitive to the way it is attached to the pipe string. Different ways of attaching the accelerometer might generate different readings for the same acoustic signal. This issue was handled by taking multiple reading at the same point and averaging the results.

- Sampling frequency: the maximum sampling frequency of the data acquisition card is relatively low. An anti-aliasing low-pass filter was added to prevent aliasing. As a drawback of this, the signal energy that lies beyond the filter cutoff frequency was not captured.

- Acoustic transmitter: the tool connects to the pipe string through a swedge, and this might contribute to the channel multiple reflections. In addition, the tool does not efficiently generate signals with frequencies lower than 100 Hz or higher than 2000 Hz.

- Pipe string: the pipe string has a length of around 200 feet for the 7" setup and about 240 feet for the 2-7/8" setup. The measurements from a longer string are believed to provide a more accurate decay analysis.

- Acoustical noise: the current setup does not provide a noise signal similar to that in an actual oil or gas well.

3.6 Signal Analysis

After measurements were captured from the testbed, several signal analysis methods were usually conducted in order to get a better understanding of the measure-

ments and the acoustic channel. Other than inspecting the signal level variations and their decay rate, it is also worth looking to examine the frequency content of the measured signals and study the variation over the pipe string. A delay spread measure is a different way to investigate a measurement as it is an indication of the dispersion and the mulipath richness of the acoustic channel.

3.6.1 Power Spectral Density

The power spectral density (PSD) is a measure that describes how the power of the signal is distributed with frequency. The unit of PSD is power per Hz. The signal power within a specific frequency range can be obtained by integrating the PSD within that frequency range. Computation of the PSD of a measurement can be accomplished by taking the Fourier transform of the autocorrelation function of that signal [86].

3.6.2 Signal-to-Noise Ratio

One of the most important measures of signal quality is the Signal-to-Noise Ratio (SNR) value. SNR value is calculated in a measurement by defining a message portion and noise portion. The message portion is the measurement segment which contains the actual transmitted burst, and it will contain also an unavoidable measured noise signal in that time window. The duration of the message portion is longer than that of the transmitted burst in order to account for the channel dispersion. The noise portion, on the other hand, is the measurement segment where there is no actual data but a pure noise signal only. The power of the message portion, P_m, includes the signal power and the noise power, while the power of the noise portion, P_n, includes only the noise power. The SNR value is defined as the ratio of the signal power to the noise power. Dividing P_m by P_n yields SNR + 1; accordingly, the SNR value in a measurement is calculated as $\frac{P_m}{P_n} - 1$.

3.6.3 Decay Rate

The SNR decay rate of a series of measurements is found by formulating the signal's SNR value as a function of the measurement distance in a linear manner; linear least squares methods can be used to find this relationship. Least square estimation minimizes the sum of squared distances between the observed SNR in the measurements and the SNR value predicted by the linear approximation. More details about least square estimation can be found in [87, 88].

3.6.4 Power Delay Profile

The power delay profile (PDP) of a measurement is an indication about the intensity of the signal received through the channel as a function of time delay. Assuming the received signal is called $\boldsymbol{y}$, then the PDP of $\boldsymbol{y}$ can be found as $10\log_{10}\boldsymbol{y}^2$. On the other hand, the normalized PDP of $\boldsymbol{y}$ is defined as $10\log_{10}(\frac{\boldsymbol{y}}{\max|\boldsymbol{y}|})^2$.

3.6.5 Mean Excess Delay

The mean excess delay, $\overline{\tau}$, of $\boldsymbol{y}$ is the first moment of the power delay profile and can be found as [89]

$$\overline{\tau} = \frac{\sum_k y_k^2\ \tau_k}{\sum_k y_k^2} \tag{3.1}$$

where τ_k is the time index and y_k is the value of $\boldsymbol{y}$ at time τ_k.

3.6.6 Root Mean Square (RMS) Excess Delay Spread

The RMS delay spread, σ_τ, is the square root of the second central moment of the power delay profile of the measurement, and it can be found as [89]

$$\sigma_\tau = \sqrt{\overline{\tau^2} - (\overline{\tau})^2} \tag{3.2}$$

where

$$\overline{\tau^2} = \frac{\sum_k y_k^2 \, \tau_k^2}{\sum_k y_k^2} \tag{3.3}$$

3.6.7 Maximum Excess Delay (X dB)

The maximum excess delay (X dB) is defined as $\tau_X - \tau_0$, where τ_0 is the time of the first arriving multipath and τ_X is the maximum time delay at which a signal multipath is within X dB of the strongest multipath signal [89]. This measure defines the extent of the multipath energy that is above a particular threshold (X dB).

3.6.8 Coherence Bandwidth

Coherence bandwidth, B_c, of a channel is a measure of the range of frequencies over which the channel frequency response can be considered relatively fixed; i.e., the channel passes all the frequencies in that range with approximately equal gain and linear phase. This measure defines the range of frequencies over which frequency components have a strong correlation.

Although they are inversely proportional, the exact relationship between the coherence bandwidth and the RMS delay spread of a channel is not exactly known. As a rough estimate, if B_c is defined as the bandwidth over which the frequency components have a correlation above 0.5, then B_c can be approximated as [89]

$$B_c \approx \frac{1}{5 \, \sigma_\tau} \tag{3.4}$$

4. 2-7/8" Pipe String

The 2-7/8" pipe string experiment is detailed in this chapter. The designed testbed is described in Section 4.1, and some of the propagation results are displayed. In Section 4.2, the propagation results after installing the first concrete segment on the pipe string are shown. Finally, the propagation results are shown in Section 4.3 for the case when another concrete segment was installed on the pipe string.

4.1 Testbed Setup

Eight segments of 2-7/8 inch production tubing were assembled to form the pipe string for this experiment. Figure 4.1 depicts a photograph of the actual pipe string.

Figure 4.1: Photograph of the 2-7/8" pipe string - no concrete case

The function generator was used to generate the input signal on a specific frequency; this signal was used to trigger the acoustic tool. Consequently, the acoustic tool would generate an acoustic wave that propagates through the 2-7/8" pipe

string. The acoustic receiver was used to measure the propagating acoustic wave. Signal measurements were taken at different points along the pipe sting. In each measurement, five bursts were recorded for each input frequency. Figure 4.2 displays a schematic for the described testbed.

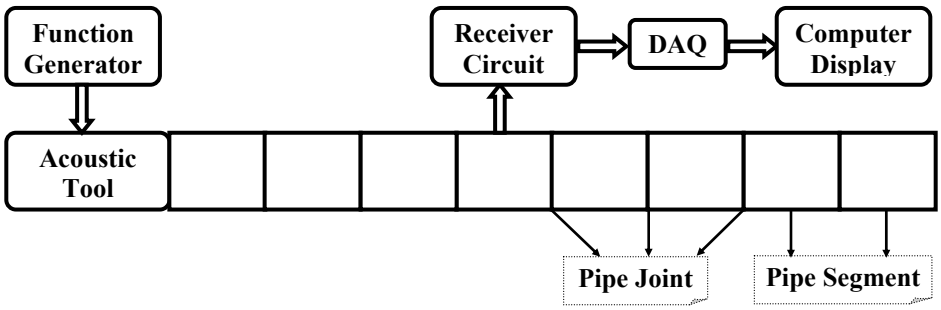

Figure 4.2: Testbed for the 2-7/8" pipe string - no concrete case

4.1.1 Measurement Results

The results of the propagation measurements are explained in this subsection.

4.1.1.1 Power Spectral Density

Figure 4.3 shows the power spectral density of the 500 Hz signal measured at different locations along the 2-7/8" pipe string. It is noted that the measurement recorded at the beginning of the pipe string contains many of the 500 Hz harmonics. But as the wave propagates down the pipe string, different harmonics seem to decay in different rates.

Figure 4.4 shows the power spectral density of the 1000 Hz signal. It can be seen here that the measurement taken near the transmitter contains all the harmonics up to 20 kHz. It is also noted that the fundamental harmonic almost disappeared from the measurements taken away from the transmitter.

Figure 4.5 shows the power spectral density of the 1500 Hz signal. In this case,

it is seen that the low-frequency harmonics preserve more of their energy compared to the higher harmonics.

Finally, Figure 4.6 shows the power spectral density of the 2000 Hz signal. Conclusions similar to those made for the 500 Hz, 1000 Hz, and 1500 Hz signals are found for this case as well.

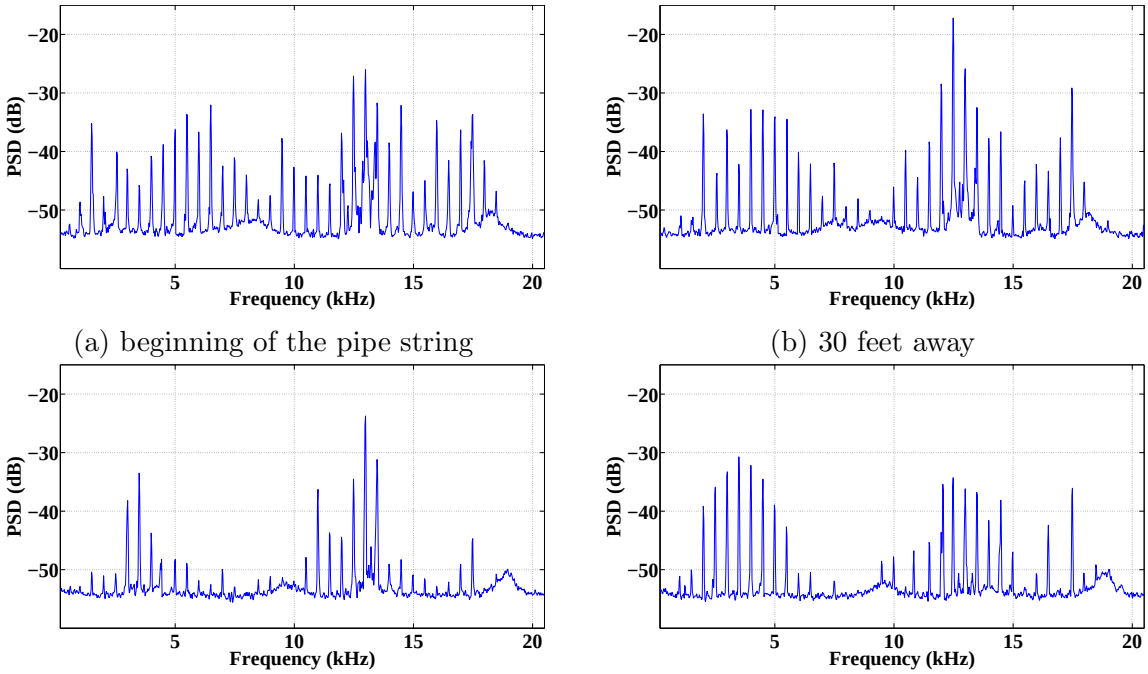

(a) beginning of the pipe string

(b) 30 feet away

(c) 90 feet away

(d) 220 feet away

Figure 4.3: Power spectral density of the 500 Hz signal measured over the 2-7/8" pipe string - no concrete case

The results in the previous four figures indicate that different harmonics decay in different rates. Harmonics up to 20 kHz can be found in the measurements recorded close to the transmitter unit. It can be said that, in general, as the acoustic signal propagates down the pipe string, the high-order harmonics decay faster than the lower-order harmonics. Consequently, it is expected to see most of the signal energy concentrated in the lower frequency range for a longer pipe string.

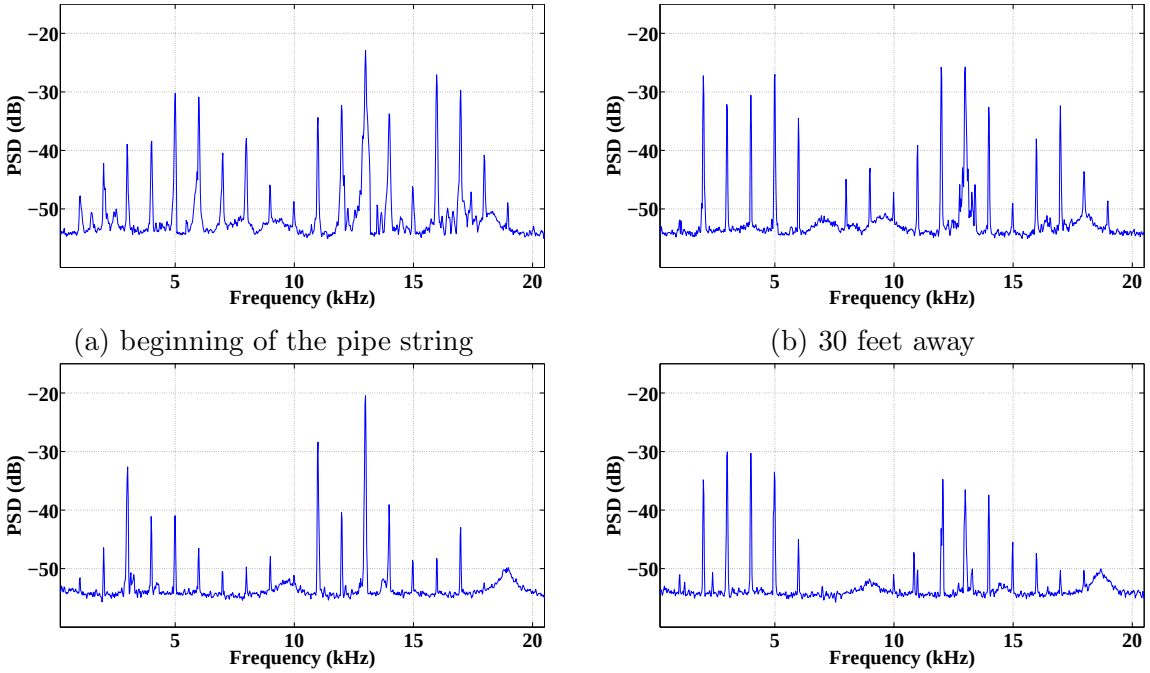

(a) beginning of the pipe string

(b) 30 feet away

(c) 90 feet away

(d) 220 feet away

Figure 4.4: Power spectral density of the 1000 Hz signal measured over the 2-7/8" pipe string - no concrete case

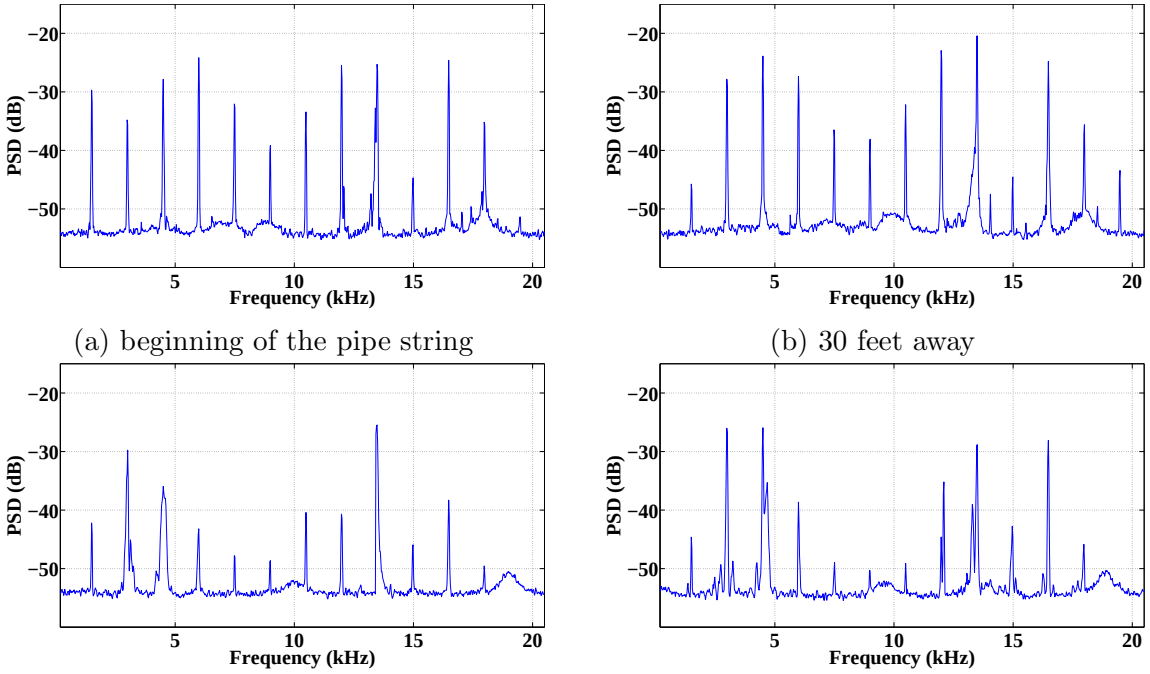

(a) beginning of the pipe string

(b) 30 feet away

(c) 90 feet away

(d) 220 feet away

Figure 4.5: Power spectral density of the 1500 Hz signal measured over the 2-7/8" pipe string - no concrete case

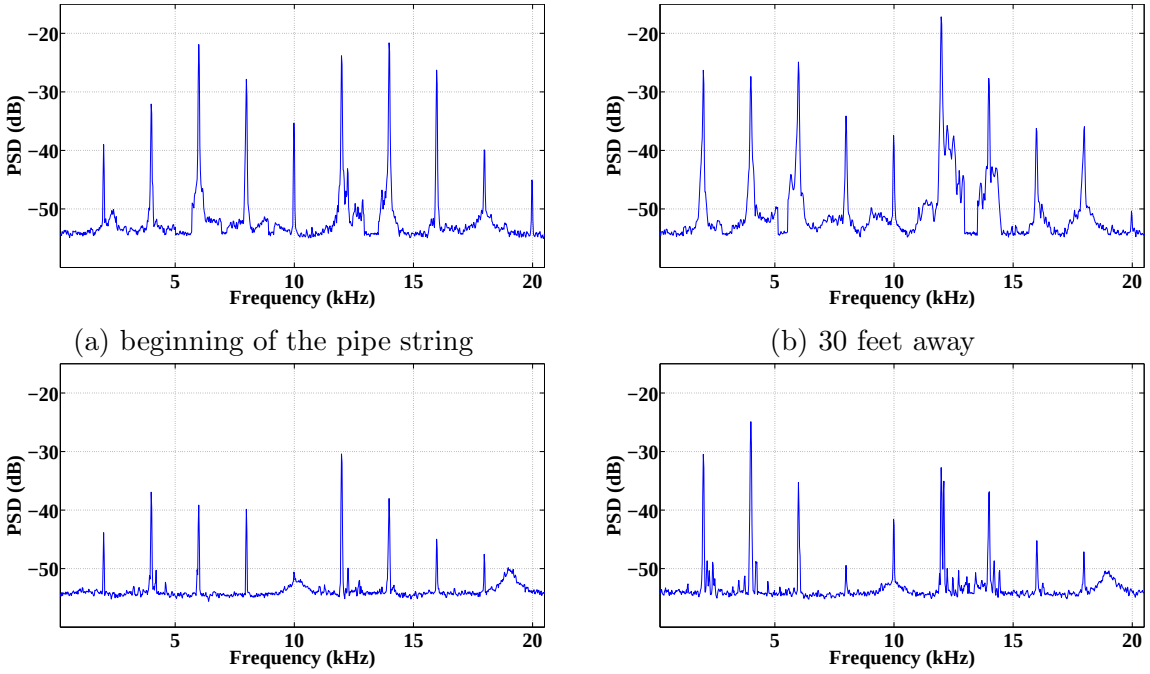

(a) beginning of the pipe string

(b) 30 feet away

(c) 90 feet away

(d) 220 feet away

Figure 4.6: Power spectral density of the 2000 Hz signal measured over the 2-7/8" pipe string - no concrete case

4.1.1.2 Signal-to-Noise Ratio

The signal-to-noise ratio results of the measurements are now discussed. Figure 4.7 displays the SNR results for the 20 tested input frequencies. A general decline in SNR values with increasing the propagation distance is observed for the different acoustic waves. From the result of this figure, it can be speculated that some of the frequencies have a less dramatic decline in their SNR values compared to others. For example, it can be seen that the 1000 Hz and 2000 Hz signals decline in a lower pace compared to the other frequencies.

4.1.1.3 Signal Decay Rate

In order to picture the situation with a longer pipe string, the SNR rate of decay is investigated. This measure helps in deciding what frequencies to use and where to put repeaters, if needed, along the pipe string.

Figure 4.8 displays the SNR decays rate, in dB per 1000 feet, for the different input frequencies. The same results are shown, in tabulated form, in Table 4.1. In this case, it is seen that the least decay rate appears for the 1000 Hz signal which has a decay rate around 27.6 dB per 1000 feet. On the other hand, the 1800 Hz signal has the highest decay rate in this experiment.

Table 4.1: Channel decay rate for the 2-7/8" pipe string

Frequency (Hz)	100	200	300	400	500
Decay Rate (dB/1000 feet)	44.8	32.9	42.6	34.7	36.1
Frequency (Hz)	600	700	800	900	1000
Decay Rate (dB/1000 feet)	41.3	57.7	31.5	48.4	27.6
Frequency (Hz)	1100	1200	1300	1400	1500
Decay Rate (dB/1000 feet)	51.9	55.3	44.7	56.7	41.0
Frequency (Hz)	1600	1700	1800	1900	2000
Decay Rate (dB/1000 feet)	50.1	40.5	63.6	54.3	33.6

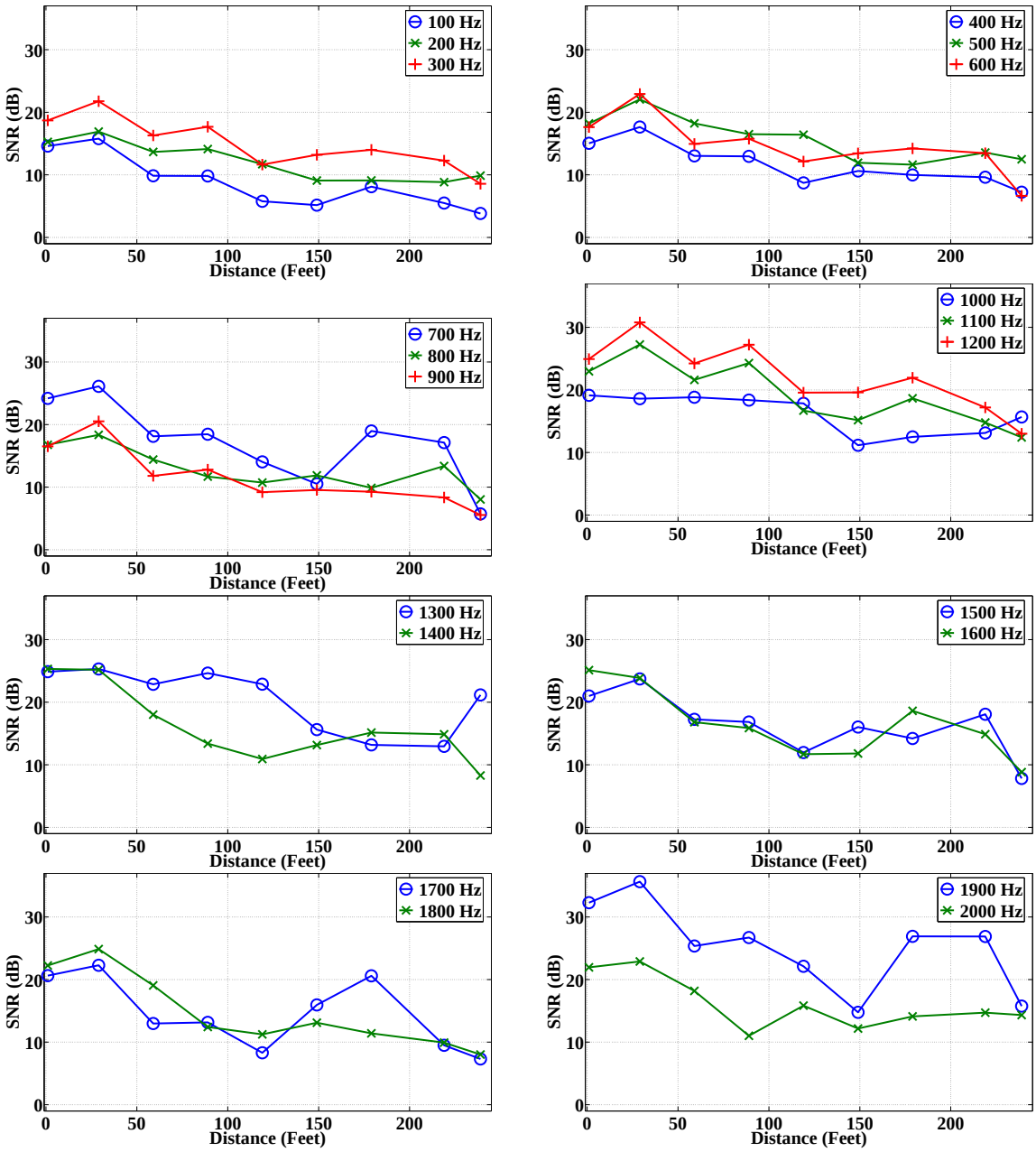

Figure 4.7: Signal-to-noise ratio vs. distance for the 2-7/8" pipe string - no concrete case

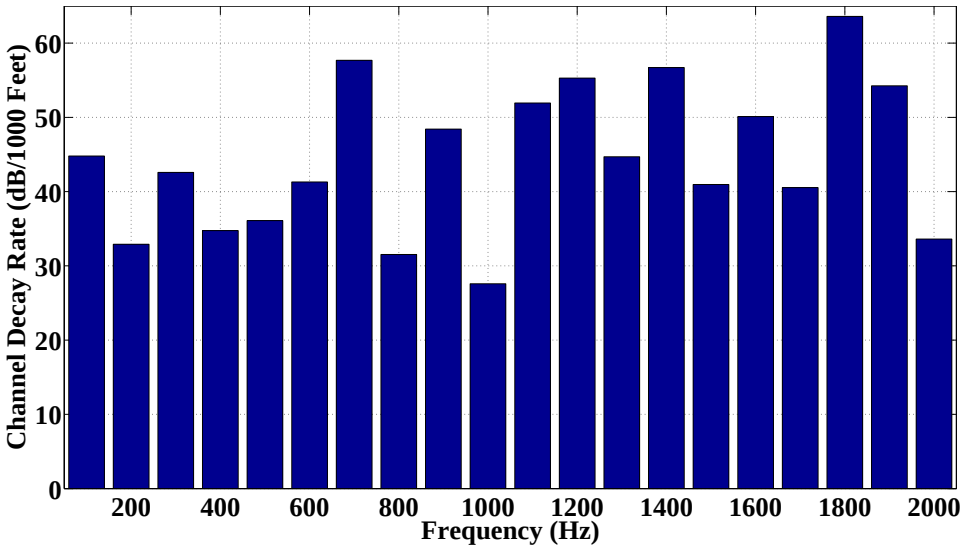

Figure 4.8: Signal decay rate (dB/1000 feet) for the 2-7/8" pipe string - no concrete case

4.2 First Concrete Segment Experiment

In order to study the effect of concrete on acoustic wave propagation, the exterior of the second pipe segment (with a length around 30 feet) was encased in a doughnut-shaped concrete segment of 1.5 inch thickness. The same propagation measurements were repeated for this setup. Figures 4.9 and 4.10 show photographs of the concrete segment structure before and after pouring the concrete. The propagation experiments are similar to those of the no-concrete case. Figure 4.11 displays a schematic for the testbed after encasing the second pipe segment in concrete.

4.2.1 Measurement Results

In order to appreciate the effect of concrete on the propagation of acoustic waves, the propagation results are shown in this subsection.

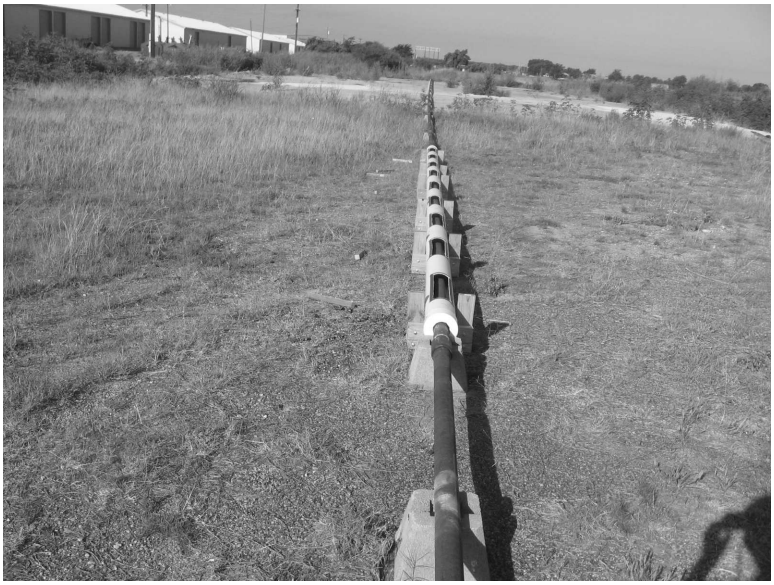

Figure 4.9: Photograph of the setup of the first concrete segment on the 2-7/8" pipe string

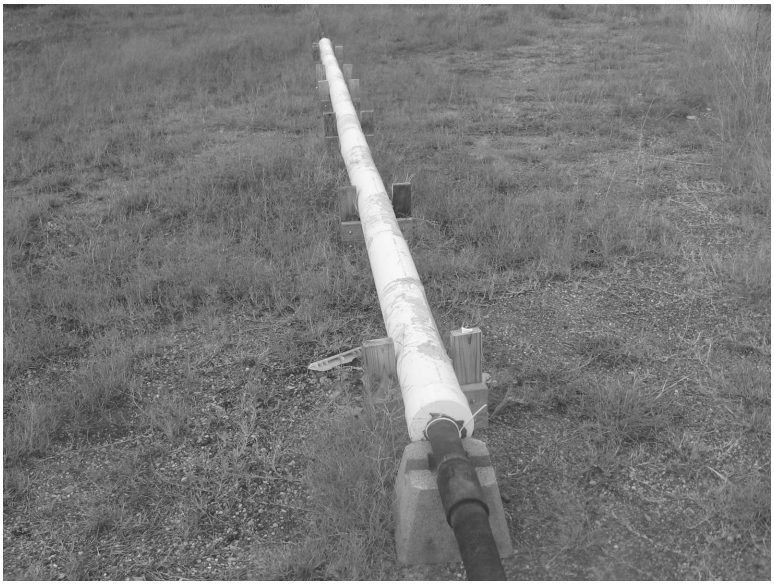

Figure 4.10: Photograph of the concrete segment on the 2-7/8" pipe string

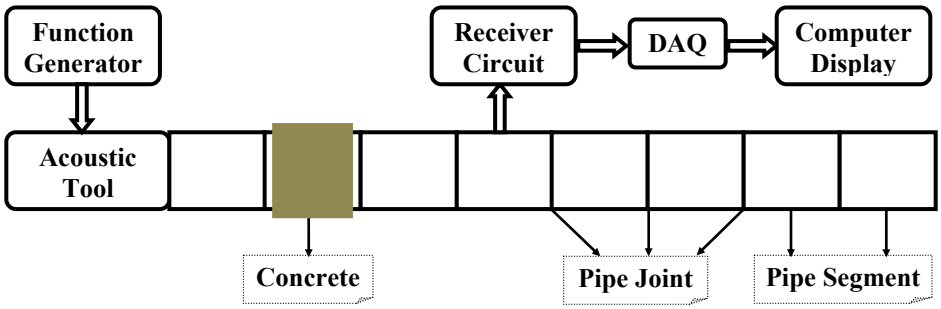

Figure 4.11: Testbed for the 2-7/8" pipe string - one concrete segment case

4.2.1.1 Power Spectral Density

Figure 4.12 shows the power spectral density of the 500 Hz signal measured at different locations along the 2-7/8" pipe string. It is noted that the measurement made at the beginning of the pipe string contains all of the 500 Hz harmonics up to 20 kHz. But as the signal propagates beyond the concrete segment, it can be seen that many of the harmonics died off. It is noted that for measurements taken beyond the concrete segment, most of the signal energy is concentrated in the lower-frequency harmonics.

Figure 4.13 shows the power spectral density of the 1000 Hz signal. A similar behavior to that in the 500 Hz case is seen for this frequency. In addition, Figures 4.14 and 4.15 display the PSD results for the 1500 Hz and 2000 Hz signals.

From these results, it is noted that different harmonics decay in a different manner. Harmonics up to 20 kHz can be found in measurements taken close to the transmitter unit. In addition, the concrete segment is filtering off many of the signal harmonics, especially the higher-frequency harmonics. Consequently, if a longer concrete segment is available, it is expected to see more filtration of the signal harmonics. It is also noted that the concrete effect depends on the input frequency of the acoustic signal.

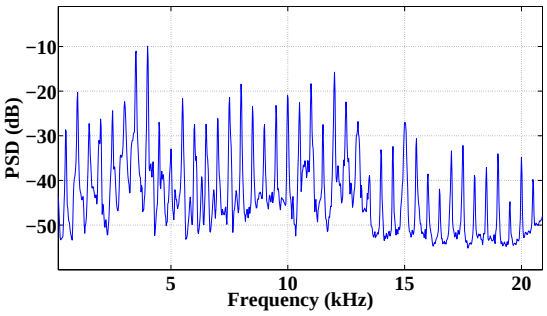

(a) beginning of the pipe string

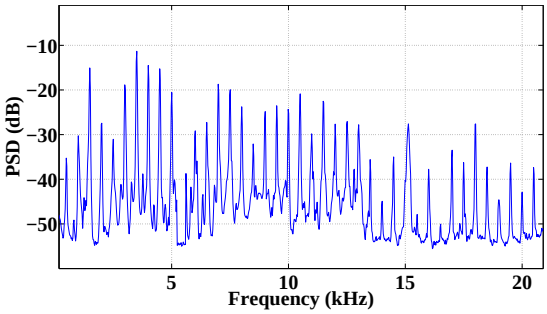

(b) 30 feet away (just before the concrete segment)

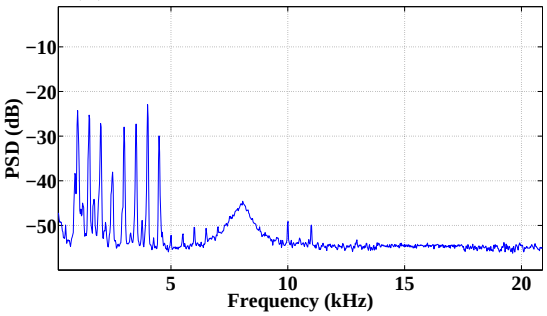

(c) 90 feet away

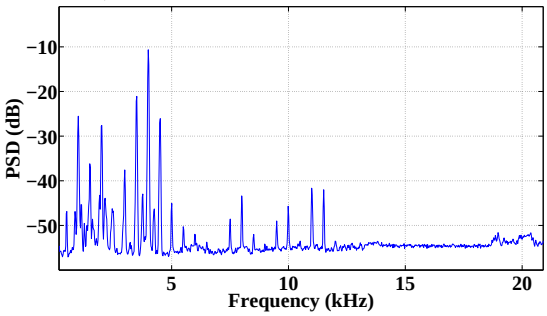

(d) 220 feet away

Figure 4.12: Power spectral density of the 500 Hz signal measured over the 2-7/8" pipe string - one concrete segment case

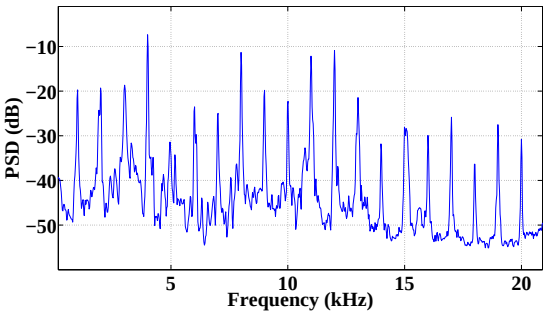

(a) beginning of the pipe string

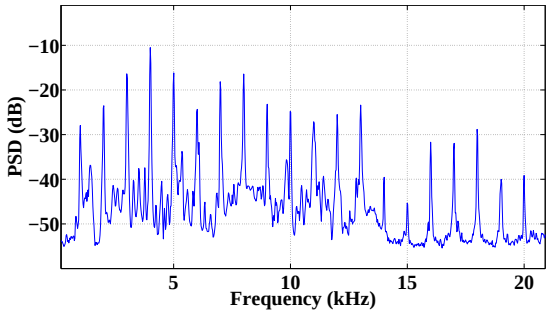

(b) 30 feet away (just before the concrete segment)

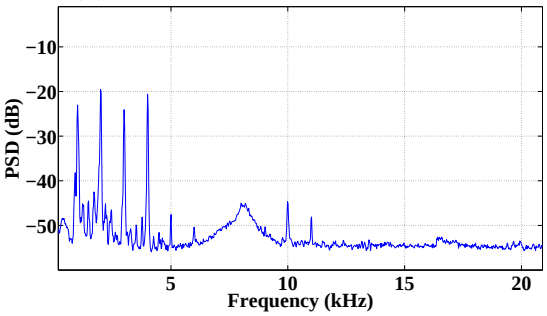

(c) 90 feet away

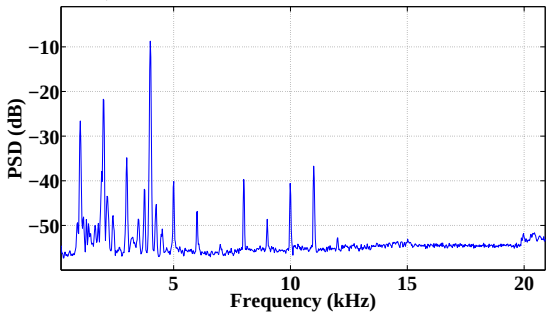

(d) 220 feet away

Figure 4.13: Power spectral density of the 1000 Hz signal measured over the 2-7/8" pipe string - one concrete segment case

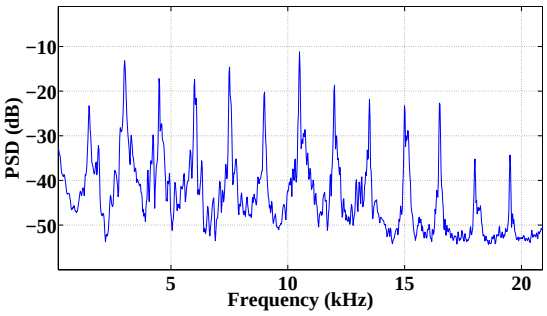

(a) beginning of the pipe string

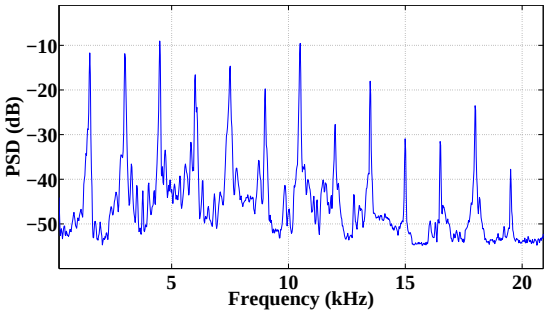

(b) 30 feet away (just before the concrete segment)

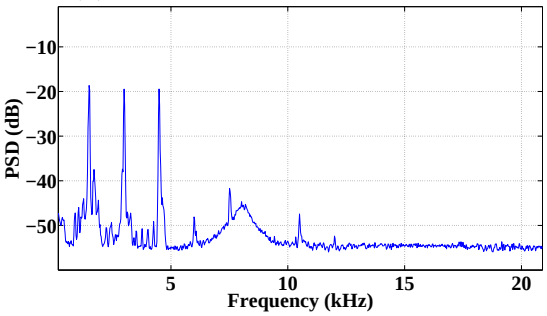

(c) 90 feet away

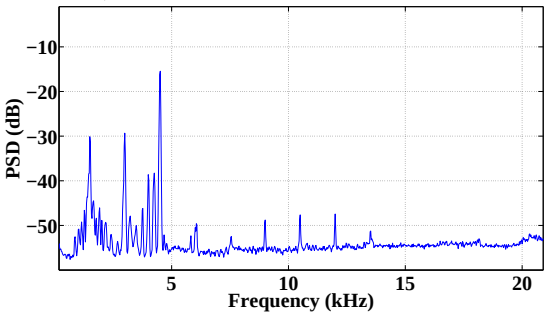

(d) 220 feet away

Figure 4.14: Power spectral density of the 1500 Hz signal measured over the 2-7/8" pipe string - one concrete segment case

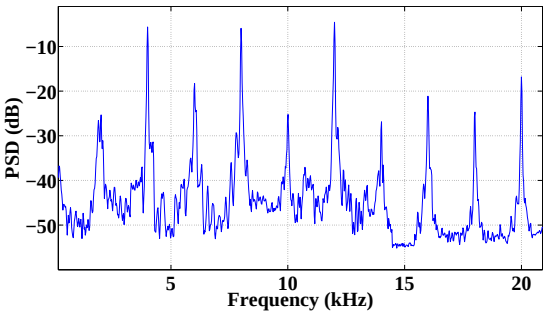

(a) beginning of the pipe string

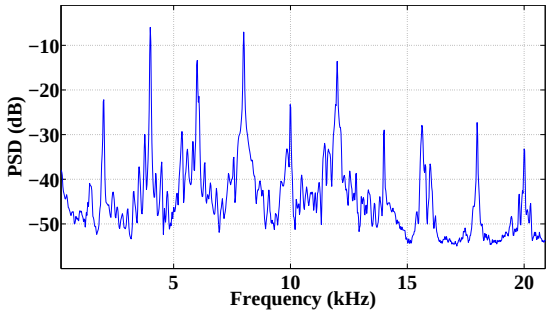

(b) 30 feet away (just before the concrete segment)

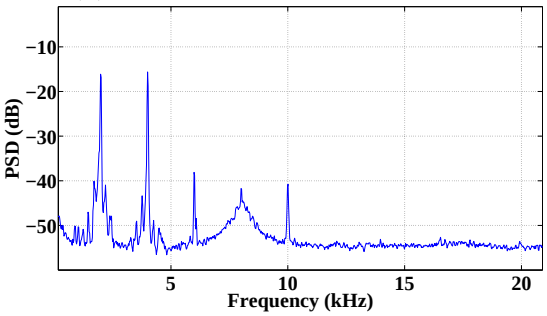

(c) 90 feet away

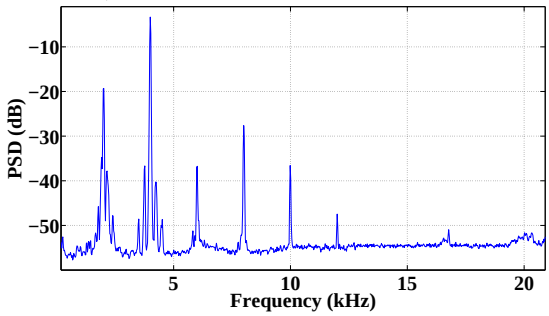

(d) 220 feet away

Figure 4.15: Power spectral density of the 2000 Hz signal measured over the 2-7/8" pipe string - one concrete segment case

4.2.1.2 Signal-to-Noise Ratio

Figure 4.16 displays the SNR results for the 20 tested input frequencies. An immediate decline in SNR values is observed after pouring concrete over the second pipe segment. The decline can be seen by comparing the SNR values taken just before the concrete segment with those taken immediately after the concrete segment. For the measurements taken beyond the concrete segment, a general decline in SNR values is noted with increasing the propagation distance for the different acoustic signals.

4.3 Second Concrete Segment Experiment

There was a need to conduct more propagation experiments in order to understand the effect of concrete on signal propagation in more depth. Accordingly, another concrete segment was added over the pipe string. The third pipe segment was encased in concrete; the concrete segment was around 30 feet of length and 1.5 inch of thickness. After the cement dried off, the aforementioned propagation measurements were repeated on this setup. Figure 4.17 shows a photograph of the new concrete segment around the third pipe segment along with the one around the second pipe segment. The experiment setup is similar to that of the no-concrete case. Figure 4.18 displays a schematic for the testbed after cementing the second and third pipe segments.

4.3.1 Measurement Results

Measurements results taken after including the second concrete segment are discussed in this subsection.

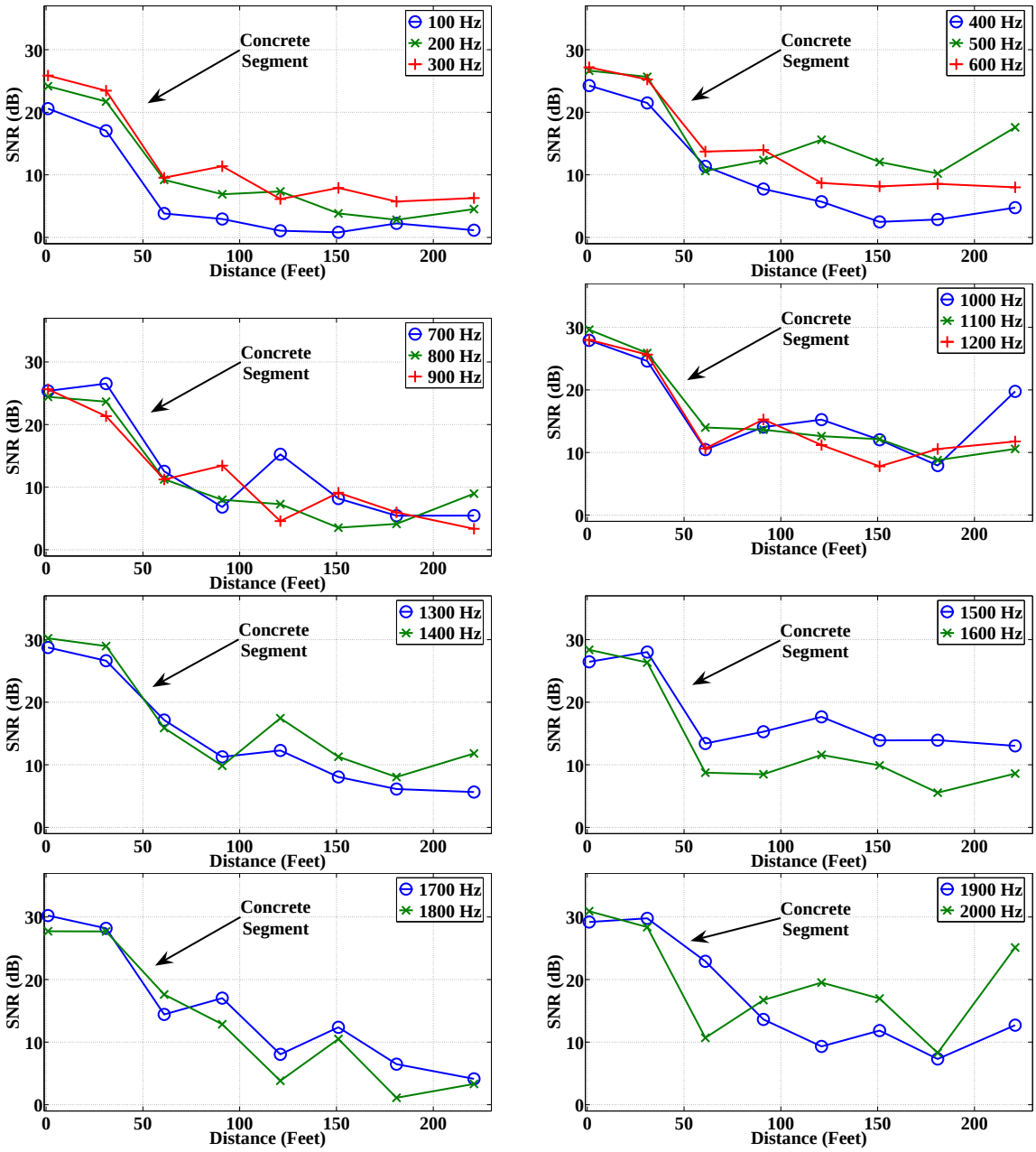

Figure 4.16: Signal-to-noise ratio vs. distance for the 2-7/8" pipe string - one concrete segment case

Figure 4.17: Photograph of the two concrete segments on the 2-7/8” pipe string

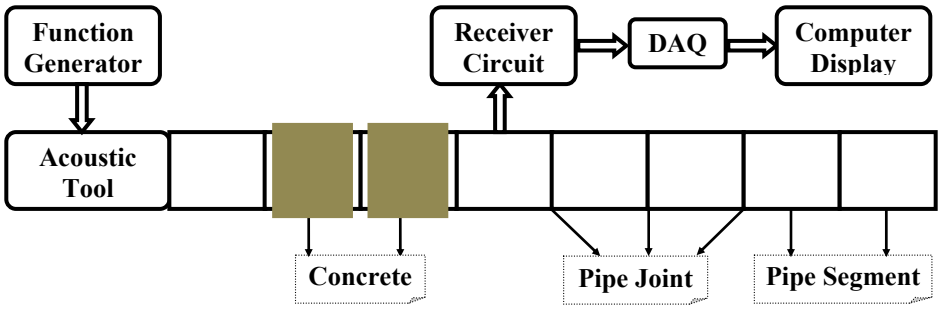

Figure 4.18: Testbed for the 2-7/8” pipe string - two concrete segments case

4.3.1.1 Power Spectral Density

Figure 4.19 shows the power spectral density of the 500 Hz signal. As the signal propagates beyond the concrete segments, many of the high-frequency harmonics died off. Comparing the results here to those when there was one concrete segment, it is noted that less harmonics are available for the measurements taken beyond the concrete segments. This is an indication that as the concrete segment gets longer, less harmonics can survive.

Figure 4.20 shows the power spectral density of the 1000 Hz signal. As can be seen in the figure, only the harmonics with frequencies less than 5 kHz survived for the measurements taken beyond the concrete segments. Figures 4.21 and 4.22 display the results for the 1500 Hz and 2000 Hz signals. The results here are similar to those of in the previous two figures.

In the two concrete segments case, the measurements recorded beyond the concrete segments seem to have an operating bandwidth that is much smaller than that of the measurements taken when there was only one concrete segment. This is a clear indication of the severity of concrete on the propagation of acoustic waves.

4.3.1.2 Signal-to-Noise Ratio

Figure 4.23 displays the SNR results for the 20 tested input frequencies for the two concrete segments case. An immediate sharp decline in SNR values is observed after pouring concrete over the second and third pipe segments. This conclusion can be seen by comparing the SNR values taken just before the concrete segments with those taken just after the concrete segments. For measurements taken beyond the concrete segments, the different acoustic signals have, worrying, low SNR values.

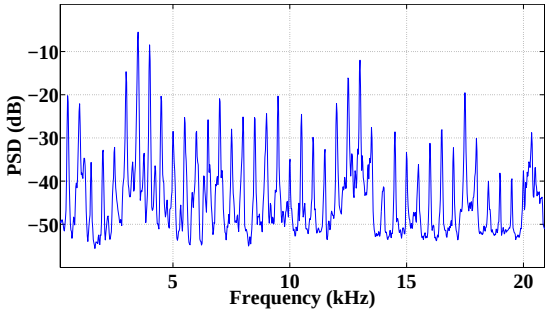

(a) beginning of the pipe string

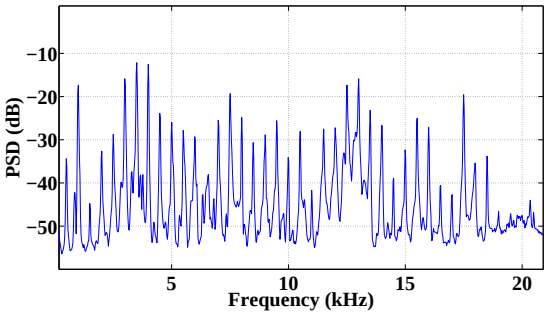

(b) 30 feet away (just before the first concrete segment)

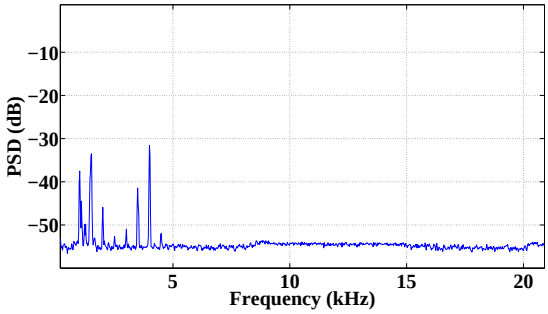

(c) 90 feet away (just after the second concrete segment)

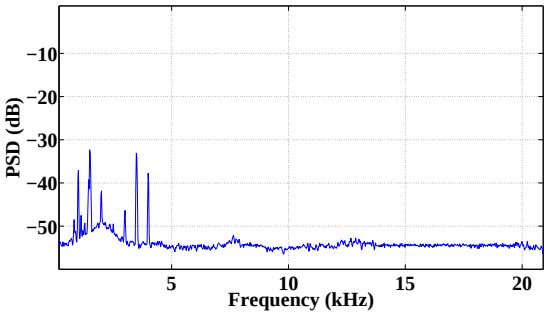

(d) 220 feet away

Figure 4.19: Power spectral density of the 500 Hz signal measured over the 2-7/8" pipe string - two concrete segments case

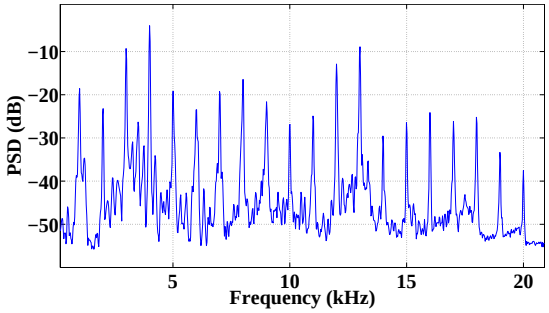

(a) beginning of the pipe string

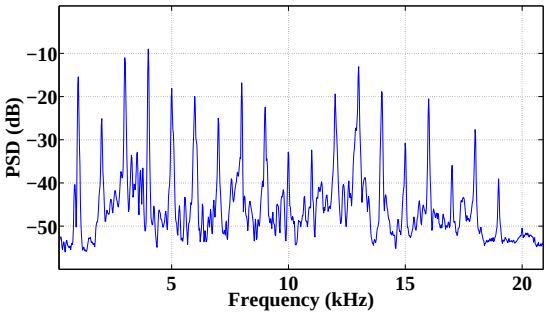

(b) 30 feet away (just before the first concrete segment)

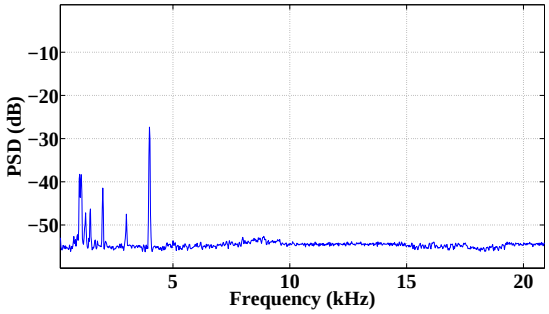

(c) 90 feet away (just after the second concrete segment)

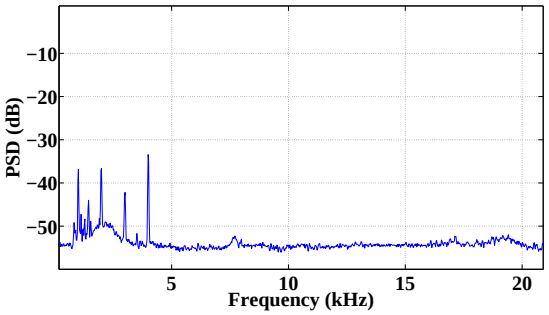

(d) 220 feet away

Figure 4.20: Power spectral density of the 1000 Hz signal measured over the 2-7/8" pipe string - two concrete segments case

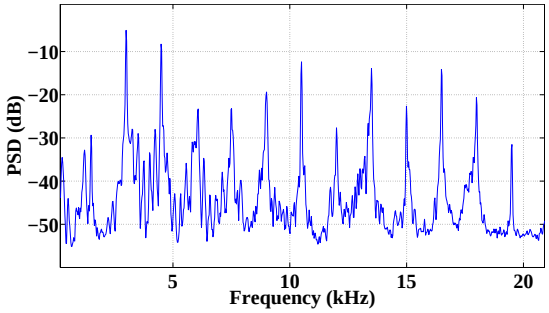

(a) beginning of the pipe string

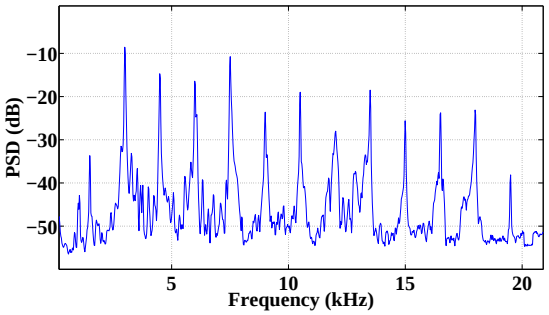

(b) 30 feet away (just before the first concrete segment)

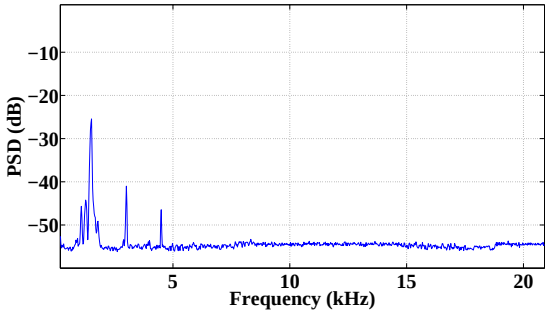

(c) 90 feet away (just after the second concrete segment)

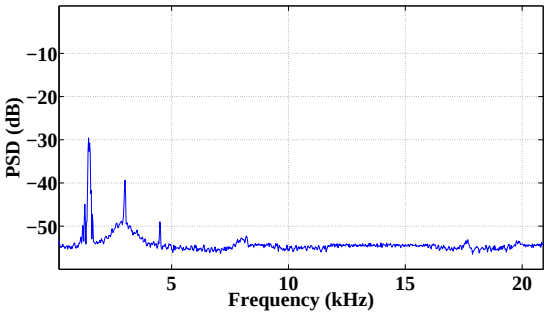

(d) 220 feet away

Figure 4.21: Power spectral density of the 1500 Hz signal measured over the 2-7/8" pipe string - two concrete segments case

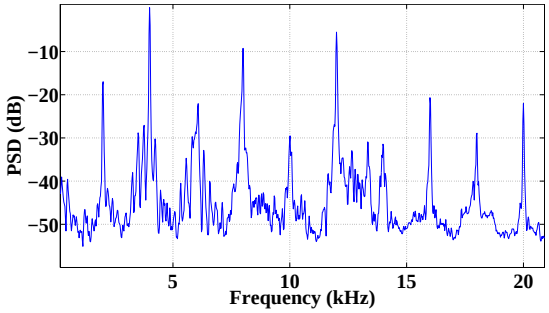

(a) beginning of the pipe string

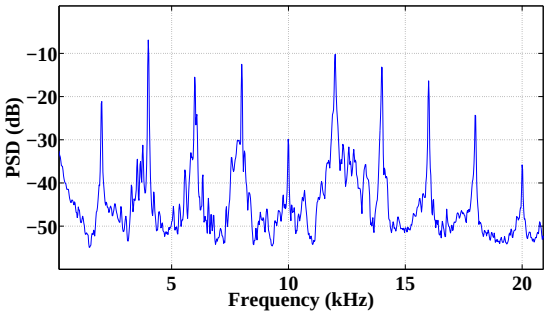

(b) 30 feet away (just before the first concrete segment)

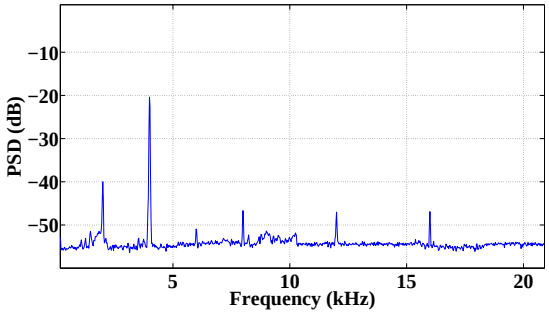

(c) 90 feet away (just after the second concrete segment)

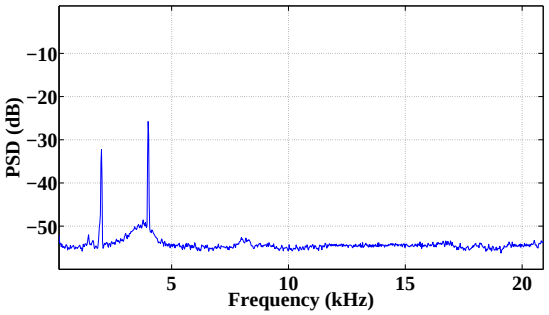

(d) 220 feet away

Figure 4.22: Power spectral density of the 2000 Hz signal measured over the 2-7/8" pipe string - two concrete segments case

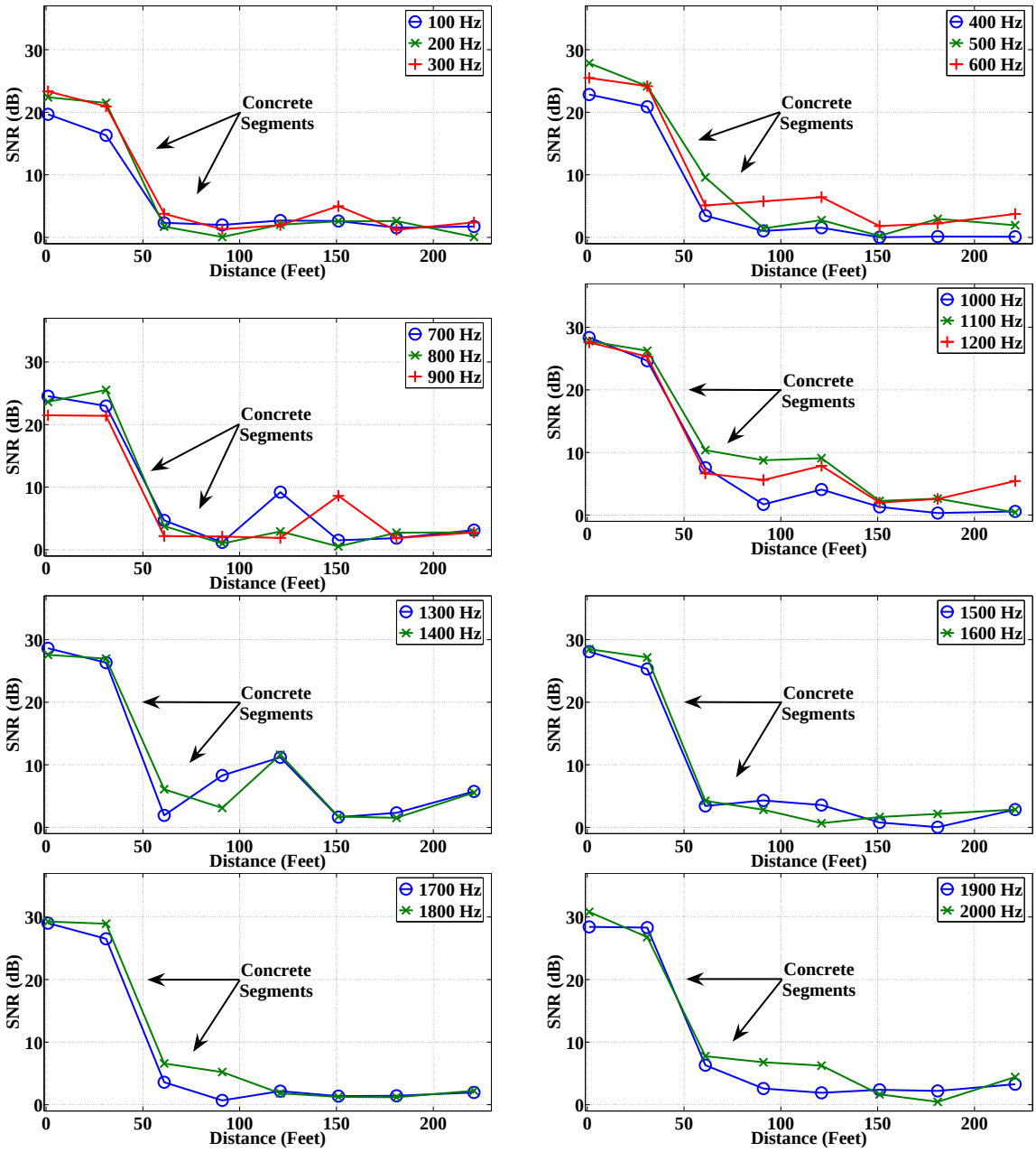

Figure 4.23: Signal-to-noise ratio vs. distance for the 2-7/8" pipe string - two concrete segments case

5. 7" Pipe String

This chapter details the 7" pipe string experiment. An overview of the designed testbed is given in Section 5.1, and the propagation results are displayed as well. Section 5.2 details the propagation results after the first concrete segment was installed on the pipe string. Finally, the propagation results are shown in Section 5.3 for the case when another concrete segment was installed on the pipe string.

5.1 Testbed Setup

Five segments of 7 inch production tubing were assembled to form the pipe string for this testbed. Signal measurements were taken at the beginning, middle, and end of each pipe segment. In each measurement, five bursts were recorded for each input frequency. Acoustic waves with different input frequencies were transmitted over the pipe and data were measured over the pipe segments using the acoustic receiver. The goal of the conducted propagation experiments was to find the acoustic channel response as a function of distance and frequency. The block diagram of the testbed is shown in Figure 5.1.

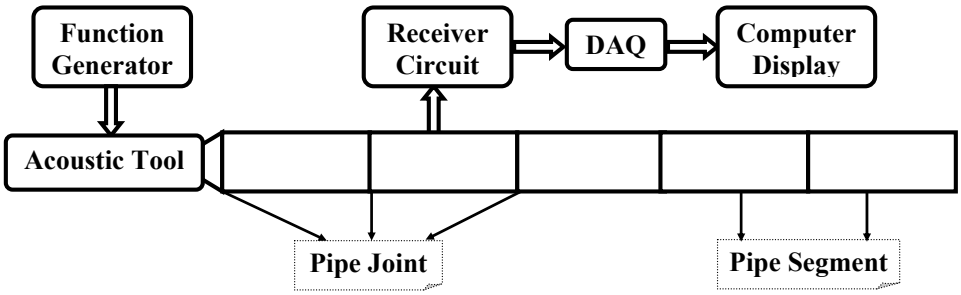

Figure 5.1: Testbed for the 7" pipe string - no concrete case

5.1.1 Measurement Results

The propagation measurements are discussed in this subsection.

5.1.1.1 Power Spectral Density

Figure 5.2 shows the power spectral density of the 500 Hz signal measured at different locations along the 7" pipe string. The measurement recorded at the beginning of the pipe string contains many of the 500 Hz harmonics. But as the signal propagates down the pipe string, different harmonics seem to decay at different rates.

Figure 5.3 displays the PSD of the 1000 Hz signal. It is worth-noting that as the acoustic signal propagates further away from the acoustic transmitter tool, the more attenuation its higher-order harmonics undergo.

Figures 5.4 and 5.5 show the PSD of the 1500 Hz and 2000 Hz signals. With increasing the input frequency of the acoustic signal, the attenuation of the higher-order harmonics is more pronounced.

It is noted from the PSD results that the acoustic channel attenuates harmonics differently, with the higher-order harmonics undergoing more attenuation than the lower-order ones. It is expected that the signal energy will be more concentrated in the lower band for a longer pipe string.

5.1.1.2 Signal-to-Noise Ratio

SNR values are shown in Figure 5.6. It is obvious that acoustic waves with different input frequencies propagate differently along the pipe string. It is also noted that the transmitter tool outputs the acoustic signals with different levels according to their input frequency. In general, the higher the input frequency, the higher the signal power. By comparing the SNR values at the beginning and the end of the pipe string, it is seen that the acoustic waves experience, in general, little decay as

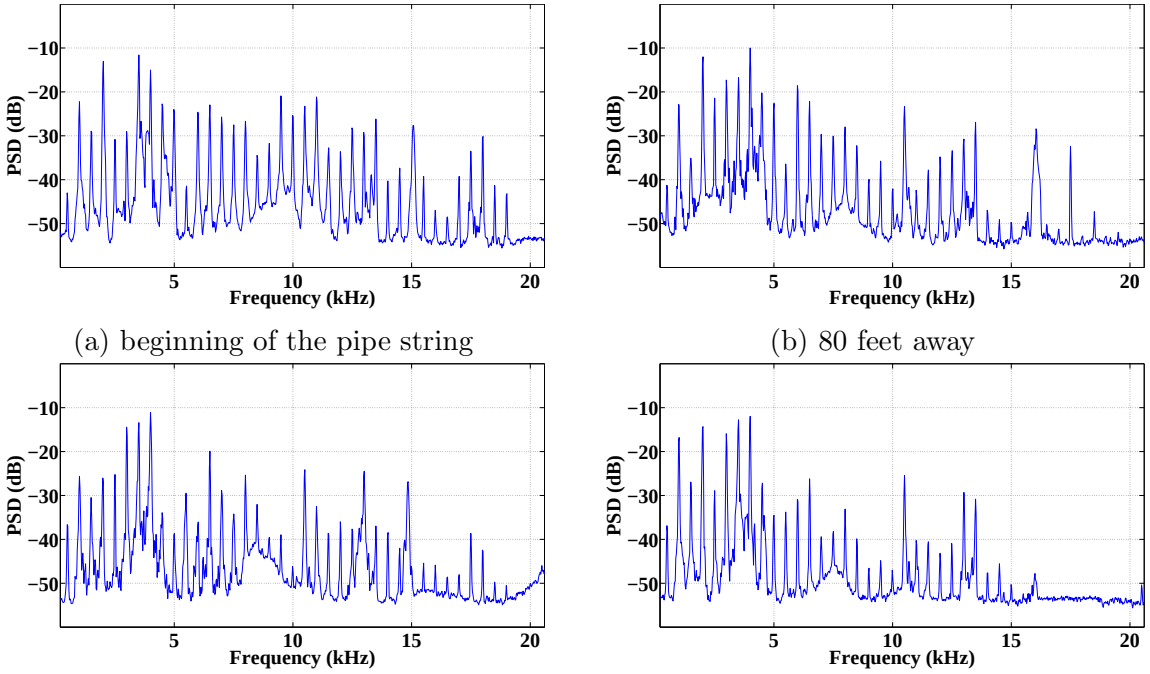

(a) beginning of the pipe string

(b) 80 feet away

(c) 120 feet away

(d) 200 feet away

Figure 5.2: Power spectral density of the 500 Hz signal measured over the 7" pipe string - no concrete case

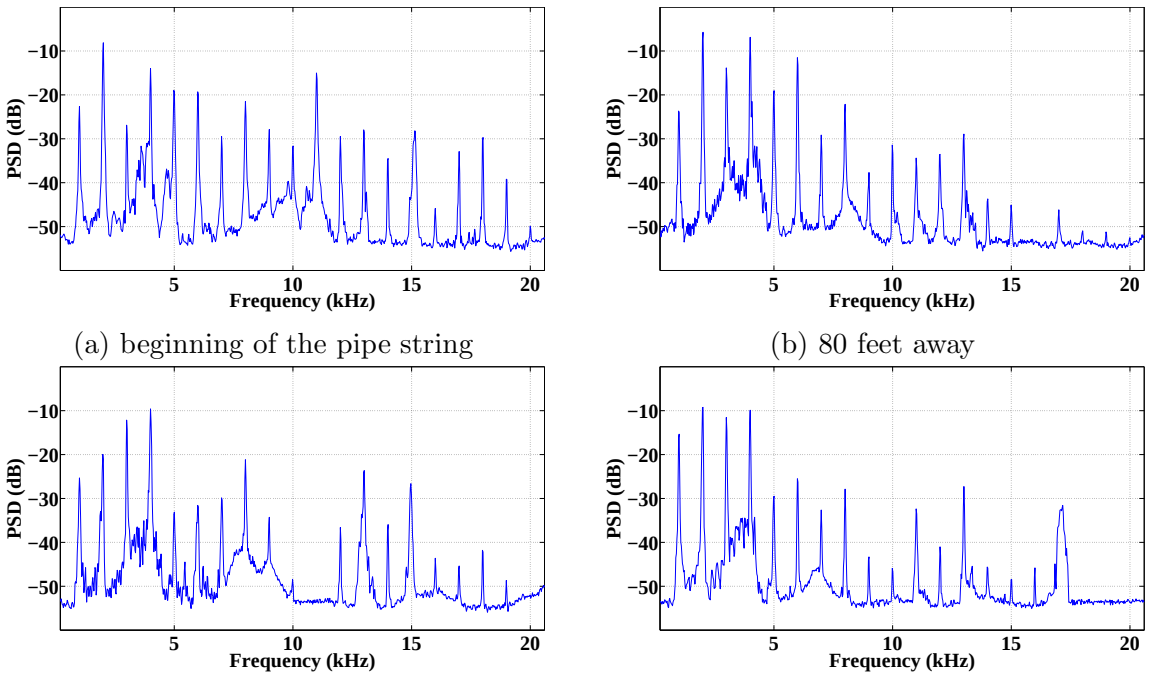

(a) beginning of the pipe string

(b) 80 feet away

(c) 120 feet away

(d) 200 feet away

Figure 5.3: Power spectral density of the 1000 Hz signal measured over the 7" pipe string - no concrete case

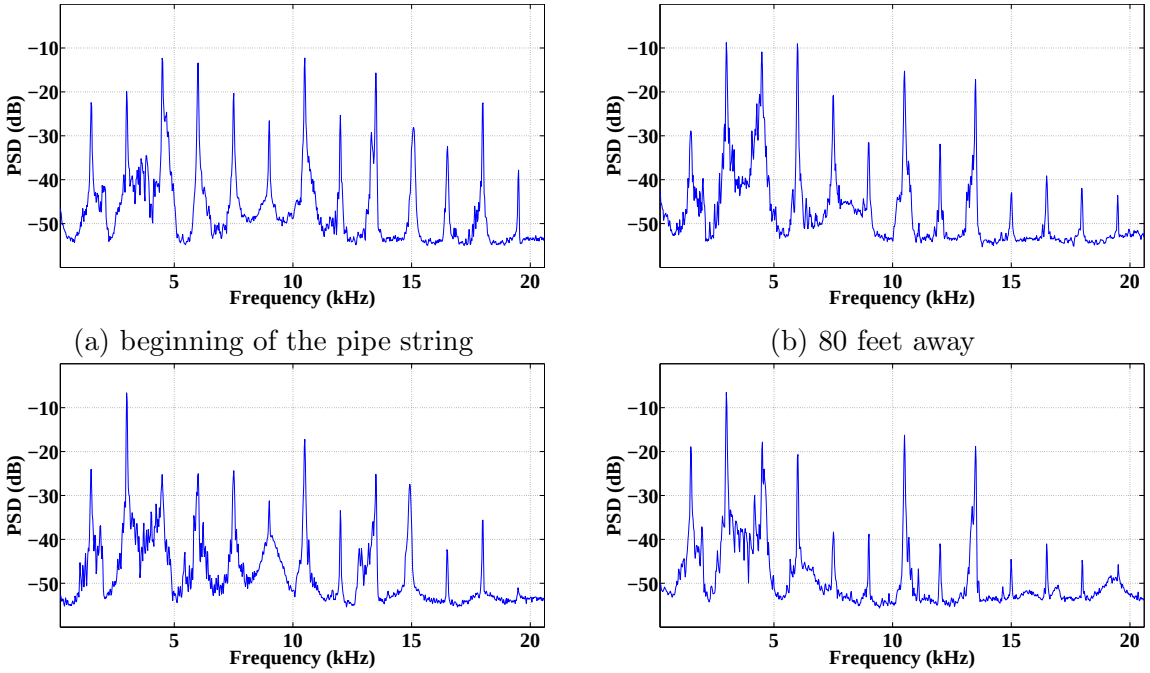

(a) beginning of the pipe string

(b) 80 feet away

(c) 120 feet away

(d) 200 feet away

Figure 5.4: Power spectral density of the 1500 Hz signal measured over the 7" pipe string - no concrete case

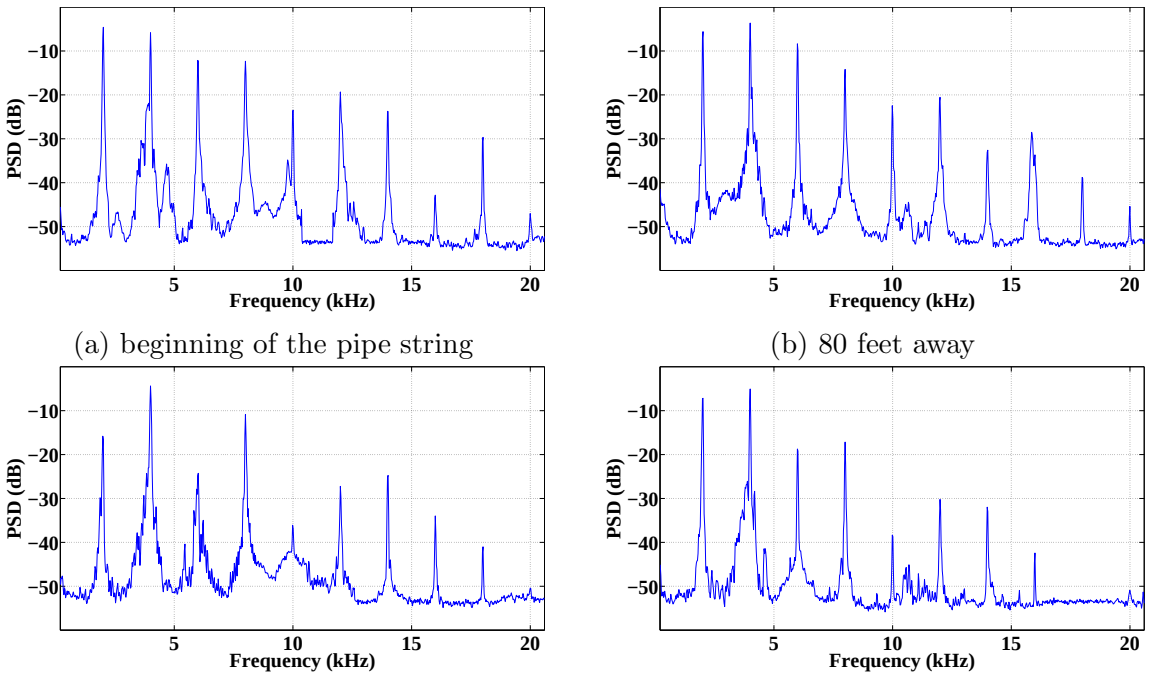

(a) beginning of the pipe string

(b) 80 feet away

(c) 120 feet away

(d) 200 feet away

Figure 5.5: Power spectral density of the 2000 Hz signal measured over the 7" pipe string - no concrete case

they progress further down the pipe string. The average SNR of all measurements along the pipe string was found to be around 21.3 dB.

5.1.1.3 Decay Rate

Figure 5.7 displays the channel attenuation rate for the 20 input frequencies. It is seen that the 200, 1000, 1700, and 2000 Hz signals experience an attenuation rate of less than 5 dB per 1000 feet. On the other hand, the acoustic waves of input frequencies of 100, 700, and 1500 Hz attenuate at a rate of more than 15 dB per 1000 feet. The results of this figure are tabulated in Table 5.1 as well.

Table 5.1: Channel decay rate for the 7" pipe string - no concrete case

Frequency (Hz)	100	200	300	400	500
Decay Rate (dB/1000 feet)	15.3	4.8	-0.9	3.7	-0.3
Frequency (Hz)	600	700	800	900	1000
Decay Rate (dB/1000 feet)	0.4	19.1	12.0	-0.9	2.1
Frequency (Hz)	1100	1200	1300	1400	1500
Decay Rate (dB/1000 feet)	7.0	4.1	2.8	-16.0	21.2
Frequency (Hz)	1600	1700	1800	1900	2000
Decay Rate (dB/1000 feet)	10.3	1.7	5.3	-8.9	3.3

5.2 First Concrete Segment Setup

Similar to the 2-7/8" pipe string case, it is interesting to study the effect of encasing the exterior of a pipe segment in concrete on the propagation of acoustic signals along the pipe string. As seen in the previous chapter, concrete had a significant impact on the propagation of acoustic signals through the tubing. In order to investigate this effect on the 7" pipe string, the exterior of the first half of the third pipe segment (around 20 feet) was encased in a doughnut-shaped concrete segment of 3/4 inch thickness. The propagation measurements were repeated after that. The block diagram of this testbed is shown in Figure 5.8.

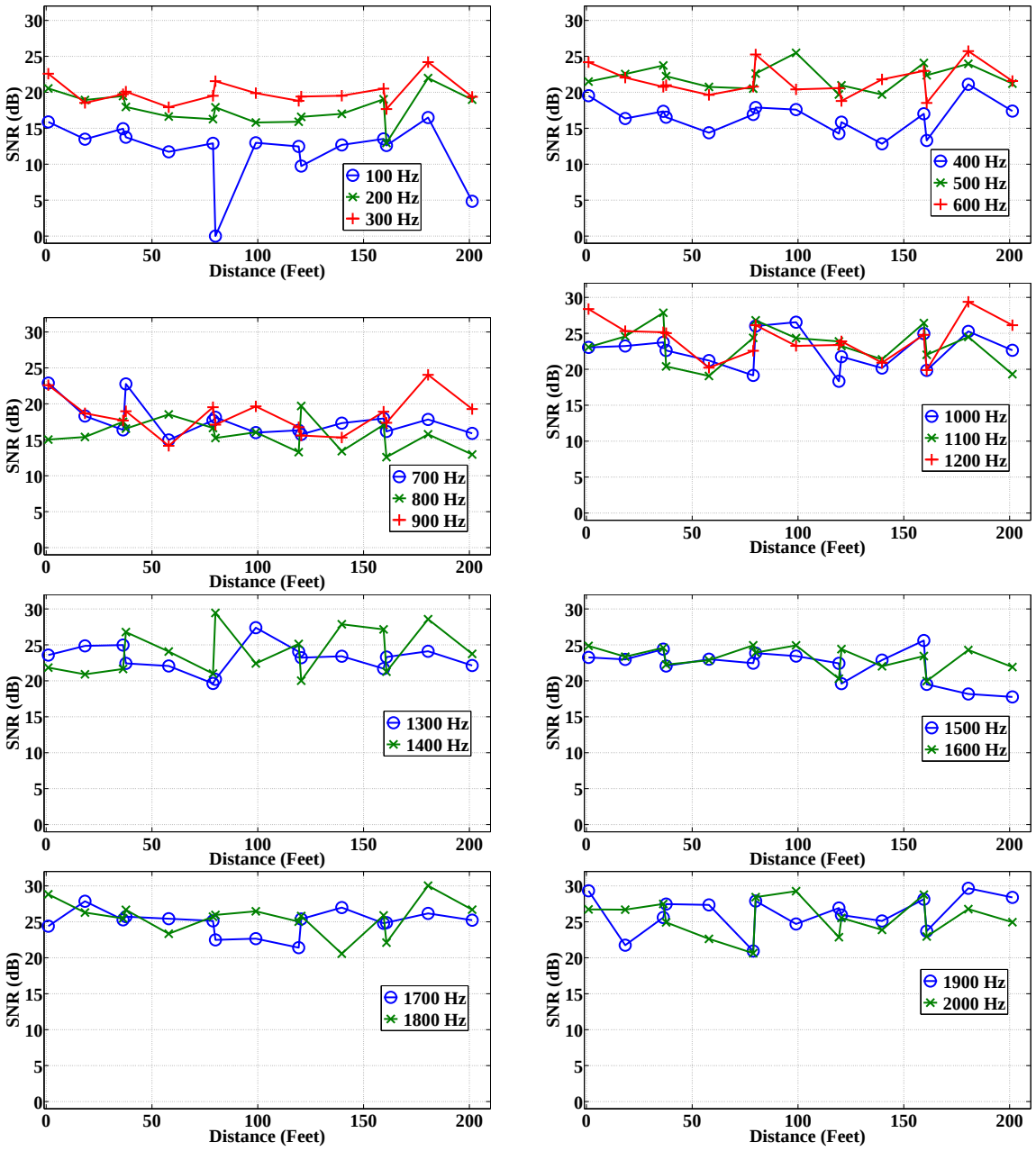

Figure 5.6: Signal-to-noise ratio vs. distance for the 7" pipe string - no concrete case

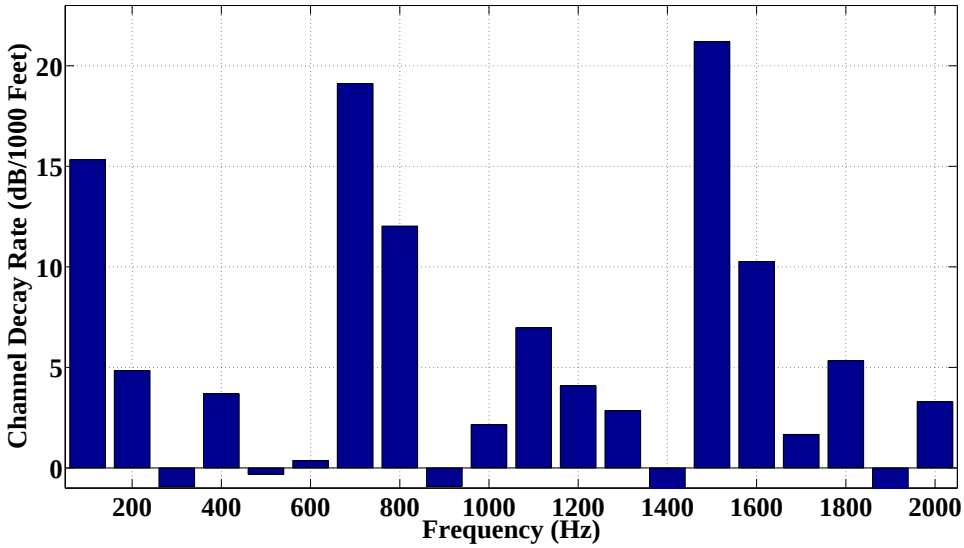

Figure 5.7: Channel decay rate (dB/1000 feet) for the 7" pipe string

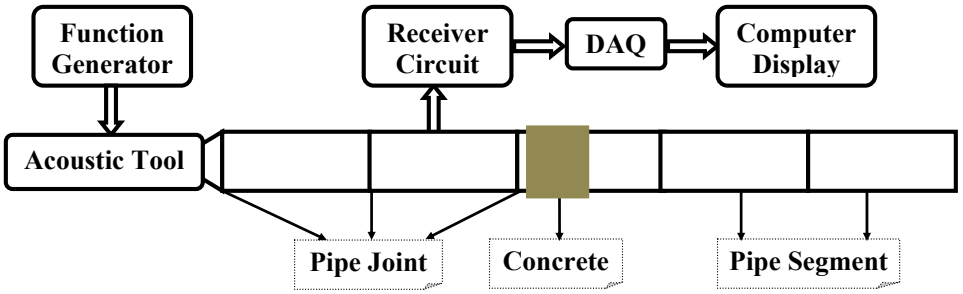

Figure 5.8: Testbed for the 7" pipe string - one concrete segment case

5.2.1 Measurement Results

The results of the propagation measurement are discussed in this subsection.

5.2.1.1 Power Spectral Density

The PSD of the 500 Hz signal along the pipe string is shown in Figure 5.9. It is noted that the concrete is filtering out few of the higher-order harmonics. Nevertheless, many of the lower-order harmonics manage to pass the concrete segment.

Figure 5.10 displays the PSD of the 1000 Hz signal. As shown in the figure, the operating bandwidth of the acoustic channel appeared to shrink. For this case of concrete length and diameter, the harmonics higher than about 10 kHz appear to be highly attenuated, while the harmonics in the lower range are slightly attenuated.

Figures 5.11 and 5.12 show the PSD results for the 1500 and 2000 Hz signals. Similar to the findings of the previous two figures, the lower band of harmonics manages to pass with lower attenuation compared to that of the higher band.

The PSD results emphasize the filtering effect of the concrete segment on the acoustic signal propagation. A longer concrete segment is thought to filter more of the higher frequency band of the acoustic wave.

5.2.1.2 Signal-to-Noise Ratio

The SNR values of the acoustic waves along the pipe string are shown in Figure 5.13. The decline in SNR values is very obvious for the measurements recoded beyond the concrete segment. On the other hand, the acoustic waves are attenuated differently depending on their input frequency. For example, the 100 Hz could not pass through the concrete segment as obvious from the very low SNR values for the measurements recorded beyond the concrete segment.

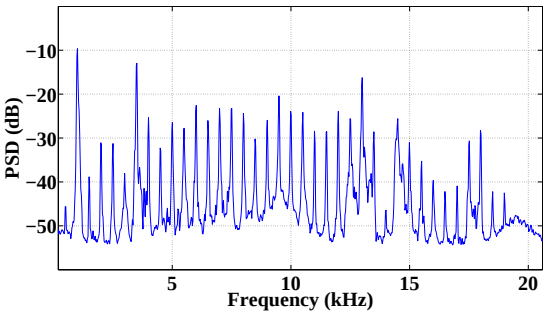

(a) beginning of the pipe string

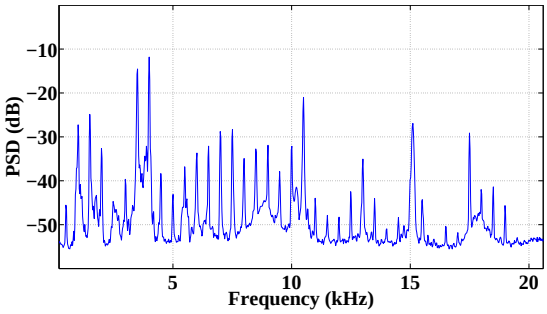

(b) 80 feet away (just before the concrete segment)

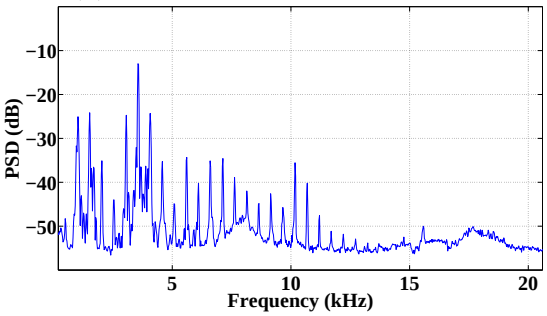

(c) 120 feet away

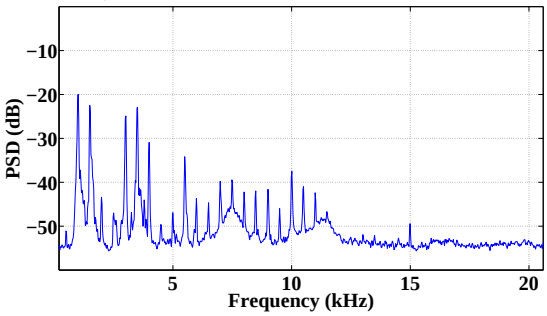

(d) 200 feet away

Figure 5.9: Power spectral density of the 500 Hz signal measured over the 7" pipe string - one concrete segment case

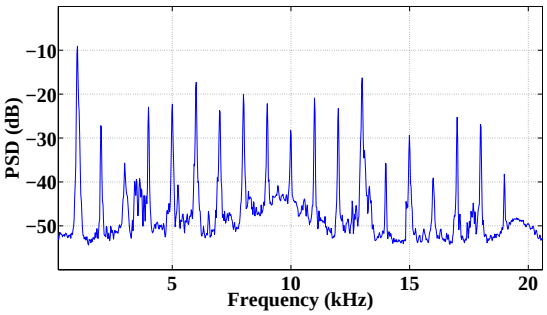

(a) beginning of the pipe string

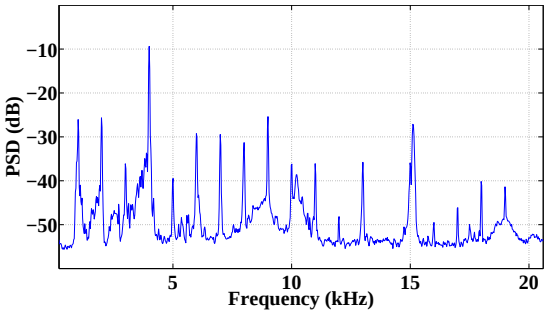

(b) 80 feet away (just before the concrete segment)

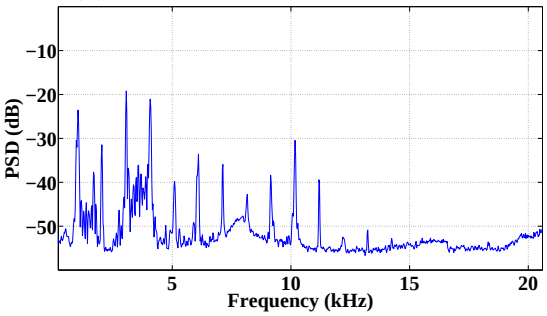

(c) 120 feet away

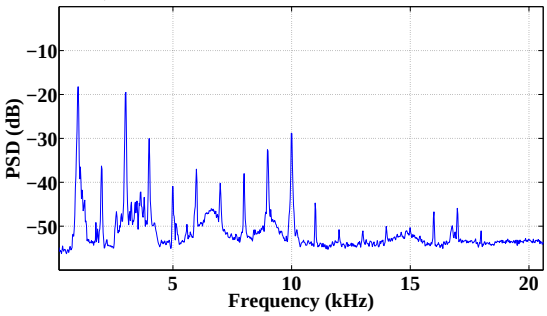

(d) 200 feet away

Figure 5.10: Power spectral density of the 1000 Hz signal measured over the 7" pipe string - one concrete segment case

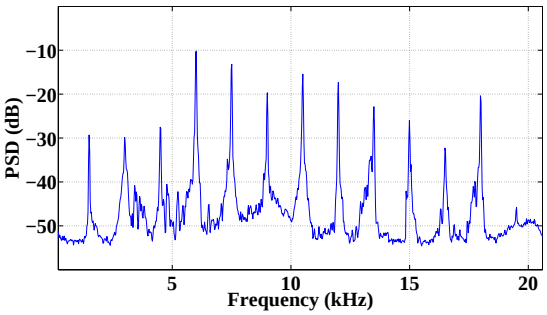

(a) beginning of the pipe string

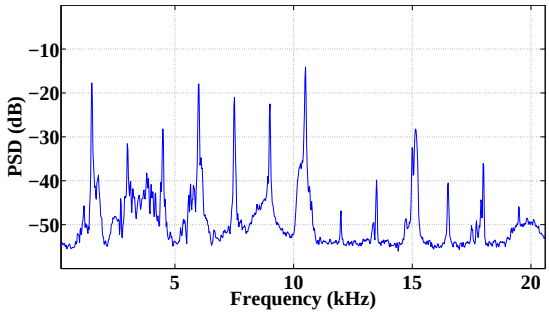

(b) 80 feet away (just before the concrete segment)

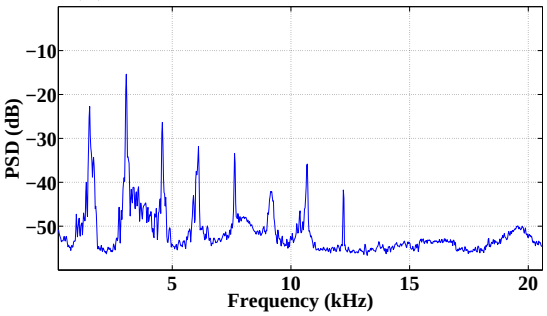

(c) 120 feet away

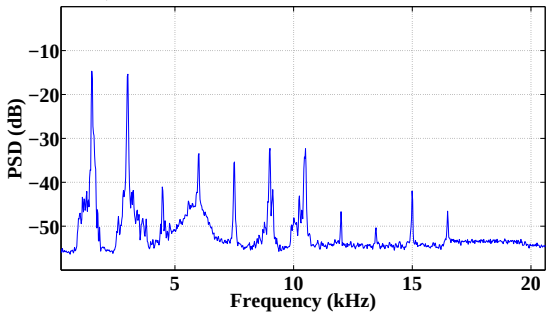

(d) 200 feet away

Figure 5.11: Power spectral density of the 1500 Hz signal measured over the 7" pipe string - one concrete segment case

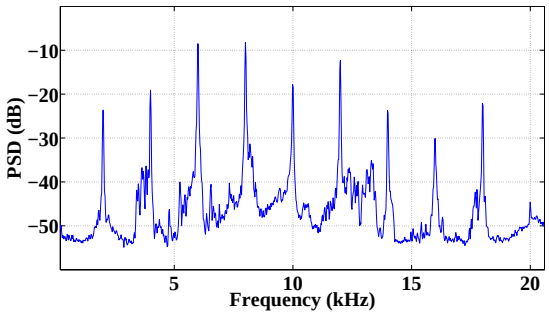

(a) beginning of the pipe string

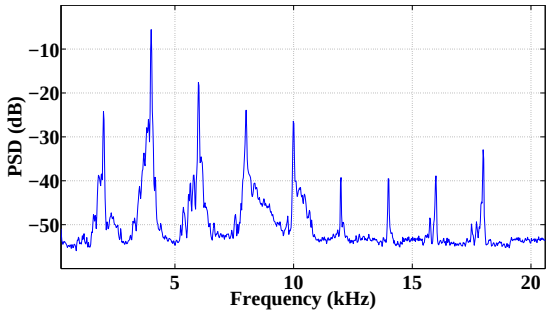

(b) 80 feet away (just before the concrete segment)

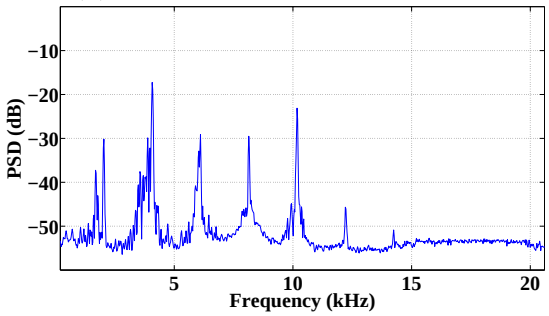

(c) 120 feet away

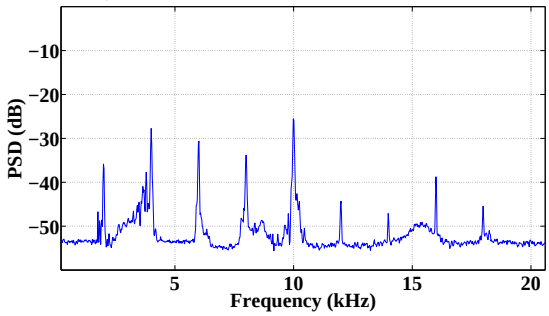

(d) 200 feet away

Figure 5.12: Power spectral density of the 2000 Hz signal measured over the 7" pipe string - one concrete segment case

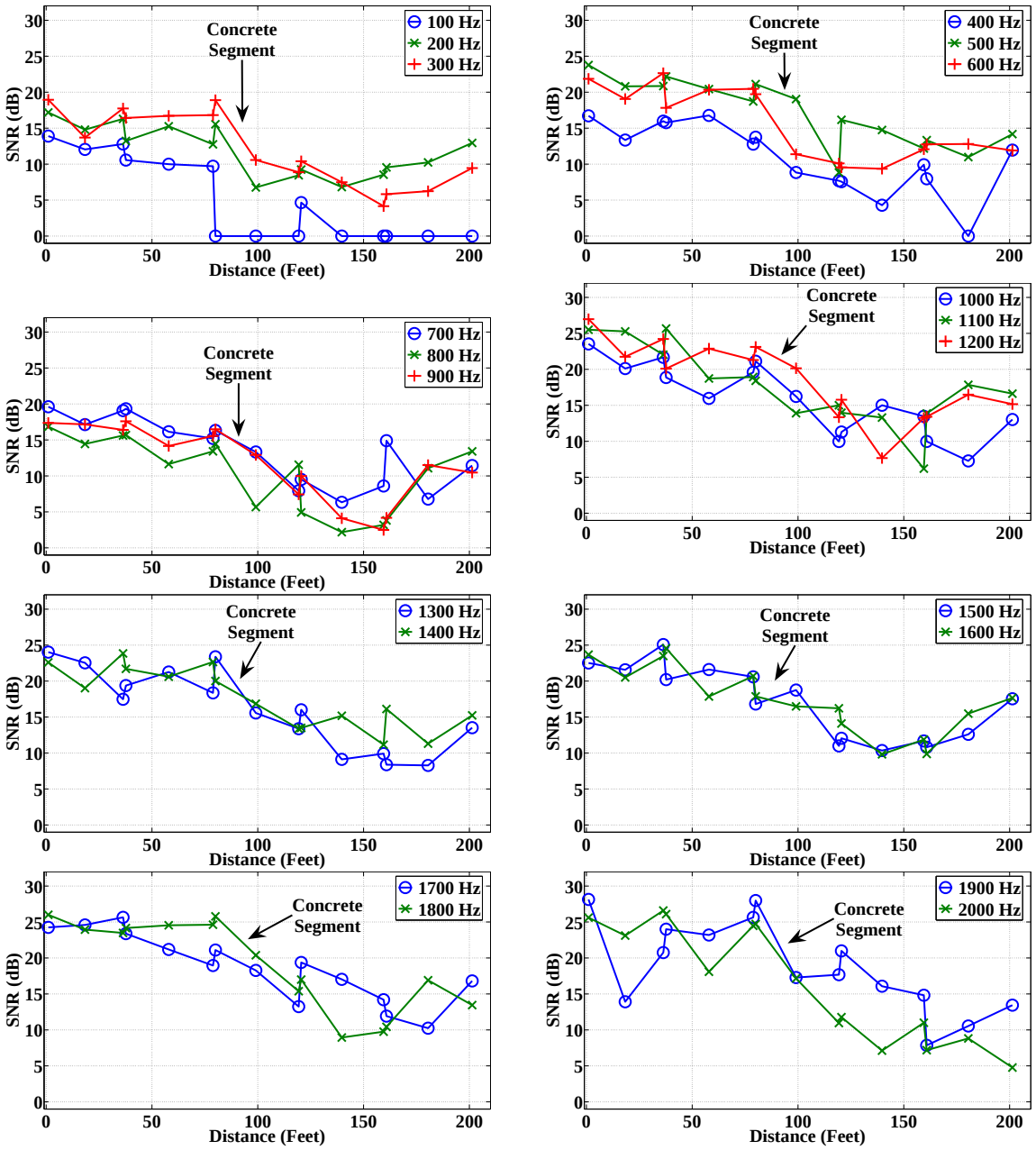

Figure 5.13: Signal-to-noise ratio vs. distance for the 7" pipe string - one concrete segment case

5.3 Second Concrete Segment Setup

To get a deeper understanding of the effect the concrete has on wave propagation, another concrete segment was added to the testbed. The later part of the third pipe was encased in concrete that has a length of around 20 feet and is 3/4 inch of thickness. The aforementioned propagation measurements were repeated on this setup. The block diagram of the testbed under two concrete segments is shown in Figure 5.14.

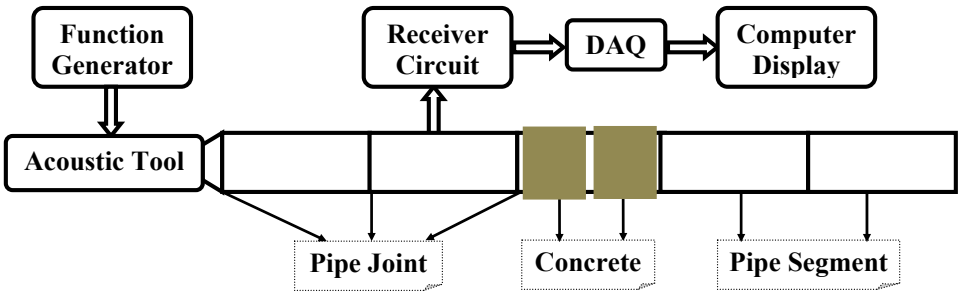

Figure 5.14: Testbed for the 7" pipe string - two concrete segments case

5.3.1 Measurement Results

The results of the propagation experiments for the case of two concrete segments are shown in this subsection.

5.3.1.1 Power Spectral Density

The power spectral density results are displayed for the 500, 1000, 1500, and 2000 Hz signals in the following four figures. Figure 5.15 shows the results for the 500 Hz signal. It is interesting to see how the introduction of the second concrete segment filtered out all the signal harmonics except the fundamental one.

The PSD results of the 1000 Hz are shown in Figure 5.16. The effect of concrete on acoustic wave propagation is very obvious; only the 1000 Hz fundamental harmonic

passed through the concrete segment, and the rest of the harmonics died off.

Figures 5.17 and 5.18 show the PSD of the 1500 and 2000 Hz signals respectively. Similar to the previous two figures, the acoustic wave are severely attenuated because of the concrete segments. For the 2000 Hz signal, almost all of the harmonics were wiped out.

The PSD results clearly emphasize the effect of concrete on acoustic wave propagation. This effect is similar to an attenuating bandpass filter with a bandwidth that is function of the concrete length and diameter.

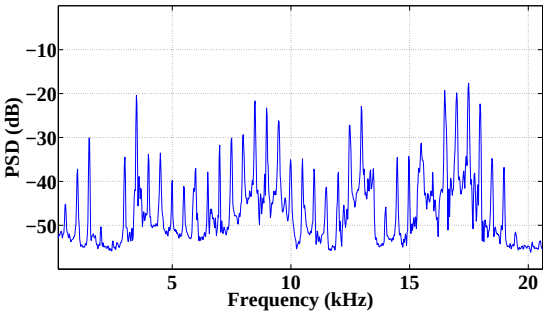

(a) beginning of the pipe string

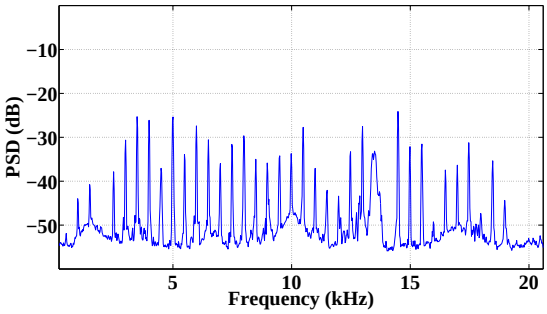

(b) 80 feet away (just before the first concrete segment)

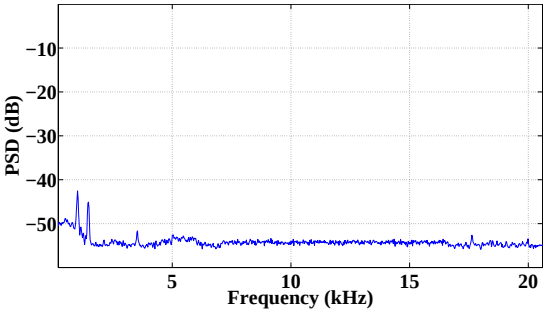

(c) 120 feet away (just after the second concrete segment)

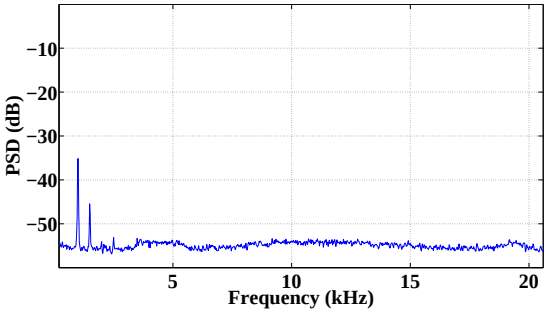

(d) 200 feet away

Figure 5.15: Power spectral density of the 500 Hz signal measured over the 7" pipe string - two concrete segments case

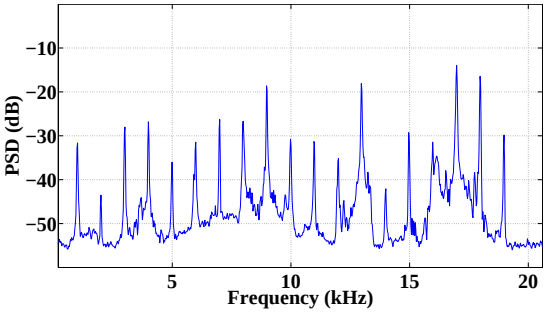

(a) beginning of the pipe string

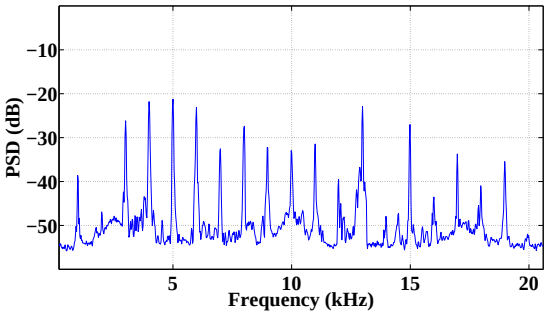

(b) 80 feet away (just before the first concrete segment)

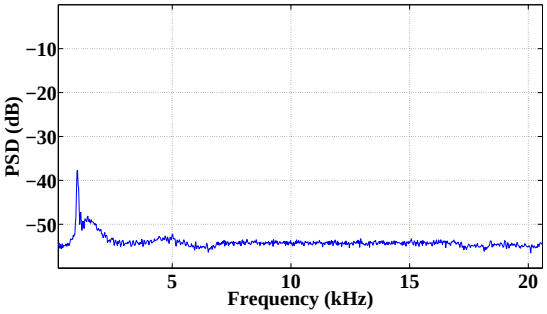

(c) 120 feet away (just after the second concrete segment)

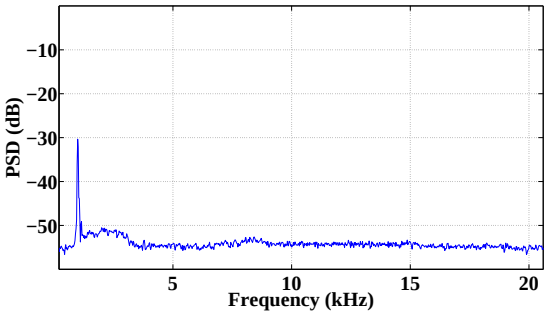

(d) 200 feet away

Figure 5.16: Power spectral density of the 1000 Hz signal measured over the 7" pipe string - two concrete segments case

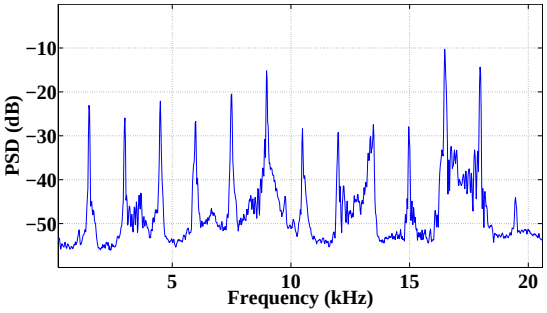

(a) beginning of the pipe string

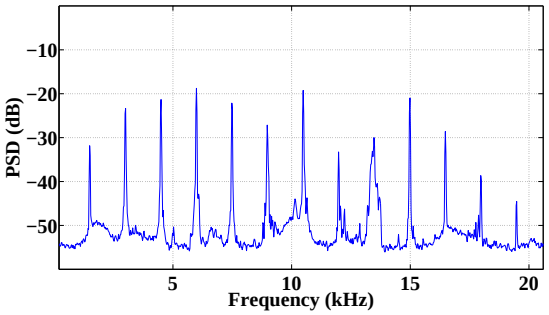

(b) 80 feet away (just before the first concrete segment)

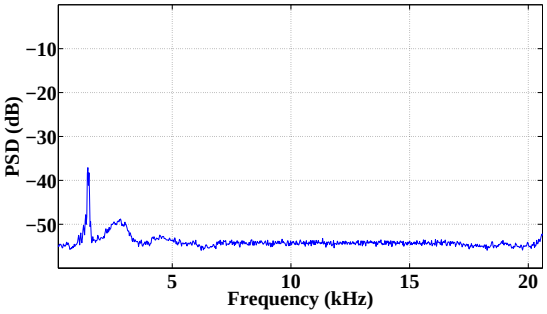

(c) 120 feet away (just after the second concrete segment)

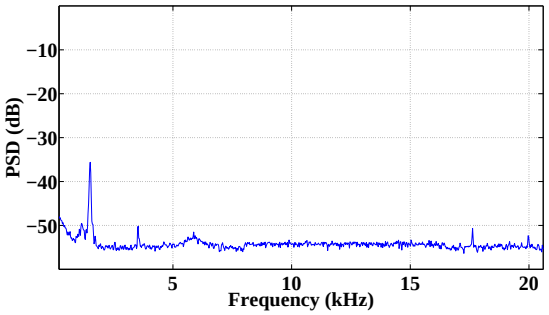

(d) 200 feet away

Figure 5.17: Power spectral density of the 1500 Hz signal measured over the 7" pipe string - two concrete segments case

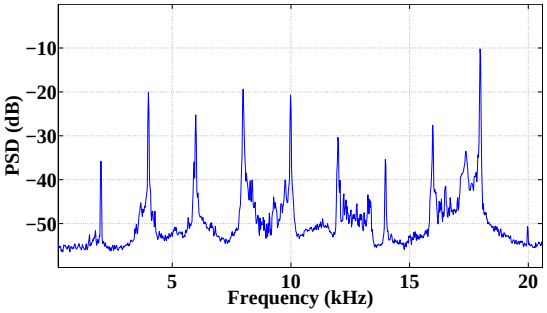

(a) beginning of the pipe string

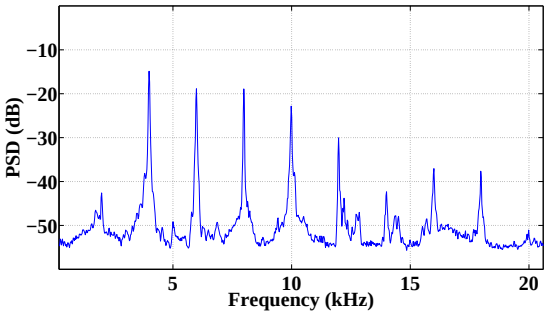

(b) 80 feet away (just before the first concrete segment)

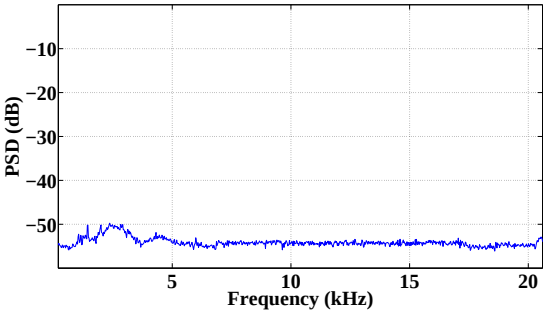

(c) 120 feet away (just after the second concrete segment)

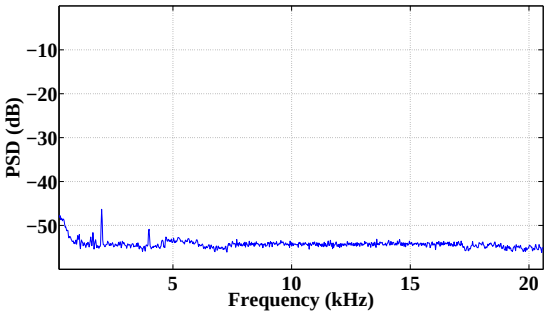

(d) 200 feet away

Figure 5.18: Power spectral density of the 2000 Hz signal measured over the 7" pipe string - two concrete segments case

5.3.1.2 Signal-to-Noise Ratio

The SNR results are displayed in Figure 5.19. As indicated from the PSD results, the acoustic waves lose most of their energy after passing through the concrete segments. Signal levels are falling to around the noise range, and so the SNR values are very close to 0 dB for most of the measurements recorded beyond the concrete segments.

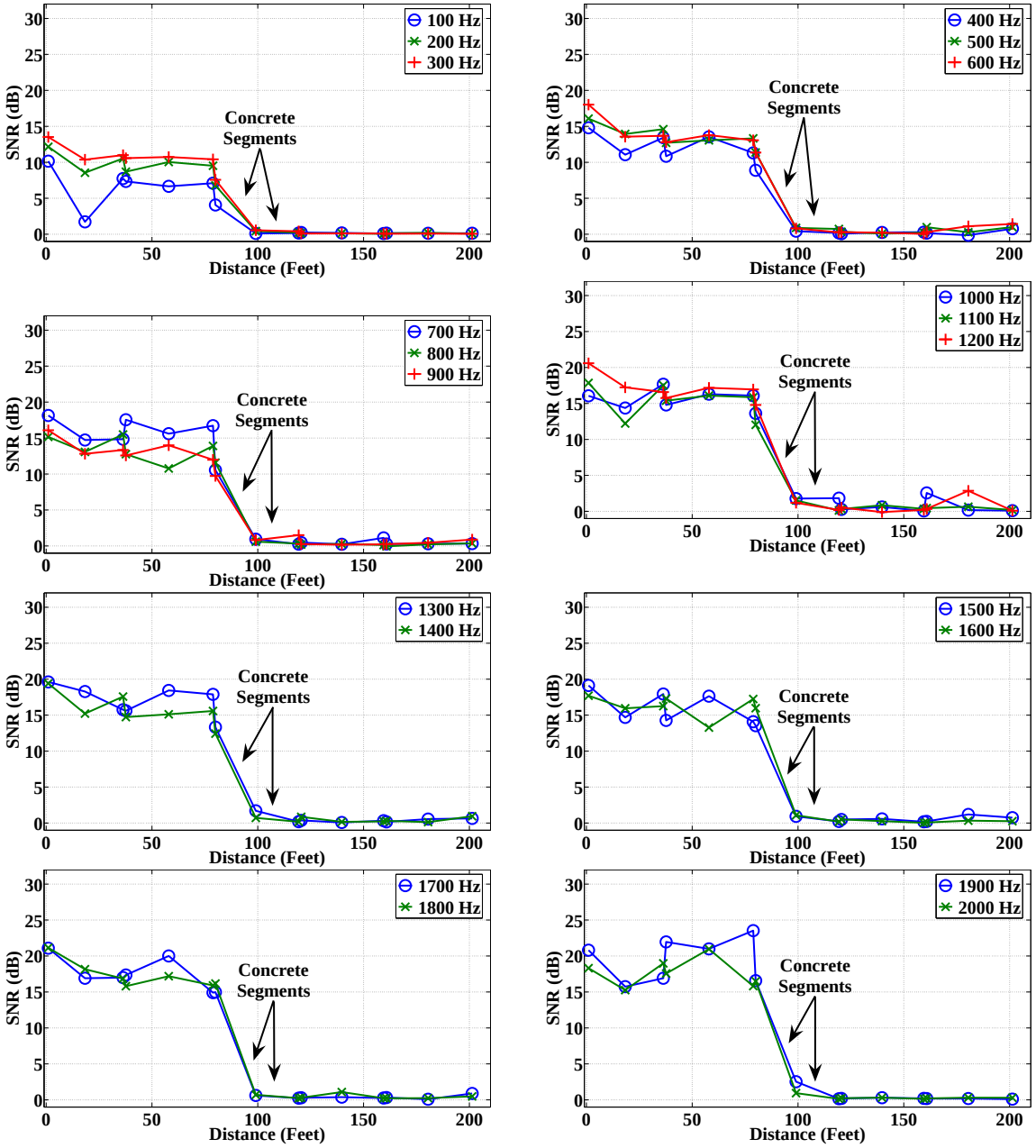

Figure 5.19: Signal-to-noise ratio vs. distance for the 7" pipe string - two concrete segments case

6. Signal Processing Algorithms

This chapter investigates the usefulness of using signal processing algorithms to counter the effects of the acoustic channel. Section 6.2 introduces the signal processing algorithms. Section 6.3 displays the results after applying the signal processing algorithms on the 7" pipe string. Finally, Sections 6.4 and 6.5 show the results for the cemented pipe string cases.

6.1 Introduction

The results of the previous two chapters indicated the need for some signal processing tools to counter the destructive effect of the acoustic channel and enhance the quality of the measurements. In order to improve the testbed, the following signal processing algorithms were investigated:

1. Filtering the fundamental harmonic
2. Coherently combining all harmonics
3. Equalizing the measured signals

6.2 Algorithms Description

Signal processing was employed at the measured signals, and the goal was to enhance the performance of the system. The block diagram of the testbed along with the signal processing tool is shown in Figure 6.1. It is assumed that the transmitted signal is denoted as $\boldsymbol{x}$, the measured signal is called $\boldsymbol{y}$, and the output of the signal processing algorithm is denoted as $\hat{\boldsymbol{x}}$ as shown in Figure 6.1.

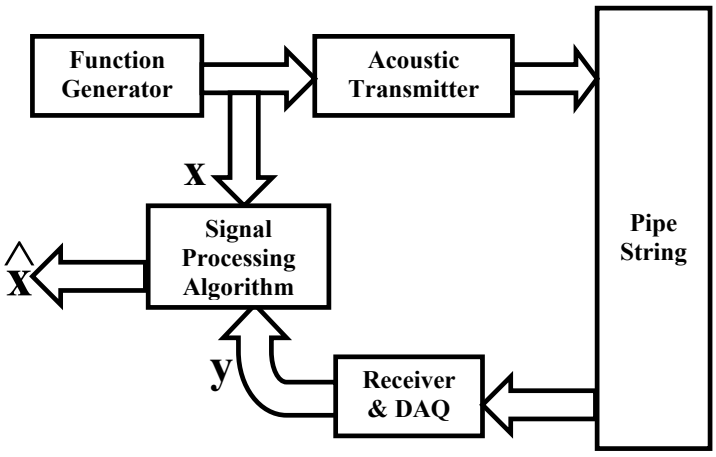

Figure 6.1: Signal processing algorithm block diagram

6.2.1 Fundamental Harmonic Filtering

A band-pass filter is used to filter the fundamental harmonic of the measured signal and remove everything else. The advantages of this method are the noise reduction as less bandwidth will be used, and the easiness of implementation. However, this algorithm does not collect all the available energy in other high-order harmonics. In addition, when the fundamental harmonic is severely attenuated (like in some of the concrete cases), the output of this algorithm is a low-SNR signal.

6.2.2 Harmonics Combining

This algorithm searches for all available harmonics and combines them coherently. The available harmonics are first band-pass filtered, then each harmonic is demodulated using sine and cosine signals to get the real and the imaginary parts of that harmonic; the frequency of the sine and cosine signals is set to equal to the frequency of that harmonic. This process is repeated for all available harmonics, then the real parts are coherently combined together; the same is done for the imaginary parts as

well. The total real and imaginary parts are then combined and the magnitude of that term is found. Finally, the result is low-pass filtered.

The advantage of this algorithm is that all the available energy in the different harmonics will be added together in a constructive manner. The drawback of this method is the possibility of adding more noise to the output signal because of the inclusion of all available harmonics; this algorithm will include noise signals from more frequency bands. It is also obvious that this algorithm has moderate complexity for filtering, demodulation, and combining.

6.2.3 Equalization

The equalizer algorithm is concerned in undoing the effects of the acoustic channel. Because the acoustic signals experience multiple reflections inside the pipe string, what is being received is actually a summation of multiple copies of the transmitted signals, each copy is delayed and attenuated differently. The obvious effect of this phenomena is that the received signal has a longer duration than that of the transmitted one. The equalizer's job is to undo the effect of the channel by combining the signal multipath copies together in a constructive manner. Consequently, the equalizer finds the optimum weight to each multipath copy and then combines the weighted copies together in order to get the desired signal.

The equalizer's goal is to find $\hat{\boldsymbol{x}}$ such that $|\boldsymbol{x} - \hat{\boldsymbol{x}}|^2$ is minimized. If the equalizer can be represented as a finite impulse response filter, $\boldsymbol{h}$, of length L with filter coefficients $\{h_0, h_1, \ldots, h_{L-1}\}$, then $\hat{\boldsymbol{x}}$ is the result of the convolution between $\boldsymbol{y}$ and $\boldsymbol{h}$. $\hat{\boldsymbol{x}}$ can be represented as

$$\hat{\boldsymbol{x}} = \boldsymbol{y} \star \boldsymbol{h} \tag{6.1}$$

However, $\hat{\boldsymbol{x}}$ can also be represented as a summation of L shifted and weighted copies

of $\boldsymbol{y}$ as

$$\hat{\boldsymbol{x}} = \sum_{j=0}^{L-1} \tilde{\boldsymbol{y}}_j h_j \tag{6.2}$$

where $\tilde{\boldsymbol{y}}_j$ is a shifted copy of $\boldsymbol{y}$ with the first j elements are zeros; for example, $\tilde{\boldsymbol{y}}_2$ is $[0, 0, y_1, \ldots, y_{N-2}]^T$, where N is the sample length. Furthermore, equation (6.2) can be rewritten as

$$\hat{\boldsymbol{x}} = \tilde{\boldsymbol{Y}}\boldsymbol{h} \tag{6.3}$$

where $\tilde{\boldsymbol{Y}}$ is $[\tilde{\boldsymbol{y}}_0, \tilde{\boldsymbol{y}}_1, \ldots, \tilde{\boldsymbol{y}}_{L-2}, \tilde{\boldsymbol{y}}_{L-1}]$. The cost function, c, is defined as

$$c = |\boldsymbol{x} - \hat{\boldsymbol{x}}|^2 = (\boldsymbol{x} - \hat{\boldsymbol{x}})^T(\boldsymbol{x} - \hat{\boldsymbol{x}}) = \boldsymbol{x}^T\boldsymbol{x} - 2\hat{\boldsymbol{x}}^T\boldsymbol{x} + \hat{\boldsymbol{x}}^T\hat{\boldsymbol{x}} \tag{6.4}$$

Using the definition of $\hat{\boldsymbol{x}}$ in (6.3), then

$$c = \boldsymbol{x}^T\boldsymbol{x} - 2\boldsymbol{h}^T\tilde{\boldsymbol{Y}}^T\boldsymbol{x} + \boldsymbol{h}^T\tilde{\boldsymbol{Y}}^T\tilde{\boldsymbol{Y}}\boldsymbol{h} \tag{6.5}$$

To get the minimum estimation error, the goal is to find $\boldsymbol{h}$ that minimizes c. Using [90], the optimum coefficients of the equalizer filter can be found as

$$\boldsymbol{h} = (\tilde{\boldsymbol{Y}}^T\tilde{\boldsymbol{Y}})^{-1}\tilde{\boldsymbol{Y}}^T\boldsymbol{x} \tag{6.6}$$

Accordingly, $\hat{\boldsymbol{x}}$ that minimizes $|\boldsymbol{x} - \hat{\boldsymbol{x}}|^2$ is found to be

$$\hat{\boldsymbol{x}} = \tilde{\boldsymbol{Y}}\boldsymbol{h} = \tilde{\boldsymbol{Y}}(\tilde{\boldsymbol{Y}}^T\tilde{\boldsymbol{Y}})^{-1}\tilde{\boldsymbol{Y}}^T\boldsymbol{x} \tag{6.7}$$

One disadvantage of using the equalization algorithm is that it needs higher processing requirements compared to the previous two algorithms. The algorithm

needs a training phase in order to get the optimum weights, and it also needs to keep tracking the channel variations and updating the weights accordingly. Its advantage is the improved gain in SNR as will be seen in the following results.

6.3 7" Pipe String Case

The results of employing the signal processing algorithms are discussed in this section for the 7" pipe string when there was no concrete. Figure 6.2 shows a sample of the output of the three signal processing algorithms for the 1800 Hz signal measured at the beginning of the pipe string. It is noted that the equalized signal appears very strong compared to the unprocessed signal and to the other algorithms' outputs.

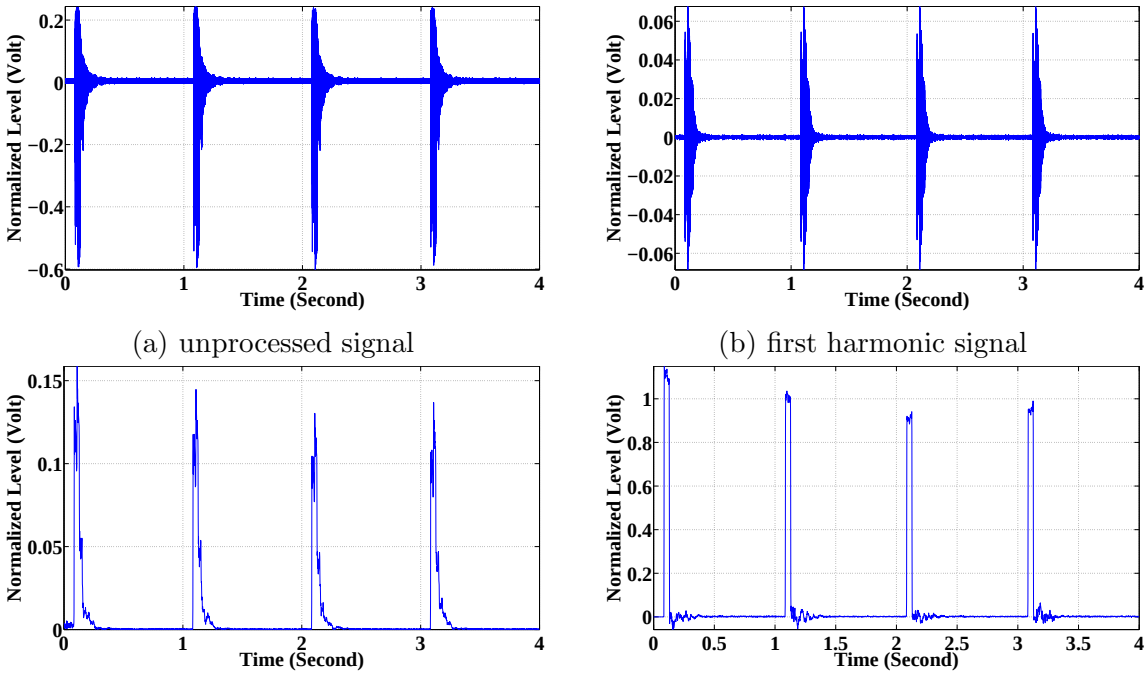

(a) unprocessed signal

(b) first harmonic signal

(c) harmonics combined signal

(d) equalized signal

Figure 6.2: Output of signal processing algorithms for the 1800 Hz signal measured at the beginning of the 7" pipe string

The SNR results are shown in Figure 6.3 for the 500 Hz signal. Obviously, the

equalized signal appears with the highest SNR values along the pipe string. In addition, the harmonics combined signal has a slightly lower SNR. It is interesting to see how the output of the third algorithm, first harmonic, appears with mixed results. In many instances, its SNR is lower than that of the unprocessed signal.

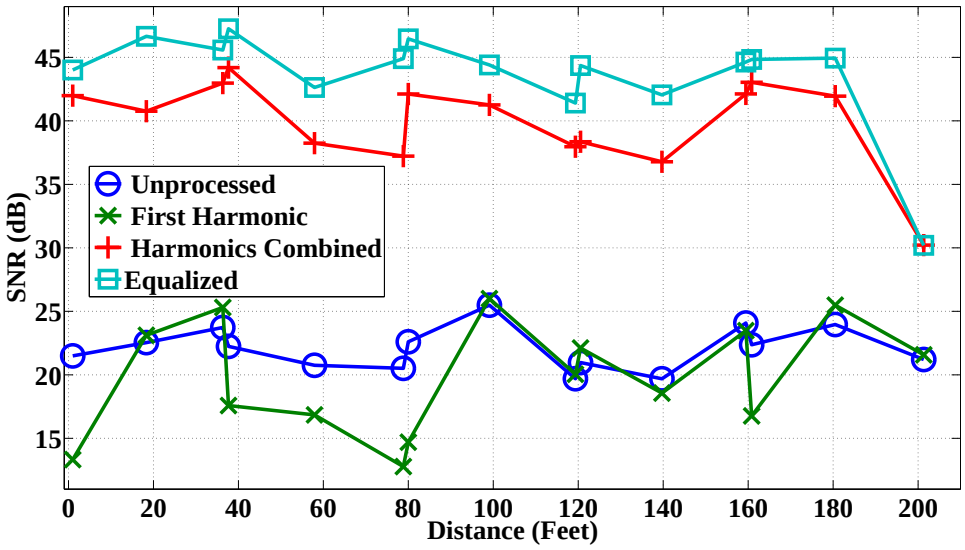

Figure 6.3: Signal-to-noise ratio of the 500 Hz signal under different signal processing algorithms measured over the 7" pipe string - no concrete case

The results for the 1000 Hz signal are shown in Figure 6.4. Both the equalization and harmonics combining algorithms produce superior results. On the other hand, compared to the 500 Hz signal, the first harmonic algorithm is producing an output that is, in most cases, greater than that of the unprocessed signal.

Figures 6.5 and 6.6 display the SNR values for the 1500 and 2000 Hz signals respectively. It is noted that the first harmonic algorithm is getting better with increasing the signal input frequency. On the other hand, both equalization and harmonic collection algorithms outperform the first harmonic algorithm.

The previous results emphasize the usefulness of the signal processing algorithms, especially the equalizer, in enhancing the SNR values for the measurements along

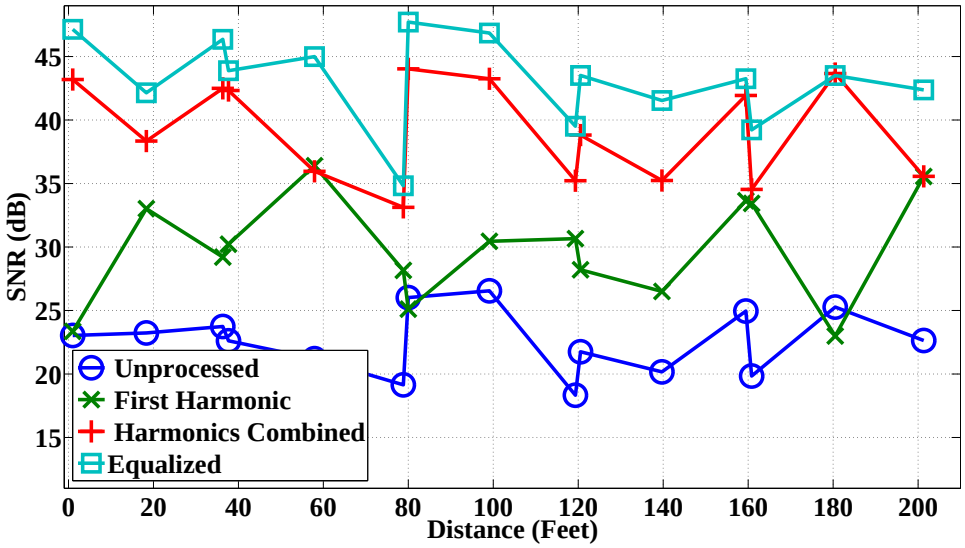

Figure 6.4: Signal-to-noise ratio of the 1000 Hz signal under different signal processing algorithms measured over the 7" pipe string - no concrete case

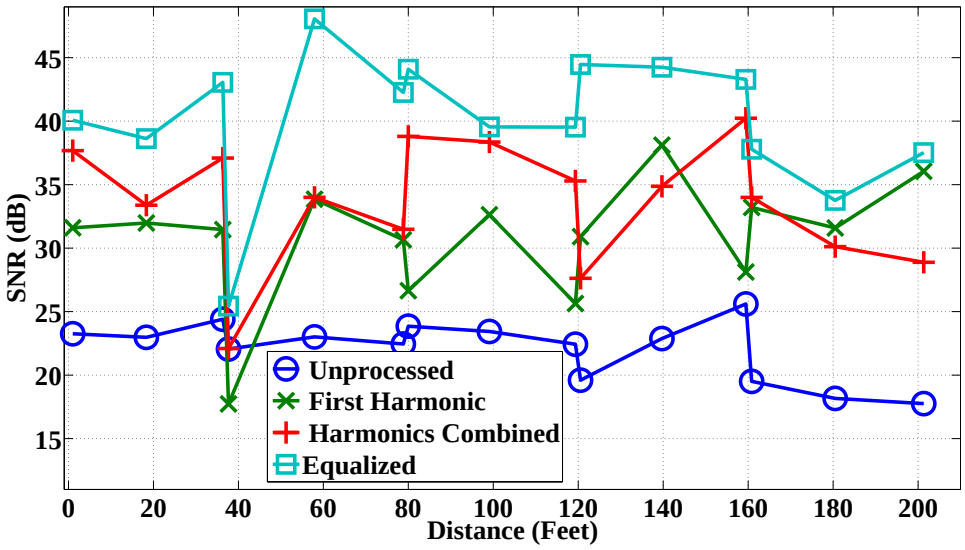

Figure 6.5: Signal-to-noise ratio of the 1500 Hz signal under different signal processing algorithms measured over the 7" pipe string - no concrete case

the pipe string.

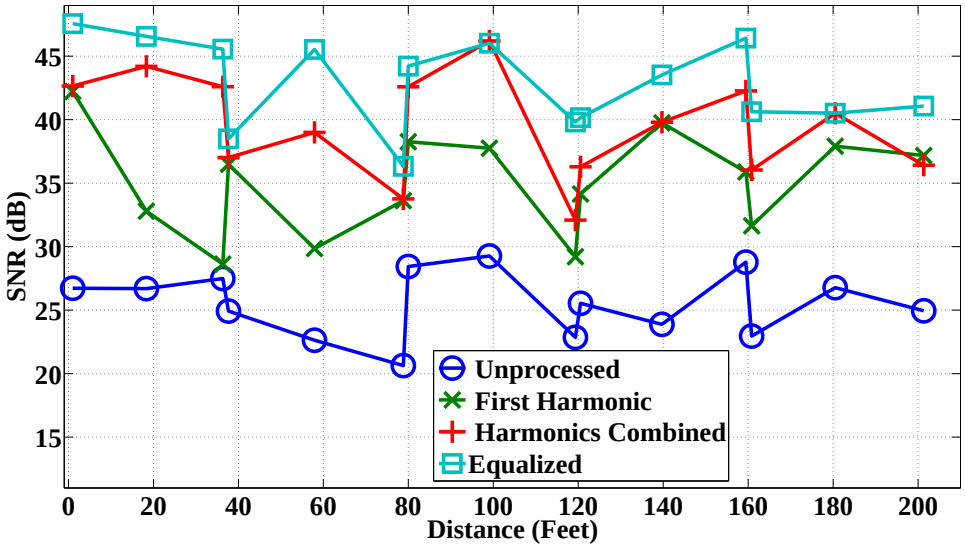

Figure 6.6: Signal-to-noise ratio of the 2000 Hz signal under different signal processing algorithms measured over the 7" pipe string - no concrete case

A detailed record of the SNR gain per input frequency is shown in Table 6.1. For signals with input frequencies of 700 Hz or less, the first harmonic algorithm is producing a loss in SNR values. Results, however, get better with increasing the input frequency. On the other hand, the other two algorithms provide higher, and more steady, gain in SNR for all input frequencies.

The average SNR gain for each algorithm is shown in Table 6.2. The equalization algorithm is producing about 19.7 dB in average SNR gain. The harmonic combined scheme's average SNR gain is about 15.7 dB, while the first harmonic's average gain is about 2.9 dB.

6.4 One Concrete Segment Case

The SNR results for the single concrete segment case are shown in this section. Figure 6.7 displays the SNR values along the pipe string for the 500 Hz signal. Although the unprocessed signal experiences a decline in its SNR values for the

Table 6.1: Signal-to-noise ratio gain of signal processing algorithms for the 7" pipe string - no concrete case

Frequency (Hz)	100	200	300	400	500
First Harmonic Average Gain (dB)	-5.6	-2.3	-5.6	-4.4	-2.2
Harmonics Combined Average Gain (dB)	18.0	19.6	15.9	15.4	17.9
Equalizer Average Gain (dB)	19.6	22.8	20.7	20.6	21.5
Frequency (Hz)	600	700	800	900	1000
First Harmonic Average Gain (dB)	-5.8	-1.9	3.3	3.9	7.2
Harmonics Combined Average Gain (dB)	18.9	16.3	18.0	19.2	16.6
Equalizer Average Gain (dB)	22.3	20.4	21.3	22.9	20.6
Frequency (Hz)	1100	1200	1300	1400	1500
First Harmonic Average Gain (dB)	8.3	4.5	5.6	5.2	8.6
Harmonics Combined Average Gain (dB)	16.8	14.4	13.0	14.1	11.5
Equalizer Average Gain (dB)	19.4	18.0	18.9	17.5	18.0
Frequency (Hz)	1600	1700	1800	1900	2000
First Harmonic Average Gain (dB)	8.5	6.1	10.1	5.8	9.5
Harmonics Combined Average Gain (dB)	12.1	12.0	13.8	16.5	13.9
Equalizer Average Gain (dB)	17.8	17.3	17.7	18.8	17.3

Table 6.2: Average signal-to-noise ratio gain as a result of using signal processing algorithms over the unprocessed signals for the 7" pipe string - no concrete case

Algorithm	Average Gain (dB)
First Harmonic	2.9
Harmonics Combined	15.7
Equalizer	19.7

measurements taken beyond the concrete segment, the equalization and harmonics combined algorithm show more steady SNR values.

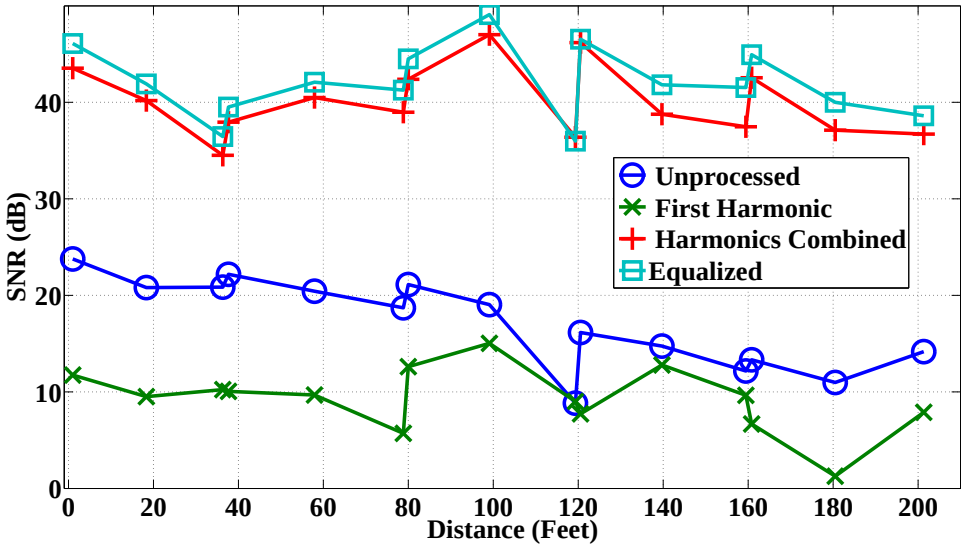

Figure 6.7: Signal-to-noise ratio of the 500 Hz signal under different signal processing algorithms measured over the 7" pipe string - one concrete segment case

The results for the 1000 Hz signal are shown in Figure 6.8. The interesting observation here is the poor performance of the first harmonic algorithm for the measurements taken beyond the concrete segment. Because of the filtering effect the concrete has, the fundamental harmonic is severely attenuated in many measurements. Accordingly, that algorithm will likely generate low-SNR results as seen in this figure.

The SNR results for the 1500 Hz signal are shown in Figure 6.9, while Figure 6.10 displays the results for the 2000 Hz signal. It is noted that because the unprocessed signals enjoy a relatively high SNR, the outputs of the three signal processing algorithms have a strong SNR gain.

It is noted from these figures that the higher the SNR values of the unprocessed signal, especially for the measurements taken beyond the concrete segment, the stead-

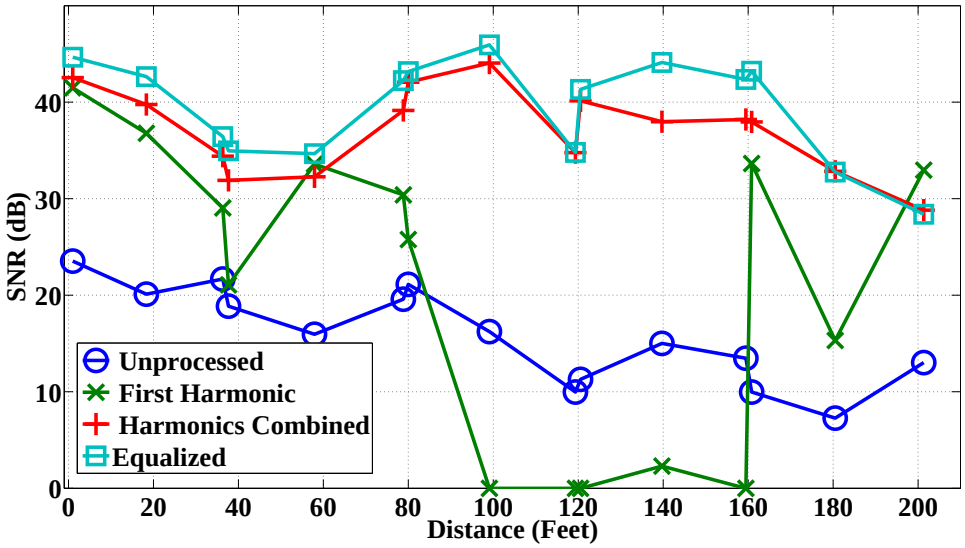

Figure 6.8: Signal-to-noise ratio of the 1000 Hz signal under different signal processing algorithms measured over the 7" pipe string - one concrete segment case

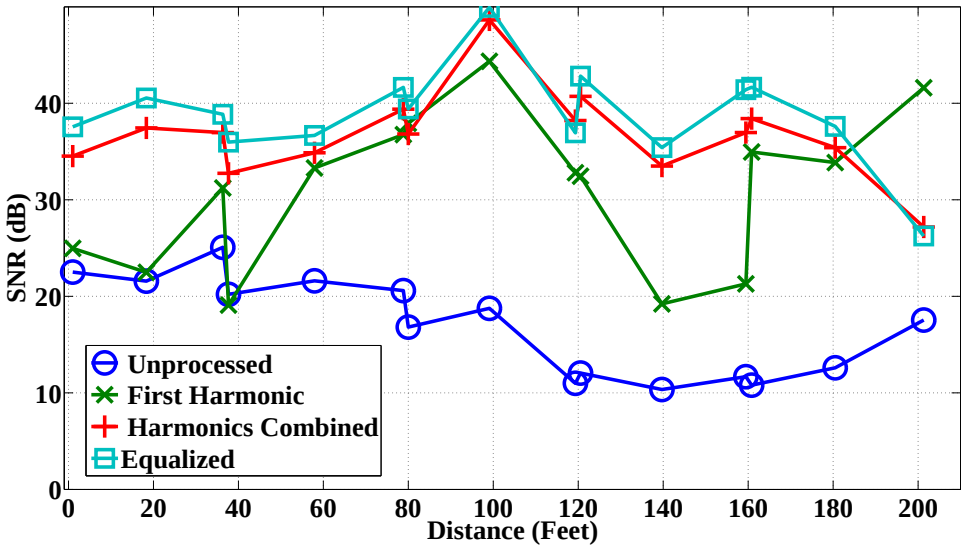

Figure 6.9: Signal-to-noise ratio of the 1500 Hz signal under different signal processing algorithms measured over the 7" pipe string - one concrete segment case

ier and higher SNR gains the signal processing algorithms can provide.

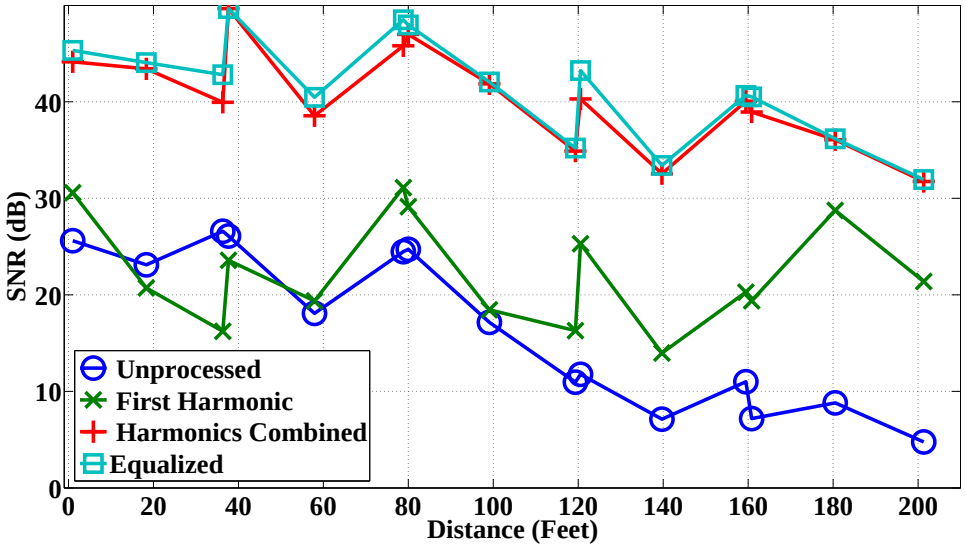

Figure 6.10: Signal-to-noise ratio of the 2000 Hz signal under different signal processing algorithms measured over the 7" pipe string - one concrete segment case

Table 6.3 includes a record of the SNR gain of the three signal processing algorithms per input frequency. As noted, the first harmonic algorithm produces a loss in SNR for the signals with low input frequency. The performance gets better, in general, with increasing the input frequency of the acoustic waves. On the other hand, the other two algorithms enjoy better SNR gain results, especially for signals with high input frequencies.

The average SNR gain for each algorithm is shown in Table 6.4. The equalization algorithm has a gain around 22 dB over the unprocessed signals. The SNR gain of the harmonic combined algorithm is about 20.4 dB, while the first harmonic algorithm has a gain of only 4.6 dB.

6.5 Two Concrete Segments Case

The goal of this section is to investigate the usefulness of using the signal processing algorithms when the level of the acoustic signals is very low as was seen in

Table 6.3: Signal-to-noise ratio gain of signal processing algorithms for the 7" pipe string - one concrete segment case

Frequency (Hz)	100	200	300	400	500
First Harmonic Average Gain (dB)	-3.1	-3.5	-10.3	-5.7	-7.8
Harmonics Combined Average Gain (dB)	15.1	16.7	15.3	14.4	22.9
Equalizer Average Gain (dB)	14.4	18.0	17.2	14.7	24.9
Frequency (Hz)	600	700	800	900	1000
First Harmonic Average Gain (dB)	-6.6	0.5	12.5	15.0	4.3
Harmonics Combined Average Gain (dB)	18.0	20.4	25.0	21.9	21.3
Equalizer Average Gain (dB)	19.3	21.9	25.8	23.4	23.6
Frequency (Hz)	1100	1200	1300	1400	1500
First Harmonic Average Gain (dB)	3.8	12.1	12.8	12.4	14.2
Harmonics Combined Average Gain (dB)	22.1	22.4	23.3	19.4	19.9
Equalizer Average Gain (dB)	24.6	23.9	26.0	22.0	22.0
Frequency (Hz)	1600	1700	1800	1900	2000
First Harmonic Average Gain (dB)	11.5	8.9	7.7	7.7	5.8
Harmonics Combined Average Gain (dB)	21.3	22.4	20.1	21.4	23.8
Equalizer Average Gain (dB)	23.7	24.7	22.4	23.2	25.0

Table 6.4: Average signal-to-noise ratio gain as a result of using signal processing algorithms over the unprocessed signals for the 7" pipe string - one concrete segment case

Algorithm	Average Gain (dB)
First Harmonic	4.6
Harmonics Combined	20.4
Equalizer	22.0

Chapter 5 for the two concrete segments setup. Figure 6.11 displays the SNR values of the signal processing algorithms along with that of the unprocessed measurements for the 500 Hz signal. It is noted that the equalization and the harmonic combining algorithms provide comparable performance. On the other hand, the results of the first harmonic algorithm are worse than that of the unprocessed signal for the measurements taken beyond the concrete segments.

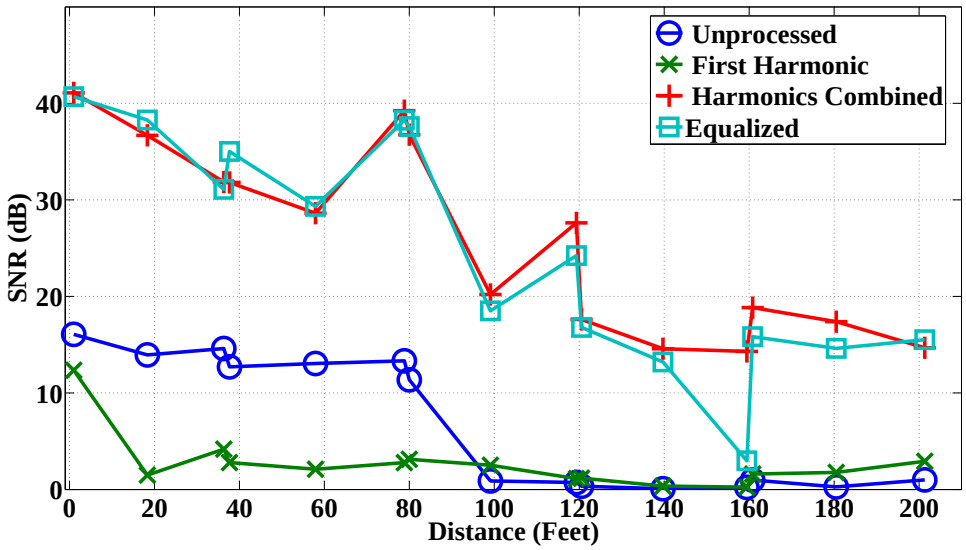

Figure 6.11: Signal-to-noise ratio of the 500 Hz signal under different signal processing algorithms measured over the 7" pipe string - two concrete segments case

Figure 6.12 shows the SNR results for the 1000 Hz signal. The decline of performance is noted for the equalization and the harmonics combined algorithms for the measurements recorded beyond the concrete segments. On the other hand, the first harmonic algorithm has a poor performance along the pipe string.

The results for the 1500 and 2000 Hz measurements are seen in Figures 6.13 and 6.14. It is obvious that the harmonics combined algorithm has slightly better results than that of the equalization algorithm.

The performance of the equalization and the harmonic combined algorithms pro-

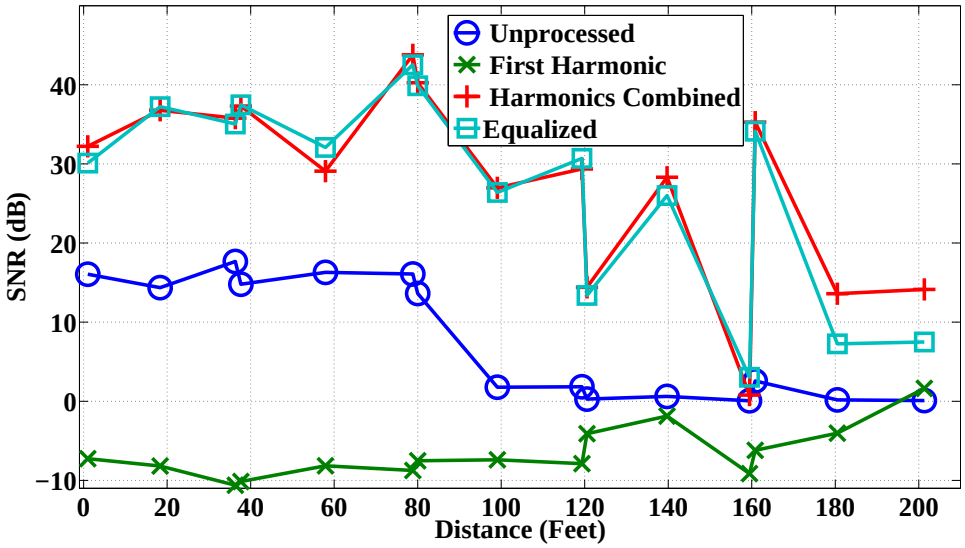

Figure 6.12: Signal-to-noise ratio of the 1000 Hz signal under different signal processing algorithms measured over the 7" pipe string - two concrete segments case

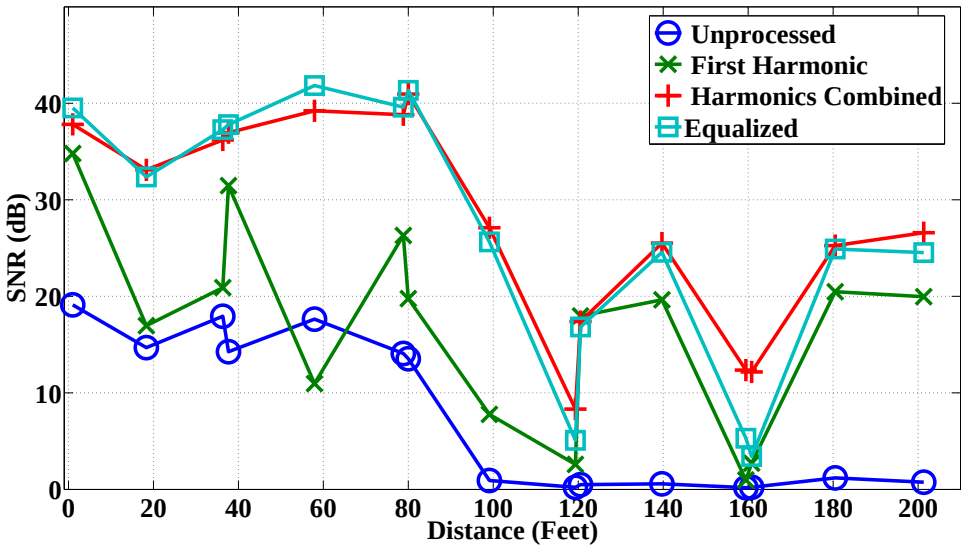

Figure 6.13: Signal-to-noise ratio of the 1500 Hz signal under different signal processing algorithms measured over the 7" pipe string - two concrete segments case

vide a substantial SNR gain over that of the unprocessed measurements. However, the SNR curves decline sharply for the measurements taken beyond the concrete segments. Apparently, if the measurements incur a substantial attenuation due to the presence of the concrete segments, the gain the signal processing algorithms can provide becomes limited.

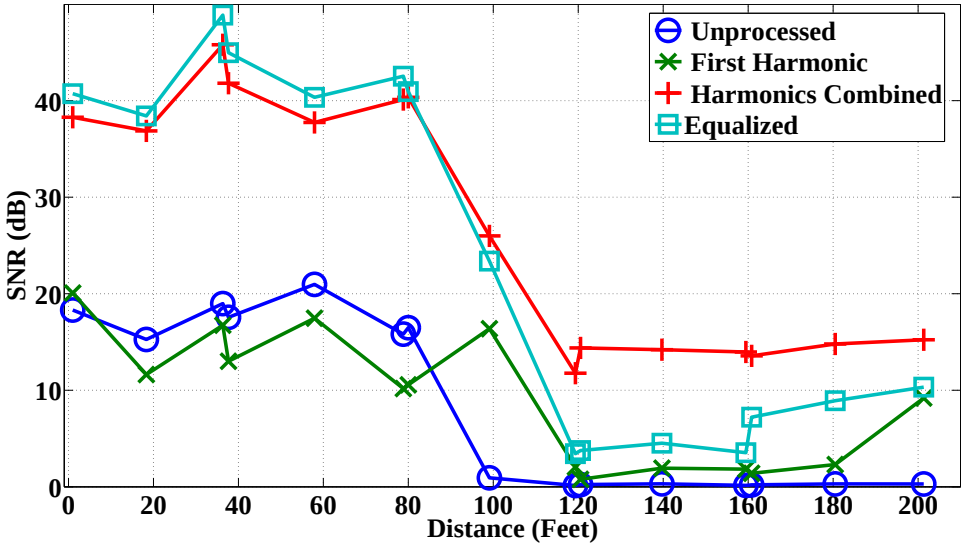

Figure 6.14: Signal-to-noise ratio of the 2000 Hz signal under different signal processing algorithms measured over the 7" pipe string - two concrete segments case

Table 6.5 details the SNR gain results for each signal processing algorithm per input frequency. The poor performance of the first harmonic algorithm is obvious from this table.

Finally, Table 6.6 lists the average gain for the three signal processing algorithms. As expected, the first harmonic algorithm has a substantial loss against the unprocessed measurements; the average loss in SNR values is around 8.4 dB. On the other hand, the equalization algorithm provided an average SNR gain of 16.1 dB which was about 1.7 dB less than that of the harmonics combined algorithm.

Table 6.5: Signal-to-noise ratio gain of signal processing algorithms for the 7" pipe string - two concrete segments case

Frequency (Hz)	100	200	300	400	500
First Harmonic Average Gain (dB)	-0.9	-2.2	-3.1	-3.4	-3.9
Harmonics Combined Average Gain (dB)	16.1	16.4	16.3	15.0	19.4
Equalizer Average Gain (dB)	13.2	13.6	14.3	13.8	18.2
Frequency (Hz)	600	700	800	900	1000
First Harmonic Average Gain (dB)	-3.6	-3.7	-1.5	6.1	-14.4
Harmonics Combined Average Gain (dB)	16.8	17.2	17.2	19.1	20.1
Equalizer Average Gain (dB)	14.2	14.5	15.4	17.0	19.1
Frequency (Hz)	1100	1200	1300	1400	1500
First Harmonic Average Gain (dB)	-187.3	7.0	5.0	5.9	9.2
Harmonics Combined Average Gain (dB)	18.9	19.7	18.1	18.3	20.1
Equalizer Average Gain (dB)	17.7	18.7	16.8	16.0	18.9
Frequency (Hz)	1600	1700	1800	1900	2000
First Harmonic Average Gain (dB)	6.0	8.3	7.0	1.1	0.6
Harmonics Combined Average Gain (dB)	17.3	19.4	17.3	15.4	18.6
Equalizer Average Gain (dB)	16.2	16.8	17.3	14.6	15.7

Table 6.6: Average signal-to-noise ratio gain as a result of using signal processing algorithms over the unprocessed signals for the 7" pipe string - two concrete segments case

Algorithm	Average Gain (dB)
First Harmonic	-8.4
Harmonics Combined	17.8
Equalizer	16.1

7. Channel Impulse Response

This chapter investigates the impulse response of the acoustic channel for the cemented 7" pipe string. Section 7.1 explains the difference between this experiment and the work in Chapter 5. Section 7.2 displays the results of this experiment; power delay profile, power spectral density, signal-to-noise ratio, and delay spread measures are investigated.

7.1 Testbed Setup

The impulse input signal to the acoustic transmitter in this setup is a voltage signal controlled by a function generator. The function generator creates a 200 microsecond square signal (i.e., the input impulse signal), which repeats every second. This signal is fed to the acoustic tool, and the transmitter generates the acoustic waves accordingly.

Extensive propagation experiments were conducted on this system to find the channel impulse response as a function of the propagation distance. Signal measurements were taken at the beginning, middle, and end of each pipe segment. In each measurement, five bursts were recorded. Afterward, the accelerometer would be disconnected from the pipe string and then reconnected again to make two more independent measurements.

7.2 Measurement Results

The impulse response propagation results are shown in this section. The impulse response is shown in Figure 7.1 for measurements made at the beginning of the pipe string, before and after the concrete segments, and at the end of the pipe string. The two obvious observations from this figure are the enormous attenuation and the

dispersion the acoustic waves undergo after passing through the concrete segments.

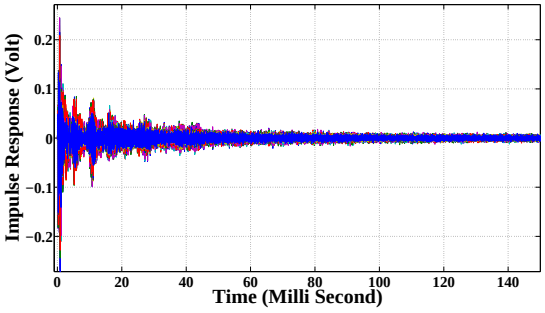

(a) beginning of the pipe string

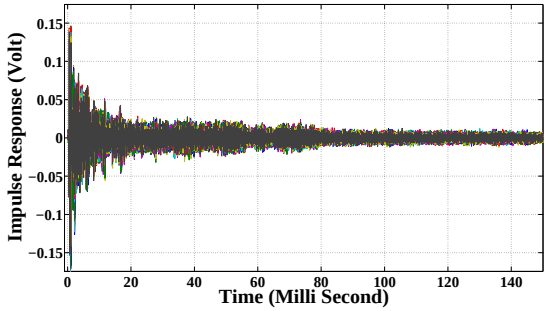

(b) 80 feet away (just before the first concrete segment)

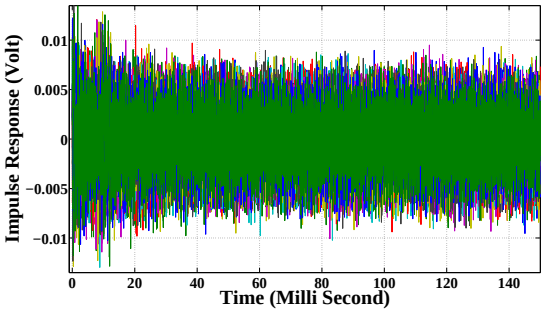

(c) 120 feet away (just after the second concrete segment)

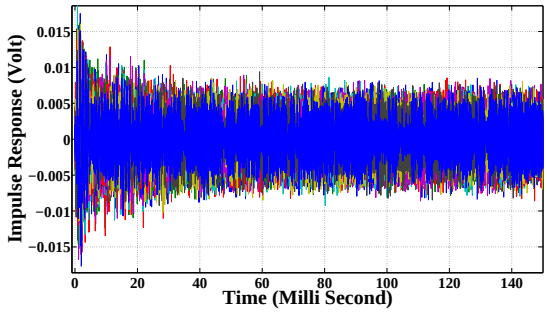

(d) 200 feet away

Figure 7.1: Channel impulse response measured over the 7" pipe string - two concrete segments case

Figure 7.2 shows the normalized power delay profile of the impulse response for the measurements described at Figure 7.1. For the measurement taken at the beginning of the pipe string, it is noted that the channel response extends over a duration of about 40 milliseconds, which is far longer than the impulse actual duration (0.2 milliseconds). Channel multipaths are believed to cause the spread of the channel impulse response at this early stage in the pipe string. In addition, the figure displays the same measures for the channel response measurement taken at the end of the pipe string. It is obvious that the signal energy extends over a longer duration compared to that at the beginning of the pipe string. Because this reading was taken beyond the concrete segment, the effect of concrete is very obvious

in smearing out the acoustic signal.

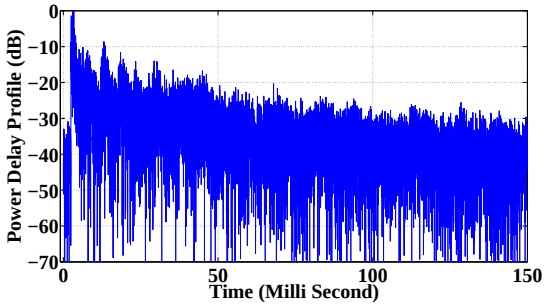

(a) beginning of the pipe string

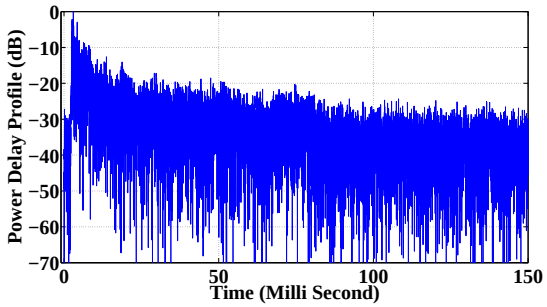

(b) 80 feet away (just before the first concrete segment)

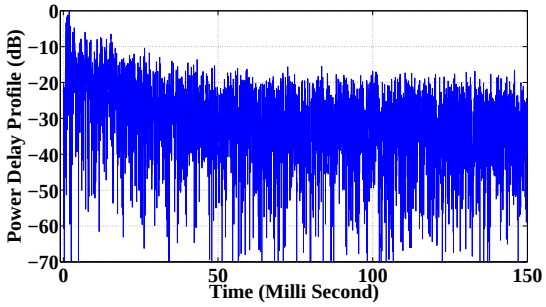

(c) 120 feet away (just after the second concrete segment)

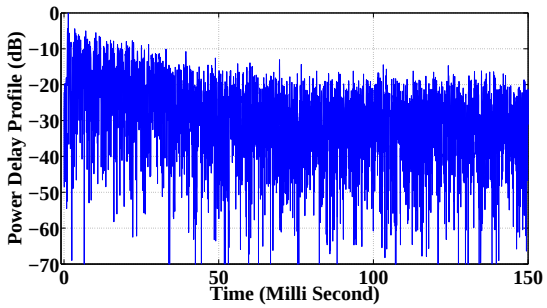

(d) 200 feet away

Figure 7.2: Power delay profile of the channel impulse response measured over the 7" pipe string - two concrete segments case

The power spectral density of the channel impulse response is shown in Figure 7.3. It is noted that the channel impulse response contains frequency components from 700 Hz up to 20 kHz when it was measured at the beginning of the pipe string. As the acoustic wave propagates down the pipe string, high frequency content seems to decay more rapidly than the low frequency content. Most of the energy of the signal measured just before the concrete segment seems to be contained in a lower frequency range (i.e., 700 Hz – 11 kHz). On the other hand, for the measurements taken beyond the concrete segment, it is noted that most of the available energy is available in the 700 Hz – 2.5 kHz frequency band. It is thought that the concrete effect on the propagation of the acoustic wave is like a filter whose bandwidth depends

on the length and thickness of the concrete segment.

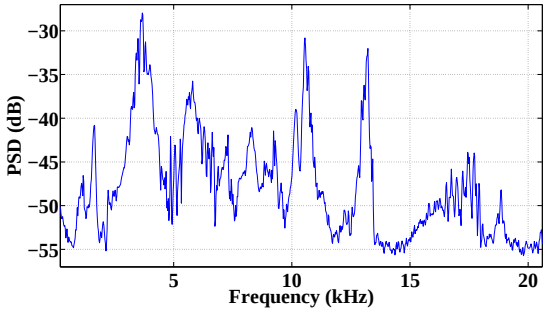

(a) beginning of the pipe string

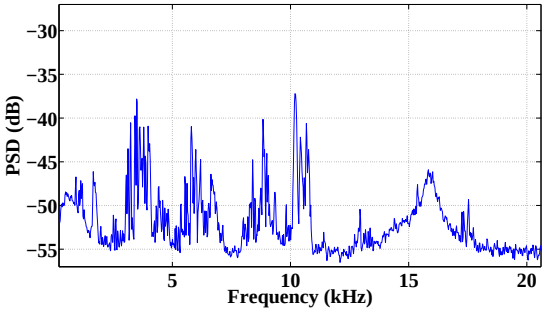

(b) 80 feet away (just before the first concrete segment)

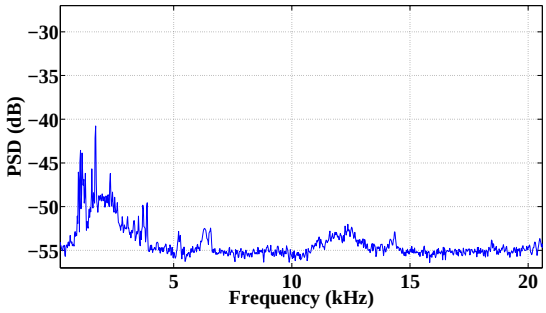

(c) 120 feet away (just after the second concrete segment)

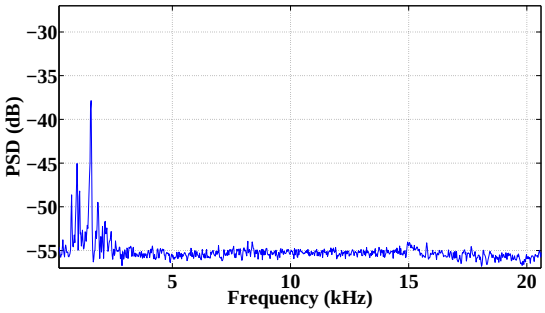

(d) 200 feet away

Figure 7.3: Power spectral density of the channel impulse response measured over the 7" pipe string - two concrete segments case

Figure 7.4 displays the SNR values of the channel impulse response along the pipe string. It is noted that the measured channel response does not experience a notable decay for the measurements taken before the concrete segments. However, the concrete effect is obvious for the readings taken beyond the concrete segments. The channel impulse response readings experience a noticeable attenuation as the SNR value decreases rapidly. Consequently, acoustic signal propagation is very limited beyond the concrete segment. It is obvious from these results that the concrete segment is heavily attenuating the acoustic signal; this behavior occurred because the acoustic waves propagate from one point to another by vibrating the pipe string. The presence of concrete over part of the string makes it more difficult to vibrate

the pipe string. Accordingly, acoustic waves are attenuated.

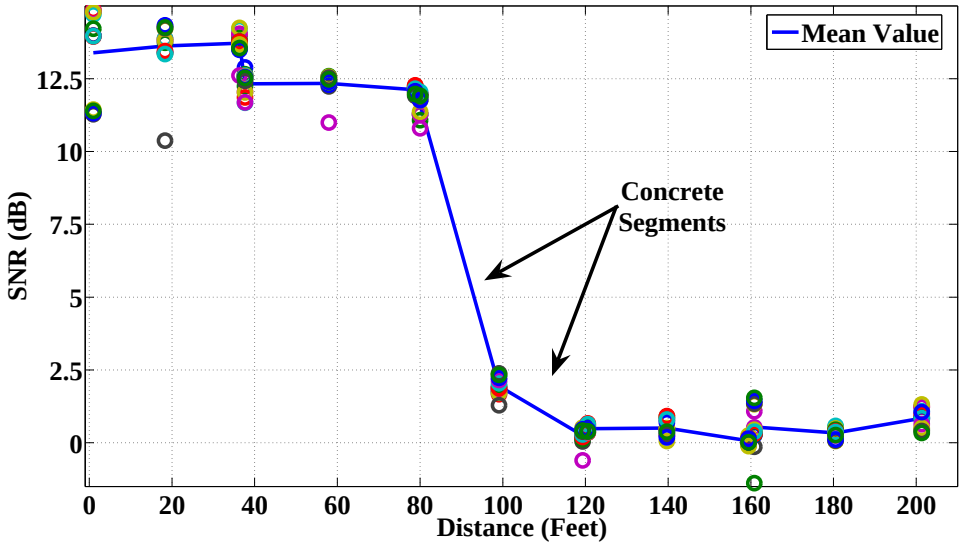

Figure 7.4: Signal-to-noise ratio of the channel impulse response measured over the 7" pipe string - two concrete segments case

Figures 7.5, 7.6, 7.7, and 7.8 show the delay spread measures of the channel impulse response measurements. As obvious from these results, the acoustic waves experience dispersion while propagating though the pipe string, with mean excess delay of around 17 milliseconds and RMS delay spread of around 27 milliseconds for the measurements taken before the concrete segment. Comparing these values to the actual duration of the impulse signal (i.e., 0.2 milliseconds) gives an indication of the severity of the dispersion in the channel. This severe dispersion is believed to be, at least in part, due to the multipath reflections in the pipe string. Because of the presence of the pipe joints that have higher acoustic impedance than the rest of the pipe body, the variations in the acoustic impedance along the pipe string will cause multiple reflections and/or transmissions of the acoustic energy.

For the measurements taken beyond the concrete segment, signal dispersion is very obvious. In this case, the mean excess delay appears to be around 68 millisec-

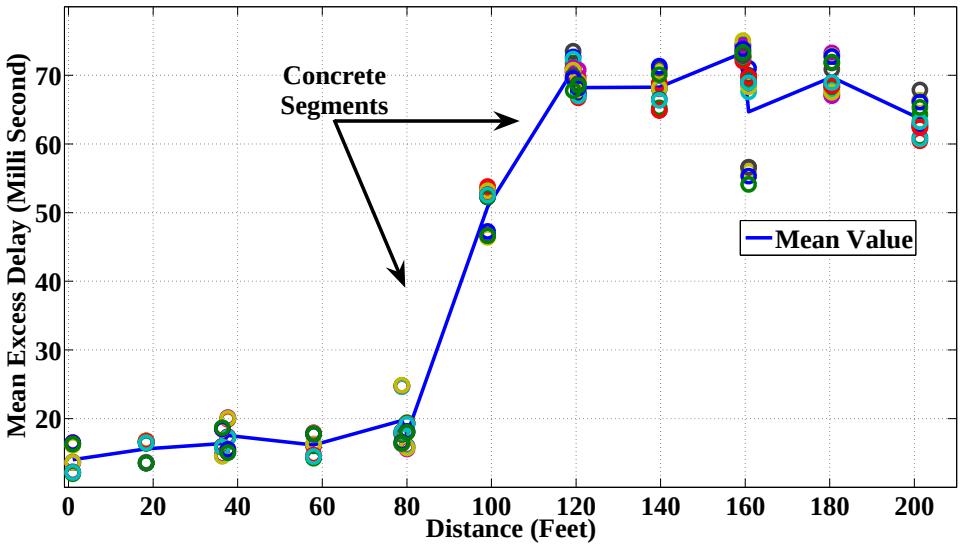

Figure 7.5: Mean excess delay of the channel impulse response measured over the 7" pipe string - two concrete segments case

onds, RMS delay spread around 45 milliseconds, and maximum excess delay (10 dB) is around 340 milliseconds. It is thought that in addition to the multipath reflections in the acoustic channel, the concrete segment filters out most of the signal frequency content. This will smear out the acoustic waves; consequently, the delay spread measures will show larger dispersion values. In addition, the low values of the coherence bandwidth indicate that the pipe string, when used as a transmission medium, appears as a frequency selective channel. Accordingly, different frequency components of the acoustic wave are expected to experience an uncorrelated fading. This result suggests that an equalizer is beneficial for this setup to reduce the effects of channel distortion and signal dispersion.

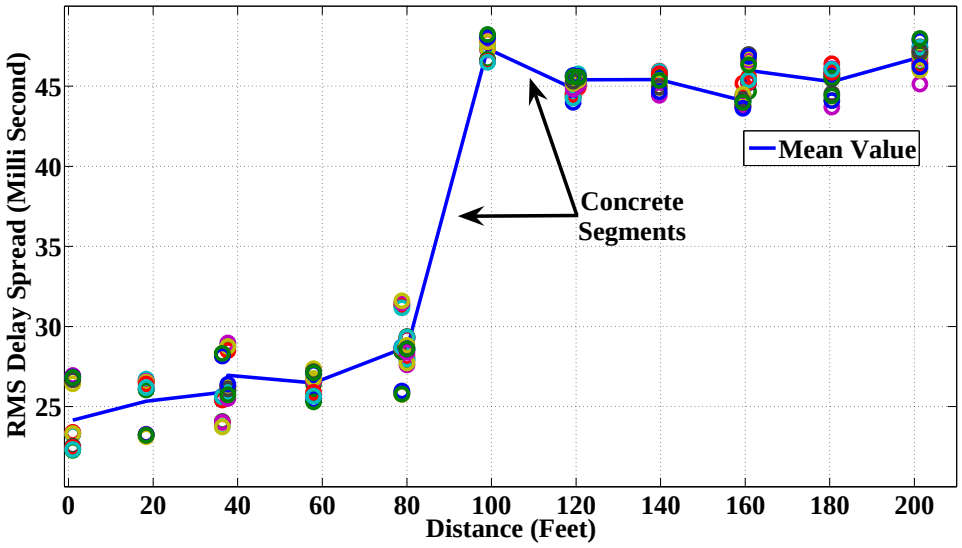

Figure 7.6: RMS delay spread of the channel impulse response measured over the 7" pipe string - two concrete segments case

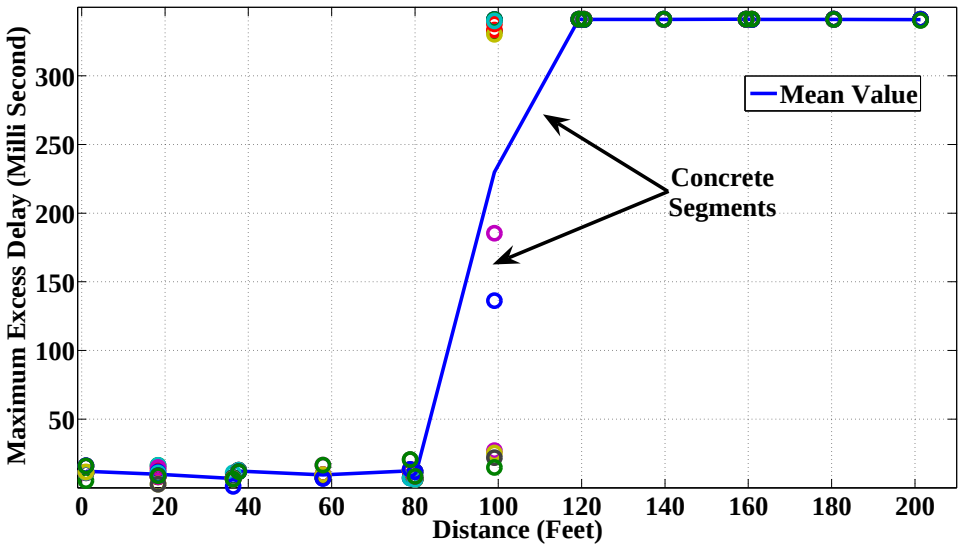

Figure 7.7: Maximum excess delay (10 dB) of the channel impulse response measured over the 7" pipe string - two concrete segments case

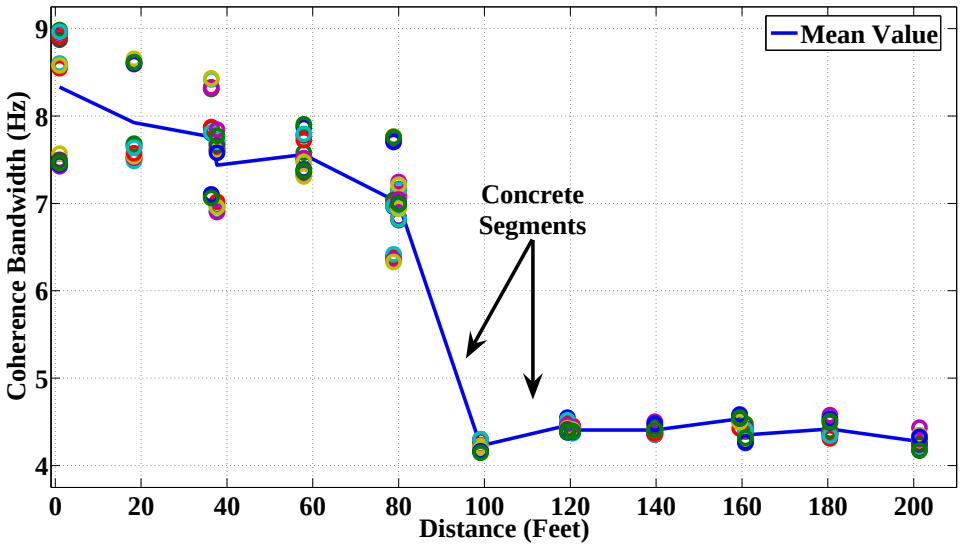

Figure 7.8: Coherence bandwidth of the channel impulse response measured over the 7" pipe string - two concrete segments case

8. Sound Wave Propagation Inside Pipe String

This chapter describes a testbed that was designed to study the propagation aspects of sound waves inside the interior of the production pipes. Section 8.1 motivates the work in this chapter. Section 8.2 describes the testbed setup. Finally, Section 8.3 includes the propagation results of this setup.

8.1 Introduction

The results of the previous chapters illustrated the severity of the impact the concrete has on the propagation of the acoustic waves that propagate though vibrating the body of the pipe string. In order to find an alternative to conducting communications through vibrating the production tubing when there is a concrete segment, this work studies the propagation of sound waves inside production tubings.

Because sound represents a longitudinal wave motion, the linear, lossless, acoustic wave equation can be expressed as [13, 14, 15, 16]

$$\nabla^2 P = \frac{1}{c^2}\frac{\partial^2 P}{\partial t^2} \tag{8.1}$$

where ∇^2 is the Laplace operator, P denotes the acoustic pressure, t is the time variable, and c is the phase speed of sound. At 0°C and 1 atmospheric pressure, the speed of sound in dry air is about 331 m/sec, and about 5790 m/sec in stainless steel, and 1402 m/sec in pure water [15].

For a circular pipe and using the cylindrical coordinates (r, θ, z), the wave equation becomes [16]

$$\frac{\partial^2 P}{\partial r^2} + \frac{1}{r}\frac{\partial P}{\partial r} + \frac{1}{r^2}\frac{\partial^2 P}{\partial \theta^2} + \frac{\partial^2 P}{\partial z^2} + k^2 P = 0 \tag{8.2}$$

Assuming a harmonic solution and using separation of variables method, a solution to Eq. (8.2) looks like [16]

$$P(r, \theta, z, t) = AJ_0(k_r r)cos(m\theta + \gamma)e^{jk_z z}e^{j\omega t} \tag{8.3}$$

where J_0 is the zeroth Bessel function of the first kind, γ and A are arbitrary constants, and ω is the angular frequency. Moreover, k_r and k_z are related as

$$(\omega/c)^2 = k_r^2 + k_z^2 \tag{8.4}$$

The expected advantage of measuring the sound waves inside the pipe string instead of measuring the vibrations over the pipe string is that the sound waves will not have to interact with concrete; accordingly, one would not expect to see any decay due to the concrete segments in this setup.

8.2 Testbed Setup

Sound wave propagation inside the interior of the pipe string is studied in this setup. The sound wave is generated using a speaker and received using a microphone. An illustration of the experiment setup is shown in Figure 8.1.

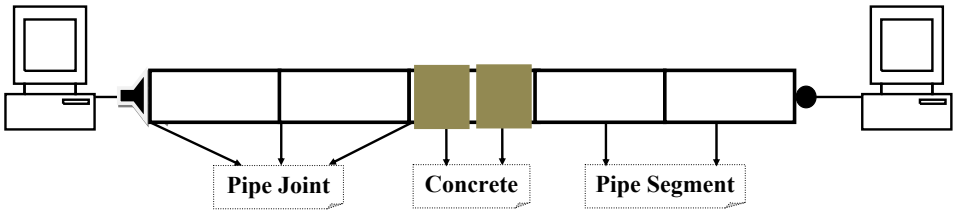

Figure 8.1: Testbed block diagram

A computer program was used in the transmitter side to generate signals that will be fed to the speaker. Twenty different frequencies (100, 200, 300, . . . , 2000 Hz)

were generated for each measurement. A 500 milliseconds signal was generated for each frequency followed by a silence period for another 500 milliseconds. So the generated signal would go like this: 100 Hz signal for 500 ms, followed by 500 ms of silence period, which is followed by 200 Hz signal for 500 ms, and so on till the end of the 2000 Hz signal. The speaker was positioned at the beginning of pipe string.

On the receiver side, a microphone was used to pick the sound wave and transform it into an electrical one. The output of the microphone connects to a computer sound card that works as a data acquisition card with a sampling rate of 44.1 kHz. Finally, a MATLAB application was developed to capture, display, and save the measurements received through the sound card. The microphone was inserted inside the pipe string itself, so the measurements examine the sound wave propagation inside the pipe string. The microphone was made as directive, in the direction of the speaker, as possible by surrounding it with a cone-shape plastic cover.

Measurements were taken all over the pipe string, and successive measurements were recorded 10 feet apart. The first measurement point was 5 feet way from the speaker, the second point was 15 feet away from the speaker (i.e., 10 feet away from the first point), and so on.

8.3 Measurement Results

Figure 8.2 shows the measured signals in different locations over the pipe string. The minimal difference between the measurements made just before and after the concrete segments can be noted; this proves that concrete has little effect on acoustic signal propagation inside the pipe string. In general, one can see that the 300 Hz and 400 Hz signals appear strong all over the pipe. It also appears that the high frequency signals decay, in general, faster than the lower frequency signals.

The power spectral density of the measurements mentioned in Figure 8.2 is dis-

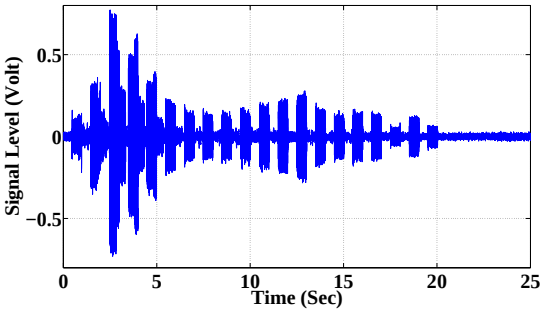

(a) beginning of the pipe string

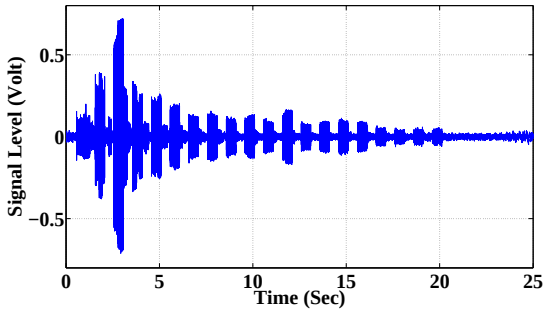

(b) 85 feet away (beginning of the first concrete segment)

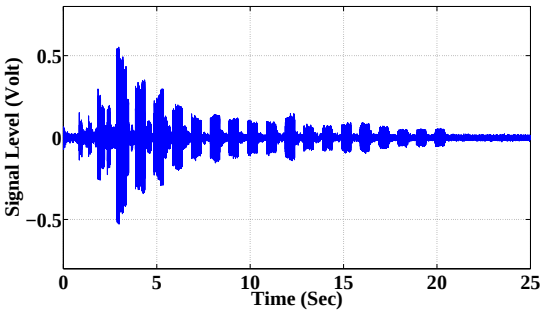

(c) 125 feet away (end of the second concrete segment)

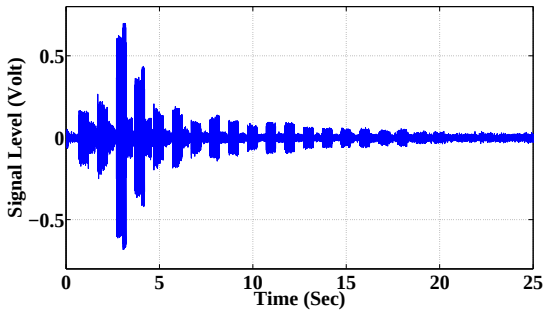

(d) 205 feet away

Figure 8.2: Signal level of the sound wave propagating inside the 7" pipe string

played in Figure 8.3. All frequencies appear strong all over the pipe string. In addition, due to the lack of any found harmonics, there is no indication of any nonlinearity in the channel. As the sound wave propagates down the pipe string, high-frequency content seems to decay a little more rapidly than the low-frequency content.

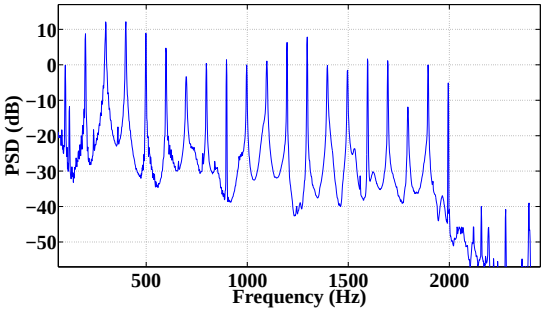

(a) beginning of the pipe string

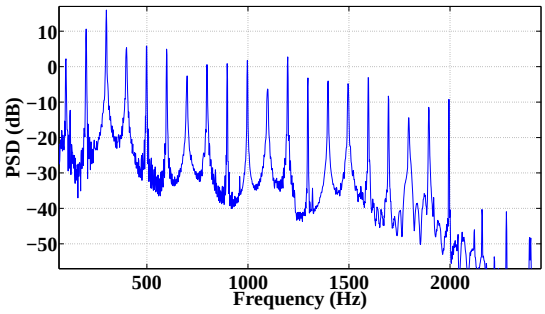

(b) 85 feet away (beginning of the first concrete segment)

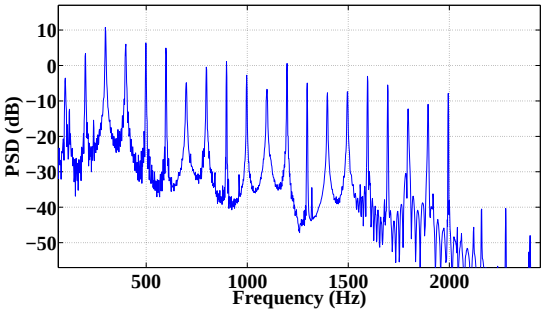

(c) 125 feet away (end of the second concrete segment)

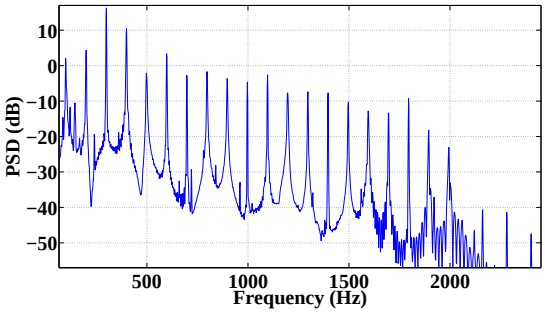

(d) 205 feet away

Figure 8.3: Power spectral density of the sound wave propagating inside the 7" pipe string

Figure 8.4 displays the SNR of the measurements taken along the pipe string. By comparing the SNR at the beginning and at the end of the pipe string, it appears that some of the signals experience little, if any, decay as the waves progress further down the pipe string. It is also obvious that different frequencies decay in a slightly different manner inside the pipe string. In addition, it is noted that the generated power of the sound wave depends on its input frequency.

The figure shows that some frequencies have very little decay; this includes the 100, 300, 800, and 900 Hz signals. On the other hand, the 1300, 1600, 1700, 1900, and 2000 Hz signals experience the highest attenuation. Fortunately, one can see from the figure that the presence of concrete, which lies over the third pipe segment (i.e., about 80–120 feet away from the transmitter), has no effect on the SNR values for any of the measurements.

From the previous results, Figure 8.5 displays the SNR decay rate per 1000 feet for each tested frequency. The general trend here is that the lower frequencies propagate better (i.e., they have a smaller decay rate) than the higher-frequency signals. In particular, it appears that if a sound wave with a frequency around 300 Hz is used to communicate inside the pipe string, this signal will decay at a rate of less than 8 dB per 1000 feet; consequently, one expects to be able to reliably communicate over a distance of few thousands feet before a repeater is needed.

Figure 8.6 displays the mean excess delay results for this experiment. It is found that the average value of the mean excess delay for all measured signals is around 288 ms, which is about 7.6% higher than that of the input signal. It is also found that the average value of the mean excess delay increases as the sound wave propagates down the pipe string at a rate around 13.6 ms per 1000 feet.

The average value of the mean excess delay measure is shown for each frequency in Figure 8.7 and for each measurement point in Figure 8.8. It is obvious that most of the frequencies have comparable results. It is noted that only the 100 Hz signal experiences a slightly higher dispersion with an average value of the mean excess delay around 332 ms, which is about 33% higher than the mean excess delay of the input 500 ms signal. On the other hand, the average value of the mean excess delay measure seems not to change along the pipe string as shown in Figure 8.8. This results emphasizes the previous conclusions that the concrete segments have no

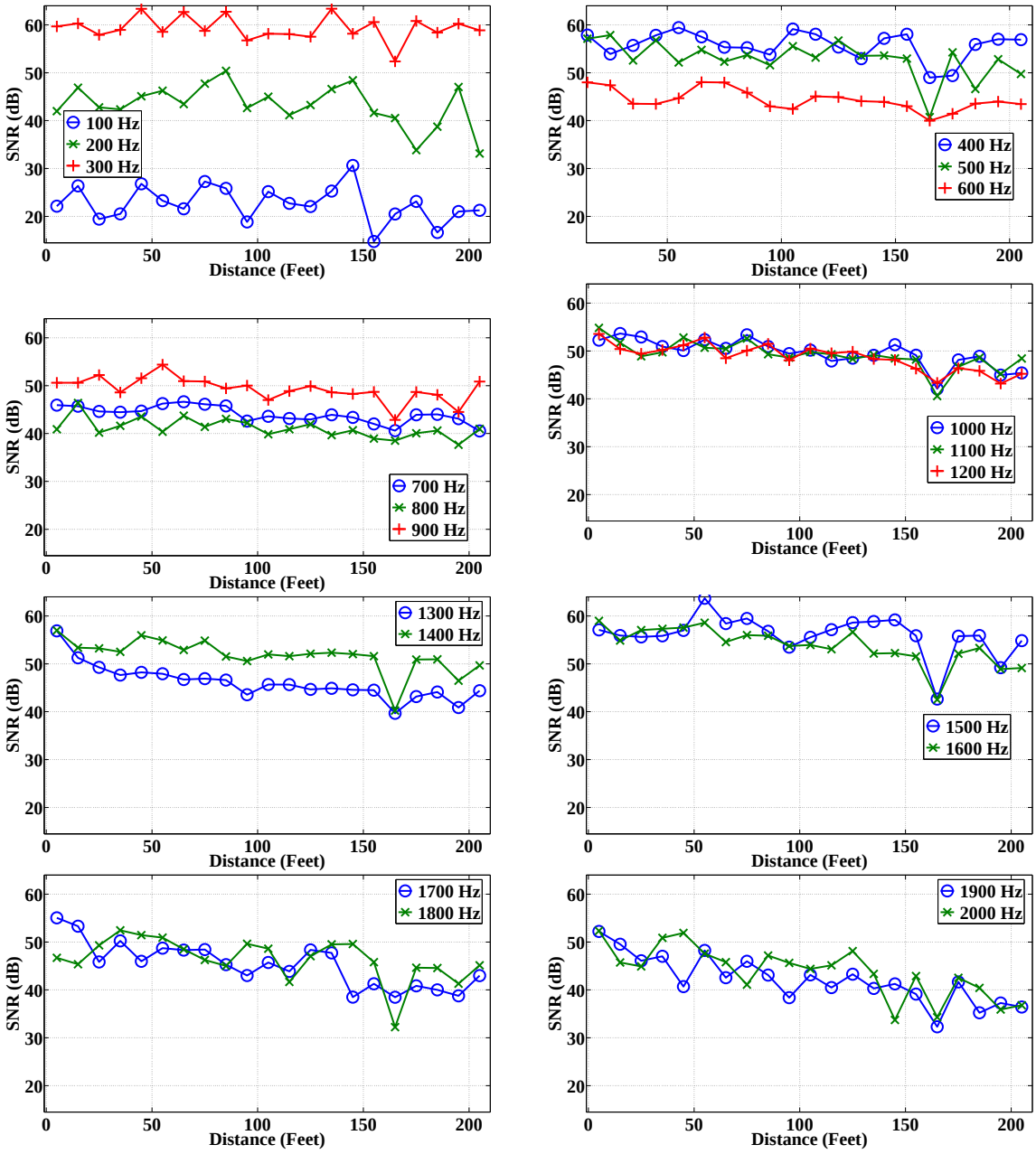

Figure 8.4: Signal-to-noise ratio of the sound wave propagating inside the 7" pipe string

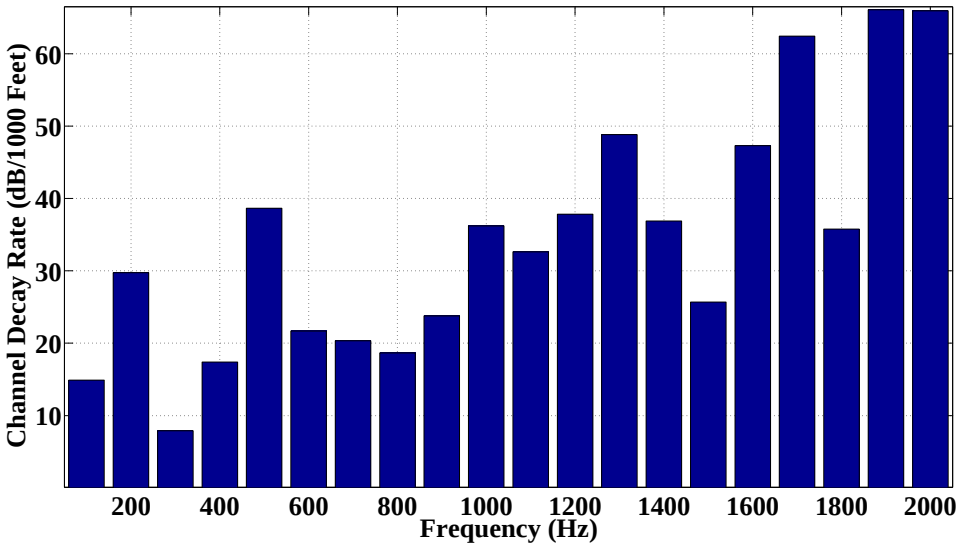

Figure 8.5: Channel decay rate (dB/1000 feet) of the sound wave propagating inside the 7" pipe string

effect on the sound waves that propagate through the interior of the pipe string.

The RMS delay spread results for the measurements are shown in Figure 8.9. It is found that the average value of the RMS delay spread for all measured signals is around 154 ms, which is about 6.4% higher than that of the input signal. Again, it is noted here that the average value of the RMS delay spread increases as the sound wave propagates down the pipe string at a rate around 13.6 ms per 1000 feet. Results found in Figures 8.6 and 8.9 emphasize that concrete has no effect on the delay spread measures for any of the measurements.

The average value of the RMS delay spread measure is shown for each frequency in Figure 8.10 and for each measurement point in Figure 8.11. It is obvious that the 100 Hz and 200 Hz signals have higher average values, while the rest of the frequencies have comparable results. On the other hand, the average value of the RMS delay spread measure does not significantly change along the pipe string.

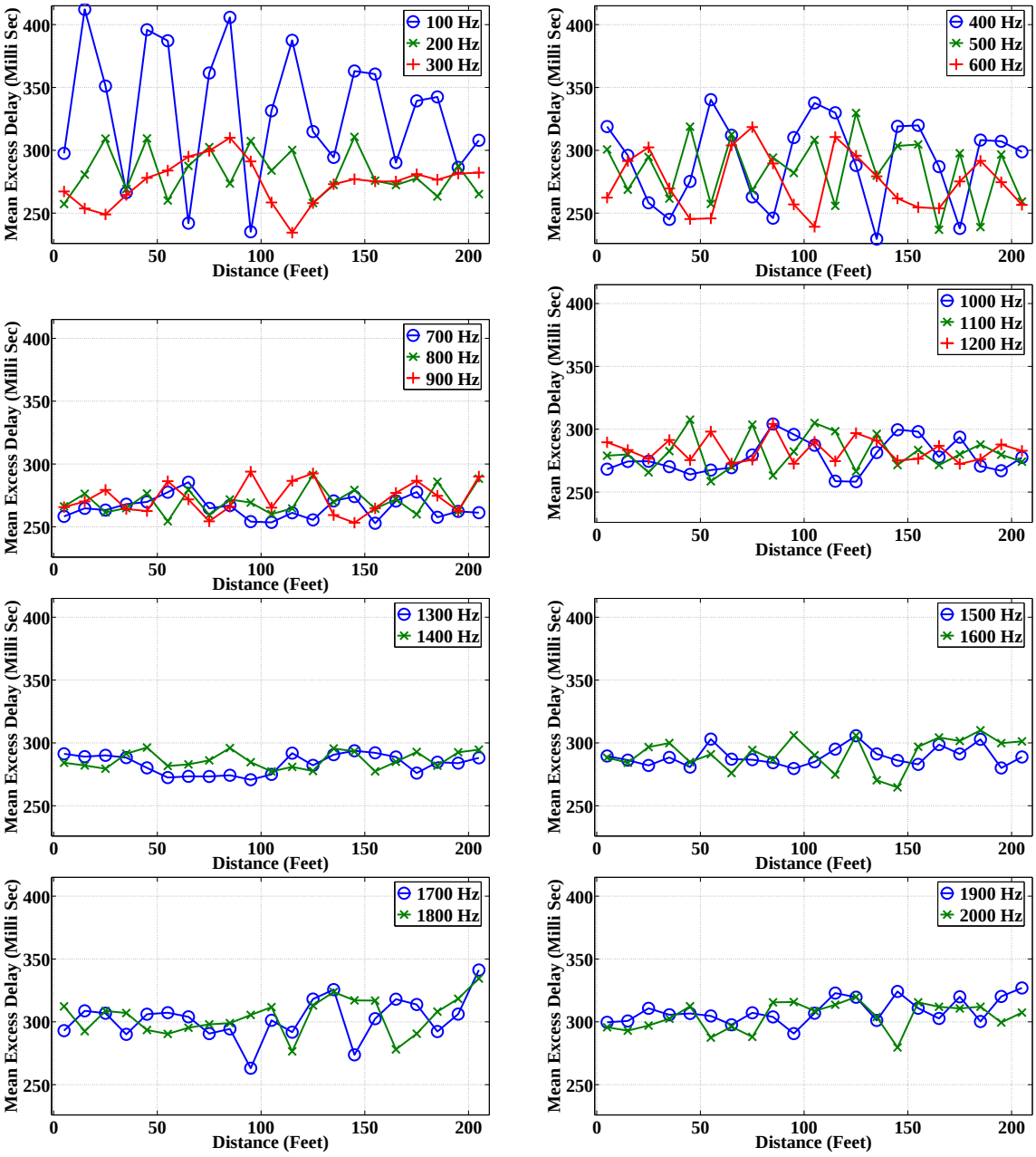

Figure 8.6: Mean excess delay values of the sound wave propagating inside the 7" pipe string

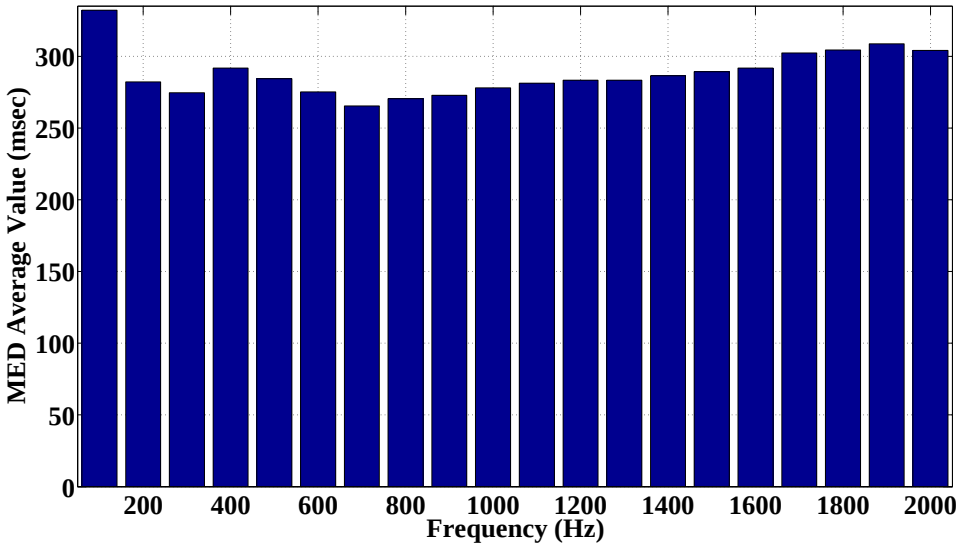

Figure 8.7: Mean excess delay average value (per frequency) of the sound wave propagating inside the 7" pipe string

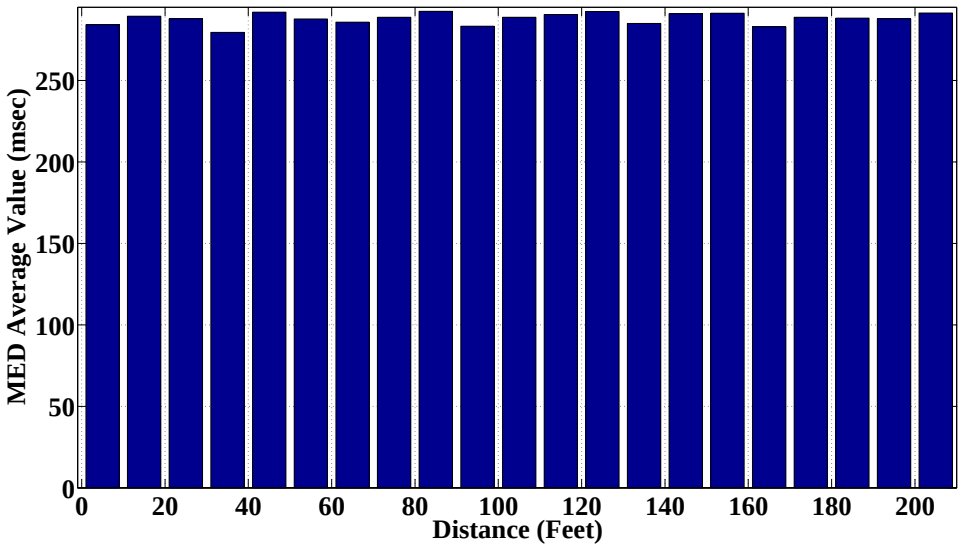

Figure 8.8: Mean excess delay average value (per measurement point) of the sound wave propagating inside the 7" pipe string

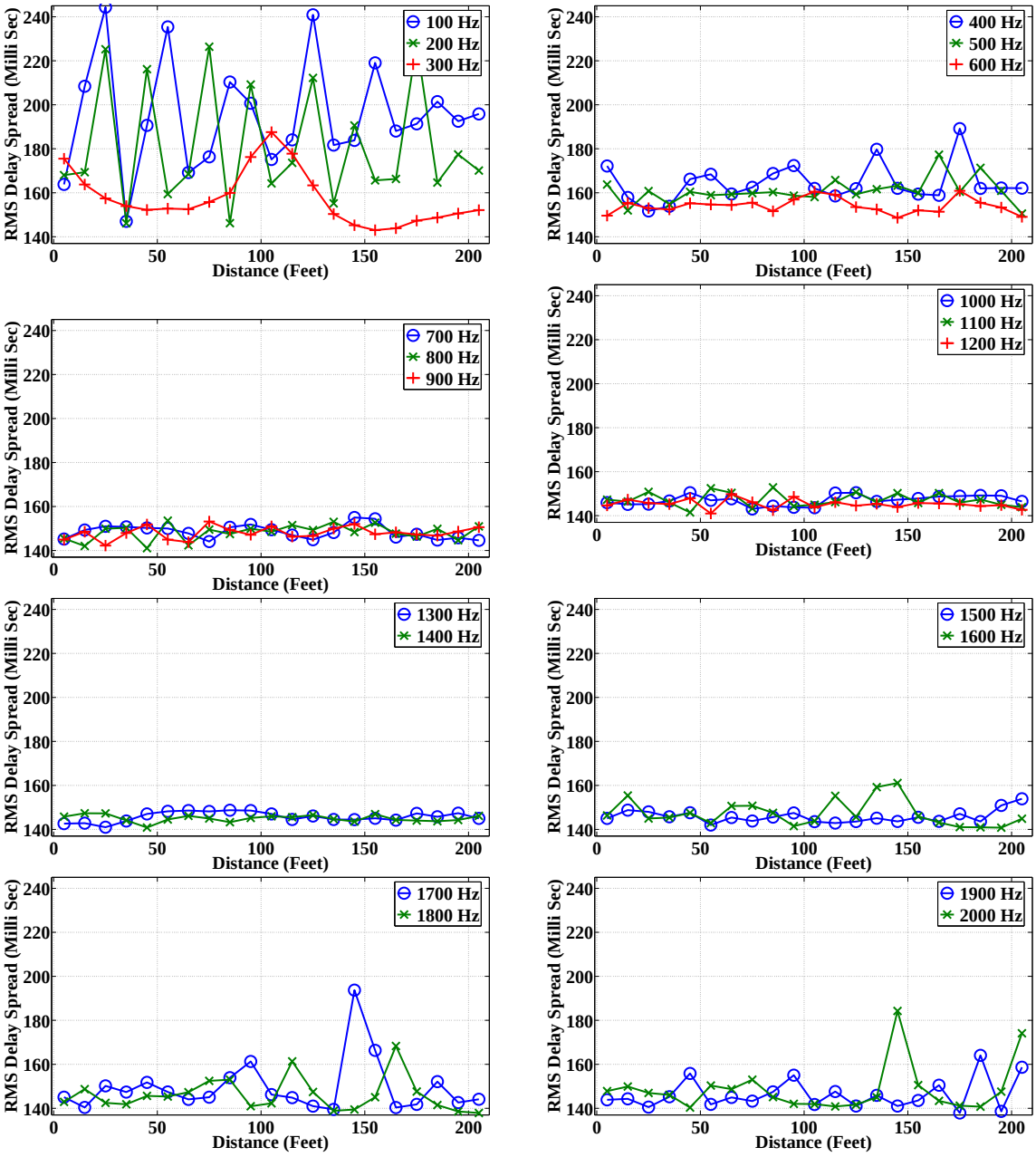

Figure 8.9: RMS delay spread values of the sound wave propagating inside the 7" pipe string

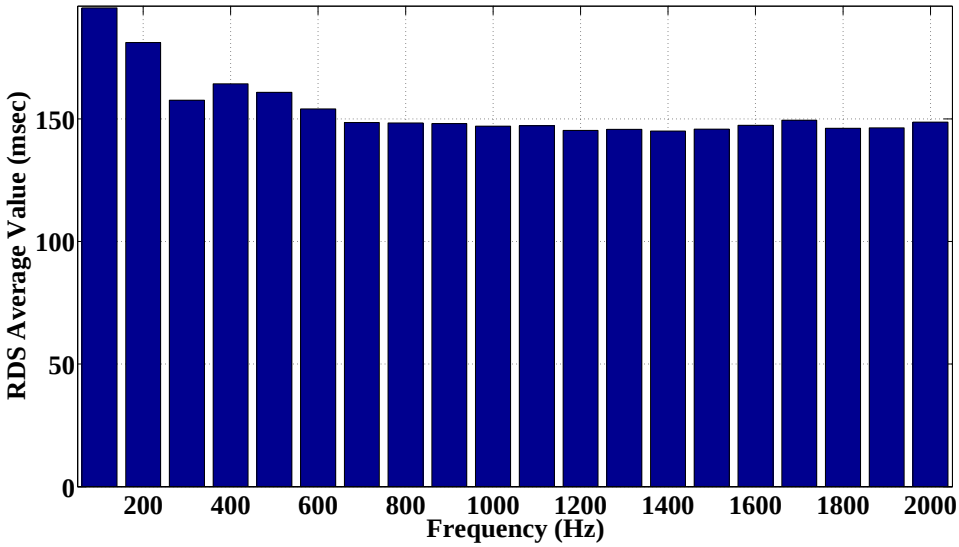

Figure 8.10: RMS delay spread average value (per frequency) of the sound wave propagating inside the 7" pipe string

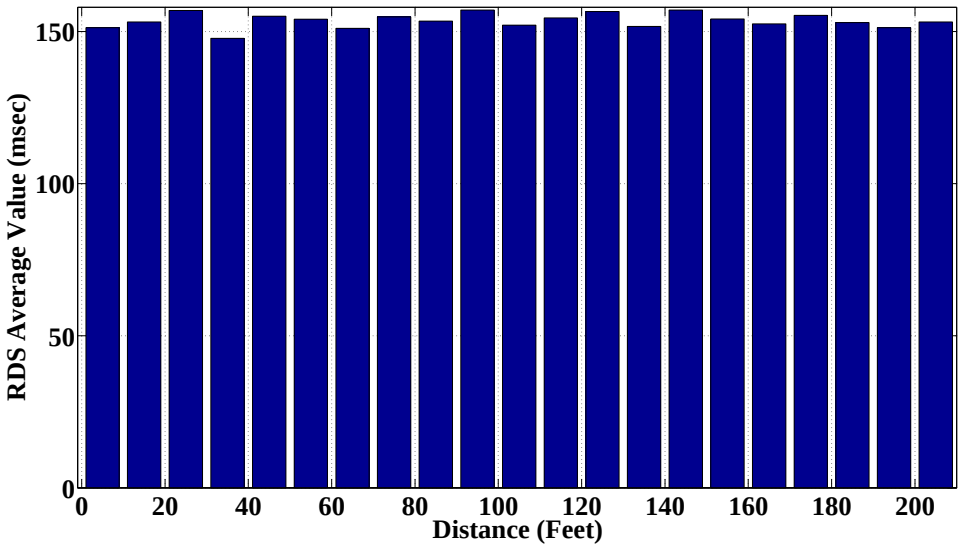

Figure 8.11: RMS delay spread average value (per measurement point) of the sound wave propagating inside the 7" pipe string

9. Conclusions

This chapter concludes the dissertation. A summary of results is provided in Section 9.1. Future work is proposed in Section 9.2.

9.1 Summary of Results

Wireless communication systems can be a feasible alternative to the low-rate, expensive, and unreliable existing wired telemetry technologies that are found in many exploration and drilling industries. In particular, using acoustic waves to communicate between two points over a pipe string is a promising technology to conduct wireless communications as they can propagate by vibrating the pipe body and so not interfering with the surrounding medium.

The study of the behavior of the communication channel is important in order to design a successful acoustic telemetry system. Accordingly, a testbed was designed to study the propagation of acoustic waves over pipe strings. In this setup, the communication medium is the pipe string itself where the acoustic waves propagate by vibrating the pipes. The effects of the signal's input frequency, pipe diameter, concrete, and propagation distance on wave propagation were studied.

Propagation studies revealed that many harmonics propagate through the pipe string and signal energy was found in frequencies up to 20 kHz. The acoustic waves experienced a decent frequency-dependent decay while propagating over the pipe string. In addition, multipath reflections in the pipe string were found to cause noticeable signal dispersion. The coherence bandwidth results indicated that the pipe string appears as a frequency selective channel.

The effect of encasing parts of the pipe string in concrete was also studied. Measured signals experienced noticeable attenuation due to the presence of a doughnut-

shaped concrete segment over the exterior of a pipe segment; many high-order harmonics were heavily attenuated after encasing the pipe in concrete. The concrete acts like an attenuating band-pass filter whose characteristics depend on the length and thickness of the concrete segment. Because the acoustic signals propagate by vibrating the pipe string, the presence of concrete segments over some pipes will make the pipes harder to vibrate; accordingly, it is expected that the acoustic waves lose their energy after passing through the concrete segments.

Signal processing algorithms that enhance the signal quality were studied to address the concrete and channel effects; these algorithms include using band-pass filters that retain the fundamental harmonic from a measurement and remove the rest, a harmonics-collection algorithm that constructively adds all the available harmonics in the measured signal, and channel equalization to undo the dispersive effect of channel. Results emphasized the usefulness of the signal processing algorithms, especially the equalizer, in increasing the signal-to-noise ratio. Consequently, employing these algorithms will help increase the transmission depth inside the well and/or the data rate.

Sound wave propagation inside the interior of the pipe string was investigated as an alternative propagation method to vibrating the pipe string. In this setup, the propagation medium is the air inside the pipe string. The experimental results emphasized the usefulness of using sound waves to carry information in cemented pipe strings. Although concrete was found to dampen the acoustic waves that propagate by vibrating the pipe string, using a microphone to sense the sound waves that propagate inside the pipe string may be a useful solution to this problem as concrete was found not to affect wave propagation in this medium.

Because the propagation results revealed that low-frequency harmonics experience less attenuation compared to the high-frequency harmonics during propagation,

the use of a low-frequency communication system is suggested to be beneficial for the 7" pipe string systems. This result applies to both propagation methods studied in this work. Signal processing algorithms that enhance the signal quality are also recommended to address the effects of attenuation and channel dispersion; in particular an equalizer can be useful for this setup.

A communication system that uses both a microphone and a piezoelectric accelerometer to sense acoustic signals is thought to perform well in pipe string systems that have some tubings encased in concrete. The piezoelectric accelerometer will be used to sense the acoustic waves that vibrate the body of the pipe, while the microphone will sense the sound waves that propagate in the air inside the pipe string. A diversity combining method should be used to combine the outputs of the microphone and the accelerometer into an improved signal in order to get the benefits of the independent channel paths. Finally, results of this work recommend that conducting wireless downhole communications using acoustic waves can be a promising, cost-effective, and reliable technology.

9.2 Proposed Future Work

Suggestions to enhance the current testbed or conduct more advanced research include:

- The development of improved theoretical and empirical models for acoustic wave propagation over pipe strings
- The development of improved signal processing techniques
- The enhancement of the testbed
- The design of advanced wireless downhole systems

9.2.0.1 Development of Improved Models

One limiting factor that has prevented the development of wireless downhole technology is the absence of reliable mathematical models for determining acoustic wave propagation in pipe strings. This limitation has been seen firsthand with the development of this testbed. No published models have been able to even partially predict the measurements that were seen with the current system. As a future work, finding a model that predicts the major features of wave propagation over the pipe string is needed.

9.2.0.2 Development of Improved Signal Processing Techniques

Because it has been difficult to predict which types of waves will propagate well through pipe strings, it would be helpful to design both signaling schemes and signal processing schemes in a manner that tolerates the unpredictable propagation environment. One proposed work is to investigate the effectiveness of adaptive equalization at the receiver unit by adaptively training an equalizer to undo the dispersive effects of the pipe string. Non-coherent diversity combining techniques can also be considered to enhance signal detection where the signal power in different frequency bands is combined to provide the strongest possible signal. The effect of different signaling formats on wave propagation can also be an interesting research problem. Finally, the use of error correction coding would be beneficial as the ability to detect and correct errors will be a substantial advantage to the wireless downhole system. Unfortunately, the use of error correction codes requires an overhead which will cause the transmission of extra pulses and consume the limited transmitter power. To avoid this problem, the use of non-binary codes, like Reed-Solomon codes, in conjunction with a non-binary modulation format, like non-binary Pulse Position Modulation, could be investigated.

9.2.0.3 Enhancement of the Testbed

The current testbed makes possible research that may not exist in any other academic setting. However, the types of results that can be generated could be greatly increased by certain enhancements to the testbed. Some ideas for future investigation include: increasing the testbed length, which will enhance the ability to predict wave propagation behavior over longer distances, and assembling different diameter pipes to study how the diameter of the tubing affects wave propagation. Finally, adding a device at the end of the pipe string that serves as an acoustical sink to limit the reflections in the pipe string could be investigated.

9.2.0.4 Design of Advanced Systems

The testbed has provided an ability to perform a number of interesting experiments. However, the testbed can be used to perform more experiments; more interesting experimental topics include: investigating the best locations to mount the acoustical sensor to pick the best signal, studying the usefulness of using multiple sensors in forming an echo cancellation setup, investigating the effect of pipe contact with the surrounding earth on wave propagation through the pipe string, investigating the effect of gas or oil flowing inside the pipe string on wave propagation, and generating an acoustical noise by running water through the pipe string while the acoustic waves are propagated down the testbed. Moreover, many actual wells are not completely vertical and at some point the pipe string is curved; because this curvature puts stress on the pipe that will change its acoustical properties, it would be interesting to study the effects of curvature on the acoustical properties. Finally, parts of some wells are encased in concrete to prevent gases from leaking out to the surface; therefore, quantifying the effect of concrete on acoustic wave propagation is an important topic to study. The effects of concrete length, diameter, and composi-

tion on the wave propagation are some of the parameters that could be investigated in the future.

REFERENCES

[1] R. C. Ransom, *Glossary of Terms & Expressions Used in Well Logging*. Houston, TX, USA: Society of Professional Well Log Analysts, first ed., 1975.

[2] K. Van Dyke, *Fundamentals of Petroleum*. Austin, TX, USA: Petroleum Extension Service, University of Texas, fourth ed., 1997.

[3] P. F. Lynch, *Primer in Drilling & Production Equipment: Volume 3 – Downhole Operations*. Houston, TX, USA: Gulf Publishing Company, first ed., 1981.

[4] D. E. Johnson and K. E. Pile, *Well Logging in Nontechnical Language*. Tulsa, OK, USA: PennWell Books, second ed., 2002.

[5] O. Serra, *Fundamentals of Well-Log Interpretation*. Amsterdam, The Netherlands: Elsevier, first ed., 1984.

[6] J. R. Hearst and P. H. Nelson, *Well Logging for Physical Properties*. New York, NY, USA: Mc Graw-Hill Book Co., first ed., 1985.

[7] J. R. Jorden and F. L. Campbell, *Well Logging II: Electric and Acoustic Logging*. Richardson, TX, USA: Society of Petroleum Engineers, first ed., 1986.

[8] F. L. Paillet and C. H. A. Cheng, *Acoustic Waves in Boreholes*. Boca Raton, FL, USA: CRC Press Inc., first ed., 1991.

[9] J.-L. Mari and F. Coppens, *Well Seismic Surveying*. Paris, France: Editions Technip, second ed., 2003.

[10] D. V. Ellis and J. M. Singer, *Well Logging for Earth Scientists*. Dordrecht, The Netherlands: Springer Verlag, second ed., 2007.

[11] O. Serra, *Well Logging Handbook*. Paris, France: Editions Technip, first ed., 2008.

[12] X.-M. Tang and A. C. H. Cheng, *Quantitative Borehole Acoustic Methods*. Amsterdam, The Netherlands: Elsevier Ltd., first ed., 2004.

[13] W. Gough, J. P. G. Richards, and R. P. Williams, *Vibrations and Waves*. Chichester, West Sussex, England: Ellis Horwood Ltd., first ed., 1983.

[14] A. P. Dowling and J. E. F. Williams, *Sound and Sources of Sound*. New York, NY, USA: John Wiley & Sons Inc., first ed., 1983.

[15] S. Temkin, *Elements of Acoustics*. New York, NY, USA: John Wiley & Sons Inc., first ed., 1981.

[16] L. E. Kinsler, A. R. Frey, A. B. Coppens, and J. V. Sanders, *Fundamentals of Acoustics*. New York, NY, USA: John Wiley & Sons Inc., fourth ed., 2000.

[17] L. Brillouin, *Wave Propagation in Periodic Structures*. Mineola, NY, USA: Dover Publications, second ed., 2003.

[18] A. C. Nilsson, "Wave Propagation in and Sound Transmission Through Sandwich Plates," *Journal of Sound and Vibration*, vol. 138, pp. 73–94, April 1990.

[19] R. M. Orris and M. Petyt, "A Finite Element Study of Harmonic Wave Propagation in Periodic Structures," *Journal of Sound and Vibration*, vol. 33, no. 2, pp. 223–236, 1974.

[20] D. J. Mead and S. Parthan, "Free Wave Propagation in Two-Dimensional Periodic Plates," *Journal of Sound and Vibration*, vol. 64, no. 3, pp. 325–348, 1979.

[21] A. H. Nayfeh, "The General Problem of Elastic Wave Propagation in Multi-layered Anisotropic Media," *The Journal of the Acoustical Society of America*, vol. 89, pp. 1521–1531, April 1991.

[22] M. S. Kushwaha, "Stop-Bands for Periodic Metallic Rods: Sculptures That can Filter the Noise," *Applied Physics Letters*, vol. 70, pp. 3218–3220, June 1997.

[23] B. A. Auld, *Acoustic Fields and Waves in Solids. Volume 1.* Malabar, FL, USA: Robert E. Krieger Publishing Company, second ed., 1990.

[24] B. A. Auld, *Acoustic Fields and Waves in Solids. Volume 2.* Malabar, FL, USA: Robert E. Krieger Publishing Company, second ed., 1990.

[25] D. Royer and E. Dieulesaint, *Elastic waves in Solids I – Free and Guided Propagation.* Berlin, Germany: Springer, first ed., 2000.

[26] A. Bedford and D. S. Drumheller, *Introduction to Elastic Wave Propagation.* Chichester, West Sussex, England: John Wiley & Sons Inc., first ed., 1994.

[27] D. S. Drumheller, *Introduction to Wave Propagation in Nonlinear Fluids and Solids.* New York, NY, USA: Cambridge University Press, first ed., 1998.

[28] T. G. Barnes and B. R. Kirkwood, "Passbands for Acoustic Transmission in an Idealized Drill String," *The Journal of the Acoustical Society of America*, vol. 51, pp. 1606–1608, May 1972.

[29] W. D. Squire and H. J. Whitehouse, "A New Approach to Drill-String Acoustic Telemetry," in *SPE Annual Technical Conference and Exhibition*, (Las Vegas, NV, USA), September 1979.

[30] D. S. Drumheller, "An Overview of Acoustic Telemetry," in *Conference: Proceedings of Geothermal Program Review X – Geothermal Energy and the Utility*

Market-The Opportunities and Challenges for Expanding Geothermal Energy in a Competitive Supply Market, (San Francisco, CA, USA), pp. 73–79, March 1992.

[31] D. S. Drumheller, "Acoustical Properties of Drill Strings," *The Journal of the Acoustical Society of America*, vol. 85, pp. 1048–1064, March 1989.

[32] D. S. Drumheller and S. D. Knudsen, "The Propagation of Sound Waves in Drill Strings," *The Journal of the Acoustical Society of America*, vol. 97, pp. 2116–2125, April 1995.

[33] D. S. Drumheller, "Extensional Stress Waves in One-Dimensional Elastic Waveguides," *The Journal of the Acoustical Society of America*, vol. 92, pp. 3389–3402, December 1992.

[34] D. S. Drumheller, "Attenuation of Sound Waves in Drill Strings," *The Journal of the Acoustical Society of America*, vol. 94, pp. 2387–2396, October 1993.

[35] D. S. Drumheller, "Coupled Extensional and Bending Motion in Elastic Waveguides," *Wave Motion*, vol. 17, pp. 319–327, August 1993.

[36] D. S. Drumheller, "Wave Impedances of Drill Strings and Other Periodic Media," *The Journal of the Acoustical Society of America*, vol. 112, pp. 2527–2539, December 2002.

[37] N. J. C. Lous, S. W. Rienstra, and I. J. B. F. Adan, "Sound Transmission Through a Periodic Cascade with Application to Drill Pipes," *The Journal of the Acoustical Society of America*, vol. 103, pp. 2302–2311, May 1998.

[38] J. M. Carcione and F. Poletto, "Simulation of Stress Waves in Attenuating Drill Strings, Including Piezoelectric Sources and Sensors," *The Journal of the Acoustical Society of America*, vol. 108, pp. 53–64, July 2000.

[39] R. Rao, "Acoustic Transmission Through Fluid-Filled Pipes in Boreholes," Master's thesis, Dept. of Ocean Engineering, Massachusetts Institute of Technology, Cambridge, MA, USA, June 1991.

[40] R. Rao, *The Radiation and Vibration of Drilling Tnbulars in Fluid-filled Boreholes*. PhD thesis, Dept. of Ocean Engineering, Massachusetts Institute of Technology, Cambridge, MA, USA, February 1996.

[41] H. Y. Lee, *Drillstring Axial Vibration and Wave Propagation in Boreholes*. PhD thesis, Dept. of Ocean Engineering, Massachusetts Institute of Technology, Cambridge, MA, USA, June 1991.

[42] D. E. Weston, "The Theory of the Propagation of Plane Sound Waves in Tube," *Proceedings of the Physical Society. Section B*, vol. 66, pp. 695–709, August 1953.

[43] E. J. Kerschen and J. P. Johnston, "Mode Selective Transfer of Energy From Sound Propagating Inside Circular Pipes to Pipe Wall Vibration," *The Journal of the Acoustical Society of America*, vol. 67, pp. 1931–1934, June 1980.

[44] M. P. Horne and R. J. Hansen, "Sound Propagation in a Pipe Containing a Liquid of Comparable Acoustic Impedance," *The Journal of the Acoustical Society of America*, vol. 71, pp. 1400–1405, June 1982.

[45] L.-H. Huang, G.-R. Chen, and W.-S. Hwang, "Sound Propagation Near Tunnel Outlets," *Journal of the Chinese Institute of Engineers*, vol. 24, pp. 321–328, May 2001.

[46] A. Kondis, "Acoustical Wave Propagation in Buried Water Filled Pipes," Master's thesis, Dept. of Civil and Environmental Engineering, Massachusetts Institute of Technology, Cambridge, MA, USA, February 2005.

[47] W. Łapka, "Sound Propagation Through Circular Ducts with Spiral Element Inside," in *European COMSOL Conference*, (Hanover, Germany), November 2008.

[48] S. T. Peng, "Rigorous Analogies Between Elastic and Electromagnetic Systems," *Applied Physics A: Materials Science & Processing*, vol. 1, pp. 87–91, February 1973.

[49] J. M. Carcione and F. Cavallini, "On the Acoustic-Electromagnetic Analogy," *Wave Motion*, vol. 21, pp. 149–162, March 1995.

[50] L. Nicolas, M. Furstoss, and M. A. Galland, "Analogy Electromagnetism-Acoustics: Validation and Application to Local Impedance Active Control for Sound Absorption," *The European Physical Journal – Applied Physics*, vol. 4, pp. 95–100, October 1998.

[51] B. R. Spies, "Electrical and Electromagnetic Borehole Measurements: A Review," *Surveys in Geophysics*, vol. 17, pp. 517–556, July 1996.

[52] F. Ding and L. Cheng, "Coreless Electromagnetic Coupling-Based Drillstem Telemetry Using Dual Electronic Gauges," *SPE Production & Operations*, vol. 22, pp. 128–134, February 2007.

[53] M. Stojanovic, "Underwater Acoustic Communications," *Wiley Encyclopedia of Electrical and Electronics Engineering*, vol. 22, pp. 688–698, March 1999.

[54] M. Stojanovic, "Acoustic (Underwater) Communications," *Wiley Encyclopedia of Telecommunications*, vol. 1, January 2003.

[55] M. Stojanovic and J. Preisig, "Underwater Acoustic Communication Channels: Propagation Models and Statistical Characterization," *IEEE Communications Magazine*, vol. 47, pp. 84–89, January 2009.

[56] A. B. Baggeroer, "Acoustic Telemetry – An Overview," *IEEE Journal of Oceanic Engineering*, vol. 9, pp. 229–235, October 1984.

[57] X. Lurton, *An Introduction to Underwater Acoustics: Principles and Applications*. Chichester, West Sussex, England: Springer-Praxis, first ed., 2002.

[58] M. Stojanovic, J. G. Proarkis, J. A. Rice, and M. D. Green, "Spread Spectrum Underwater Acoustic Telemetry," *OCEANS '98 Conference Proceedings*, vol. 2, pp. 650–654, September 1998.

[59] F.-S. Lu, C.-H. Tseng, and B.-C. Wu, "Design and Implementation of an All-Digital Real-Time Underwater Acoustic Transceiver Using Digital Signal Processors," *Journal of Marine Science and Technology*, vol. 16, no. 1, pp. 34–43, 2008.

[60] J. V. Leggett III and B. R. Green, "A New Method for Communicating Downhole Sensor Data Within the Annulus of a Production Well," in *SPE Annual Technical Conference and Exhibition*, (New Orleans, LA, USA), September 1994.

[61] T. Tochikawa, T. Sakai, R. Taniguchi, and T. Shimada, "Acoustic Telemetry: The New MWD System," in *SPE Annual Technical Conference and Exhibition*, (Denver, CO, USA), October 1996.

[62] G. Harper, E. Almanza, A. Fossa, D. Finley, and G. Strang, "Implementation of Advanced Acoustic Telemetry System Adds Value and Efficiency to Well Testing Operations," in *SPE Asia Pacific Oil and Gas Conference and Exhibition*, (Jakarta, Indonesia), September 2003.

[63] G. Harper, E. Almanza, A. Fossa, D. Finley, and G. Strang, "Advanced Acoustic Telemetry System Provides Real-time Data Acquisition that Increases Efficiency in Well Testing Operations," in *Offshore Technology Conference*, (Houston, TX, USA), May 2003.

[64] S. Kruegel, P. Tubel, and G. Covatch, "Real Time Half Duplex Communications Wireless Gauge with Downhole Power Monitors Deep Well Gas Production," *GasTIPS*, vol. 10, pp. 10–14, Summer 2004.

[65] V. Shah, W. R. Gardner, D. H. Johnson, and S. Sinanovic, "Design Considerations for a New High Data Rate LWD Acoustic Telemetry System," in *SPE Asia Pacific Oil and Gas Conference and Exhibition*, (Perth, Australia), October 2004.

[66] S. Sinanovic, D. H. Johnson, V. Shah, and W. R. Gardner, "Data Communication Along the Drill String Using Acoustic Waves," in *ICASSP 2004*, (Montreal, Quebec, Canada), pp. IV–909–912, May 2004.

[67] S. Sinanovic, *Limits of Acoustic Waveguide Communication*. PhD thesis, Dept. of Electrical and Computer Engineering, Rice University, Houston, TX, USA, April 2006.

[68] S. Sinanovic, D. H. Johnson, and W. R. Gardner, "Directional Propagation Cancellation for Acoustic Communication Along the Drill String," in *ICASSP 2006*, (Toulouse, France), pp. IV–521–524, May 2006.

[69] L. Gao, W. Gardner, C. Robbins, M. Memarzadeh, and D. H. Johnson, "Limits on Data Communication Along the Drillstring Using Acoustic Waves," in *SPE Annual Technical Conference and Exhibition*, (Dallas, TX, USA), October 2005.

[70] L. Gao, D. Finley, W. Gardner, C. Robbins, E. Linyaev, J. Moore, M. Memarzadeh, and D. H. Johnson, "Acoustic Telemetry Can Deliver More Real-Time Downhole Data in Underbalanced Drilling Operations," in *IADC/SPE Drilling Conference*, (Miami, FL, USA), February 2006.

[71] L. Gao, W. Gardner, C. Robbins, D. H. Johnson, and M. Memarzadeh, "Limits on Data Communication Along the Drillstring Using Acoustic Waves," *SPE Reservoir Evaluation & Engineering*, vol. 11, pp. 141–146, February 2008.

[72] M. Azari, A. Salguero, E. Almanza, and H. Kool, "Data Acquisition With Advanced Acoustic Telemetry Improves Operational Efficiency in Deep-water and Land-Well Testing-Case Histories," in *SPE Asia Pacific Oil & Gas Conference and Exhibition*, (Adelaide, Australia), September 2006.

[73] M. Azari, A. Salguero, E. Almanza, and H. Kool, "Real Time Data Acquisition with Advanced Acoustic Telemetry Improves Operational Efficiency in Deep Water Offshore Well Testing," in *SPE Asia Pacific Oil & Gas Conference and Exhibition*, (Adelaide, Australia), September 2006.

[74] M. Memarzadeh, D. H. Johnson, W. Gardner, and L. Gao, "Maximizing the Fidelity of Log Signals Transmitted via Digital Telemetry," in *SPE Annual Technical Conference and Exhibition*, (San Antonio, TX, USA), September 2006.

[75] M. Memarzadeh, *Optimal Borehole Communication Using Multicarrier Modulation*. PhD thesis, Dept. of Electrical and Computer Engineering, Rice University, Houston, TX, USA, January 2007.

[76] C.-Y. Wang, W.-X. Qiao, and W.-Q. Zhang, "Using Transfer Matrix Method to Study the Acoustic Property of Drill Strings," in *IEEE International Symposium on Signal Processing and Information Technology*, (Vancouver, BC, Canada), pp. 415–419, August 2006.

[77] C.-Y. Wang, W.-X. Qiao, W.-Q. Zhang, X.-H. Che, and J. Li, "Acoustic Waveform Design for Data Transmission by Using Drill Strings in Logging-While-Drilling," in *8th International Conference on Signal Processing*, vol. 4, (Beijing, China), November 2006.

[78] J. M. Neff and P. L. Camwell, "Field-Test Results of an Acoustic MWD System," in *SPE/IADC Drilling Conference*, (Amsterdam, The Netherlands), February 2007.

[79] D. Fyfe, L. Jarvis, T. Ing, and M. Farooqui, "Field Trial of an Acoustic Downhole Monitoring System Retrofitted in an Existing Completion," in *SPE Middle East Oil and Gas Show and Conference*, (Bahrain, Kingdom of Bahrain), March 2007.

[80] D. Finley and R. Pahmiyer, "Well Testing in the New Millennium – Real Time," in *SPE Asia Pacific Oil and Gas Conference and Exhibition*, (Jakarta, Indonesia), April 2001.

[81] R. Pahmiyer, A. Flowers, E. Almanza, and H. El Assal, "Implementation of Advanced Wellsite Data Management and Communications System Adds Value and Efficiency to Welltesting Operations," in *Offshore Europe Conference*, (Aberdeen, United Kingdom), September 2001.

[82] M. Brinsden, "A New Wireless Solution to Real Time Reservoir Surveillance," in *SPE Middle East Oil and Gas Show and Conference*, (Bahrain, Kingdom of Bahrain), March 2005.

[83] C. Fulda, O. Akimov, A. Baule, J. Bethge, T. Roessel, and R. Tilsley-Baker, "Real-Time Transmission of High-Resolution Images," in *SPE Europec/EAGE Annual Conference and Exhibition*, (Vienna, Austria), June 2006.

[84] E. Tollefsen, A. Weber, A. Kramer, G. Sirkin, D. Hartman, and L. Grant, "Logging While Drilling Measurements: From Correlation to Evaluation," in *SPE International Oil Conference and Exhibition in Mexico*, (Veracruz, Mexico), June 2007.

[85] A. Anchliya, "A Review of Seismic While Drilling (SWD) Techniques: A Journey from 1986 to 2005," in *SPE Europec/EAGE Annual Conference and Exhibition*, (Vienna, Austria), June 2006.

[86] S. L. Miller and D. G. Childers, *Probability and Random Processes: With Applications to Signal Processing and Communications*. Amsterdam, The Netherlands: Elsevier Academic Press, first ed., 2004.

[87] C. L. Lawson and R. J. Hanson, *Solving Least Squares Problems*. Philadelphia, PA, USA: Society for Industrial and Applied Mathematics, first ed., 1995.

[88] T. K. Moon and W. C. Stirling, *Mathematical Methods and Algorithms for Signal Processing*. Upper Saddle River, NJ, USA: Prentice Hall Inc., first ed., 2000.

[89] T. Rappaport, *Wireless Communications: Principles and Practice*. Upper Saddle River, NJ, USA: Prentice Hall PTR, second ed., 2001.

[90] S. J. Orfanidis, *Optimum Signal Processing: An Introduction*. New York, NY, USA: McGraw-Hill Publishing Company, second ed., 2007.